CENTRO DE INVESTIGACIÓN EN MATERIALES AVANZADOS
DEPARTAMENTO DE ESTUDIOS DE POSGRADO

AEROGEL OF CHITOSAN (CS) AND POLYVINYL ALCOHOL (PVA) REINFORCED WITH GRAPHENE OXIDE (GO): SYNTHESIS, CHARACTERIZATION, AND APPLICATION AS COMPOSITE

TESIS
QUE PARA OBTENER EL GRADO DE
MAESTRÍA EN CIENCIA DE MATERIALES
Presenta:

Guadalupe Izamar Delgado Angeles

ASESOR:
Dr. Alejandra García García
Dr. Han Zhang

APODACA, NUEVO LEÓN. **SEPTIEMBRE, 2023**

DECLARATION

EMS7100P Extended Research Project – Final Report

This report entitled A**erogel of chitosan (CS) and polyvinyl alcohol (PVA) reinforced with graphene oxide (GO): synthesis, characterization, and application as composite** was composed by me and is based on my own work. Where the work of others has been used, it is fully acknowledged in the text and in captions to tables and illustrations.

This report has not been submitted for any other qualification.

Name: Guadalupe Izamar Delgado Angeles

Signed: 

Date 06-03-2023

ABSTRACT

In the present work, the investigation of aerogels to be used as multifunctional materials was investigated, for which chitosan (CS) was chosen as reference material because of its availability in nature, polyvinyl alcohol (PVA) because of its biocompatibility, and graphene oxide (GO) because it is a novel material with great growth in the coming years, but mainly because of the availability of functional groups on its surface; hoping that the interaction between these materials and the combination of their properties will result in the fabrication of solid material with properties such as high specific surface area, low density, and small pore size typical of an aerogel. For this purpose, some blends of these substances were freeze-dried to remove the liquid phase and thus obtain the aerogel. With the intention of identifying the influence of the interactions between the materials by varying the amount of these, and thus choosing one with the best properties for characterization by X-ray Photoelectronic Spectroscopy (XPS), Atomic Force Microscopy (AFM), Fourier-Transform Infrared Spectroscopy (FTIR), Scanning Electron Microscopy (SEM), Brunauer-Emmett-Teller method (BET), Thermo Gravimetric Analysis (TGA), Differential Scanning Calorimetry (DSC) and a test with a thermographic camera.

In this way, it was found that using chitosan (CS) with small amounts of polyvinyl alcohol (PVA) as the aerogel matrix and graphene oxide (GO) as filler improves the thermal insulating properties of the material obtained; however, some other properties such as density and pore size still need to be improved in order to use this material as a multifunctional composite.

ACKNOWLEDGEMENTS

I am grateful to Queen Mary University of London (QMUL) for the opportunity to be part of their institution to develop this project and use their facilities and equipment to increase my knowledge and develop new ones. I would also be grateful to Dr. Han Zhang and his research team for their help and advice in developing the experimental work.

I would also like to thank the Advanced Materials Research Centre (Cimav) and all those involved for the support and organization of the program that allowed me to be part of this experience and represent them abroad. I would also be grateful to thank Dra. Alejandra García García for her support during the development of this project, as well as her research team, who gave me the basis to develop this work.

In addition, I would especially like to thank both my parents, Bernave and Bonifacia, as well as my siblings, Karina, Bernabe, and Agustín, for their support and motivation as I embarked on this adventure.

Finally, I would also like to give thanks to my Mexican mates with whom I started this experience, Johana, Daniel and Karen, and to those who joined, Yeremi, Reyna and Verónica, for sharing moments that we will remember with joy.

LIST OF CONTENTS

INDEX OF FIGURES

INDEX OF TABLE

1. INTRODUCTION

Aerogels are unique materials that possess extraordinary properties such as high porosity, low density, and excellent mechanical, thermal and acoustic insulation properties. They have been widely researched for various applications due to their exceptional features. Aerogels composed of chitosan (CS), polyvinyl alcohol (PVA) and graphene oxide (GO) are a recent development and have garnered significant attention due to their exceptional properties.

Chitosan (CS) is a biopolymer derived from chitin, which is a natural polymer found in the exoskeleton of crustaceans and insects. It has excellent antibacterial properties and is biodegradable. Polyvinyl alcohol (PVA) is a synthetic water-soluble polymer that is known for its high tensile and mechanical strength. Graphene oxide (GO) is a two-dimensional material that has exceptional mechanical, thermal, and electrical properties.

When combined, these materials result in an aerogel with exceptional properties that can be used in various applications. These aerogels can be used as a catalyst support, drug delivery systems, thermal insulation materials, sensors, and in energy storage systems. They are also used in aerospace and automotive industries due to their lightweight and high strength-to-weight ratio. Moreover, they are environmentally friendly and biodegradable, making them ideal for various sustainable applications.

One of the main advantages of incorporating graphene oxide (GO) as a reinforcement into aerogels is its high surface area and ability to enhance mechanical properties. Graphene oxide (GO) can also facilitate the dispersion of chitosan (CS) and polyvinyl alcohol (PVA) in the aerogel matrix due to its strong interaction with the polymers, thus improving the stability and performance of the aerogel.

The importance of aerogels composed of chitosan (CS), polyvinyl alcohol (PVA), and graphene oxide (GO) lies in their unique properties and the diverse range of potential applications they offer in various fields such as medicine, construction, and industry, leading to the development of more eco-friendly and sustainable technologies.

CONCEPTUAL FRAMEWORK

Aerogel

Aerogels are a special type of gel material in which the liquid part is replaced with gas without collapsing the overall structure, which forms a solid material with a three-dimensional (3D) porous network(1).

Therefore, the aerogels are porous nanostructured materials (up to 99.8%) with remarkable characteristics(1), such as large surface area (up to 1200 m^2/g), ultra-low density (~0.003 g/cm^3), extremely low thermal conductivity (up to 0.01 W/mk), high porosity(1), low sound velocity (up to 100 m/s), low refractive index (1.05); as well as high thermal insulation values (0.005 W/mK) (2),(3). That's the reason they are excellent candidates in the field of thermal insulation, however, they can be relatively expensive and toxic, depending on the source(4).

Hence the aerogels derived from renewable and biodegradable resources are excellent proposals for the generation of environmentally friendly insulating materials(4), and it is also possible to combine the synthesis process with some green chemistry principles; an example of this is the use of biomass or waste that can be non-toxic, renewable and biodegradable(4).

Insulating

Aerogels have a combination of low density and small pore size(5,6), which results in reduced heat transfer and therefore lower thermal conductivity values(6); they also show excellent fire resistance and sound absorption(6). They are therefore considered for applications as lightweight super insulators(7); also aerogels and aerogel-based composites are considered as new generation building thermal insulation materials(8).

Graphene oxide (GO)

Within the family of graphene materials or graphene analogues, there is graphene oxide (GO), which is a polymorph of carbon, and one of the most important graphene derivatives, as it is an oxidised form of graphene usually produced by the oxidation of graphite(9). It contains large amounts of oxygen atoms present on its surface(10), basal planes and edges(11) in the form of oxygen functional groups such as epoxy, hydroxyl and carboxyl groups(12),(13),(11), which have a lone pair of electrons(12), giving it hydrophilic properties(11),(14) and solubility in water and some solvents(9).

GO is considered a material with a high adsorption capacity(12) due to its large specific surface area; it has good mechanical properties(15), such as high hardness and excellent flexibility(16), depending on the number of layers present in the material; as well as good electrochemical, optical and chemical properties(10), it has a forbidden band that can be adjusted by varying the degree of oxidation(17), it is capable of forming stable suspensions in water, it is compatible with other materials to form covalent bonds(12),(17), as well as to be used as a substrate in materials such as aerogels(11); besides being relatively easy to obtain, it is low cost(16) and sometimes through environmentally friendly processes(11).

However, a problem with graphene and its derivatives, such as GO, is that they tend to aggregate layer by layer due to strong interplanar interactions(13); therefore, the size of GO sheets is vital in contributing to the physicochemical properties of aerogels(18).

Chitosan (CS)

It is a linear, semi-crystalline polysaccharide(19) with an Nitrogen (N) content of 7%, produced from the deacetylation of chitin, one of the main components of crustacean shells and fungal biomass(20),(6); it is therefore considered a low-cost natural biomaterial(13).

Amino (-NH) and hydroxyl (-OH) groups are present in chitosan (CS), however this polymer is positively charged(19) due to the presence of amino groups which confer many chemical and functional properties(19),(21); for example, pH-dependent solubility(22), as protonated amino groups provide solubility in dilute acidic aqueous

solutions (pH<6)(19); it tends to have a higher elastic modulus but a lower elongation (<40%) at break due to its high crystalline and glass transition temperature(23); it tends to be brittle, however this could be reduced by modifying its basic structure through mixing and chemical modification(23) with PVA being an excellent alternative.

CS is less soluble in alkaline media compared to acidic media, therefore controlling the pH during synthesis is very important, as increasing the pH increases the stiffness of the aerogel and therefore increases the Young's modulus value(16). It is also considered a crosslinking agent for GO(13), because it can strongly attract negatively charged GO sheets through electrostatic interactions(13).

Polyvinyl alcohol (PVA)

Polyvinyl alcohol (PVA) is a linear hydrophilic synthetic polymer(24),(25), which possesses prominent hydroxyl groups (-OH groups)(26). Other characteristics include high chemical resistance, good optical and physical properties, low toxicity, high biodegradability(11), high tensile strength and flexibility(27). It is also a biodegradable polymer with the ability to decompose in a relatively short period of time(28).

Its physicochemical and mechanical properties are mainly due to the number of hydroxyl groups present in the PVA polymer(29), which makes it biocompatible, thermostable(29) and easily soluble in water(11),(19).

It can also be blended with different synthetic and natural polymers due to its high hydrophilicity and processability(30) making it a good matrix for a variety of applications(29) and allowing other materials to be incorporated through hydrogen bonding(29). It is also available due to its low cost and environmental friendliness(31).

Compound material

The polymers such as PVA and CS that could crosslink them through covalent and supramolecular interactions such as hydrogen bonds are of interest for applications such as thermal insulation, acoustic insulation and flame retardants(6). Since the functional groups on the basal planes and edges of GO are well suited to form hydrogen bonds with PVA and provide enhanced charge transfer between PVA and

GO(32). On the other hand, CS aerogel is viable for use as a thermal insulator due to its mechanical and thermal properties that can be improved by the addition of GO with which a better interaction can be achieved due to the presence of functional groups on the surface of both materials(33)**.**

The approach is to take advantage of the complementary properties of the three materials, the biocompatibility associated with CS(30), the processability and versatility associated with PVA(30) and the exceptional physical properties of GO(30) to obtain a composite material that merges these properties, since due to the hydroxyl functionalities available on the surface of GO they could be employed in the formation of H-bonds with the hydroxyl functionalities of PVA and CS(30).

Aerogel as an insulating material

Usually an insulator is able to reduce heat transfer between two parts at different temperatures(5); aerogels possessing resistance to ageing, moisture(7), large surface areas and low thermal conductivity make them ideal materials for insulation(3). With the addition of nanofillers it is possible to improve the thermal and mechanical properties of an aerogel.

RATIONALE

Pollution in all its forms, from environmental to acoustic, is a serious problem today; however, thanks to materials science there is the possibility of developing and improving multifunctional composite materials in an environmentally sustainable way to be used to solve such problems. One of these innovative materials are aerogels, which are extremely light materials with high specific surface area, low thermal conductivity, but poor mechanical properties and high production costs, so their use is still limited; however, it is possible to improve their properties so that they can be used as multifunctional composites.

Due to these requirements, CS is chosen because it can be extracted from natural sources and therefore, in addition to its mechanical properties, it also provides an environmental component. While, PVA is chosen because of its high processability and thermal stability, as well as GO because of the functional groups present that are compatible with each other, achieving interaction between the substances.

In this sense, this work aims to improve the physicochemical properties of an aerogel, using GO as a reinforcing agent homogeneously dispersed in a matrix of CS and PVA polymeric materials, since previous research has shown the efficiency in the interaction between GO and CS, as well as GO and PVA to improve the mechanical properties; therefore, it is possible to use this combination to synthesise a multifunctional material that can be used as an insulator.

AIMS

Develop chitosan (CS) and polyvinyl alcohol (PVA) aerogel reinforced with graphene oxide (GO) like reinforcement to improve physico-chemical properties for a possible application as a multifunctional composite by freeze-drying synthesis.

OBJECTIVES

To perform the proposed aim, the following objectives are proposed:

- Synthesising graphene oxide (GO) by the modified Hummers method from graphite powder.
- Achieving a homogeneous solution of chitosan (CS).
- Make the homogeneous solution of polyvinyl alcohol (PVA).
- Realise homogeneous dispersion of GO in a solution with CS and PVA by stirring.
- Study the variation of the ratio of GO, PVA and CS in the formation of aerogels.
- Produce aerogel by unidirectional freeze-drying method (UFDM).
- Characterise the physicochemical properties of the generated aerogel.

2. LITERATURE REVIEW

The following chapter presents a description of the types of aerogels and their possible applications, highlighting why they are good as insulating materials, as well as the interactions that exist between the materials chosen to develop the synthesis of this material.

TYPES OF AEROGELS

According to IUPAC, aerogel is a “Gel comprised of a microporous solid in which the dispersed phase is a gas”. While S. S. Kistler, defined the aerogels as “jellies in which the liquid has been replaced by gas with limited or no shrinkage leaving behind a solid network”(34). R. Beatens, defines aerogels as the “solid structure of a gel insolate from its liquid medium”(35). S. Salimian et al., defined aerogels as porous materials in solid state consisting of a three-dimensional (3D) solid network with a large number of air-filled pores in the form of highly cross-linked structures; with unique properties such as extremely low density, large open pores and high surface area(36). A. Pierre and G. Pajonk, defined as, an aerogel is “a material that has a three-dimensionally interconnected open pore structure that is maintained after the liquid inside has been replaced by air”(36). Although different authors have their own interpretation of the meaning of an aerogel, they all agree that it is a highly porous structure, therefore with a large specific surface area, and ultra-light.

Aerogels can also be classified into different types like: organic, inorganic, hybrid and carbon.

Organic aerogels. Are those with a structure based on organic polymers, e.g., resorcinol-formaldehyde structures obtained by polycondensation in a basic medium; this classification also includes aerogels based on polysaccharides, which are derived from natural and renewable sources such as chitosan(34).

Inorganic aerogels. Are those formed with metal oxides, silica (SiO_2) are the most studied(34).

Hybrid aerogels. Are those that combine metal oxides with organic molecules, basically aerogels reinforced with nanoparticles(34).

Carbon aerogels. These come from biological origin that have been burned, they are mainly used as adsorbents and electrodes in electrical devices(34).

AEROGEL APPLICATIONS

Although there are several limitations due to cost of production, the different properties of aerogel make it ideal for a number of applications such as:

Medical devices. The properties of aerogels, such as porosity, permeability and biocompatibility, are ideal for applications in medicine as they can reply tissue structures, act as scaffolds for drug delivery, bone regeneration, wound healing and as implants for food tracking(34).

Packaging. The porous nature of aerogels (>90%) can be used to absorb moisture from biological compounds, thereby protecting packaged foods and extending their shelf life(34).

Particle detection. The aerogel was used in particle detectors and counters in space, as well as in accelerators and in balloon experiments in the upper atmosphere, due to the refractive indexes of solid aerogels, which, although fragile, are easy and safe to apply(37).

Biomedical research. Research has developed an aerogel material that possesses a moisturising property along with effective antibacterial, antioxidant and fluid-passing characteristics to aid diabetic wound healing(34).

Supercapacitors. A supercapacitor is an energy storage device based on voltage-induced charge separation at an electrolyte/solid interface. Because carbon aerogels are conductive aerogels, they are ideal for use as supercapacitors due to their large surface area and small pore size, as well as their interconnected structure(38),(37)

Oil and water separation. Aerogels are considered a very attractive adsorbent material due to their low density, large surface area, high porosity, higher adsorption capacity and good mechanical properties(39),(40).

Radiation detectors. A low density silica aerogel can be used in radiation detection vacuum tubes to support the high voltage cable because the aerogel provides both cable support and voltage separation, as its porosity allows ion transport after radiation ionisation events in the tube(37).

Optical applications. Translucent aerogels can be used for solar roofs and solar collectors, and transparent aerogels can be used for solar windows.(37)

Space applications. Lightweight silica aerogels are used as contaminant collectors to protect space mirrors from volatile organisms(37), and NASA has also used aerogel to insulate the Mars Pathfinder rover, which landed on Mars in July 1997.(38)

Thermal and acoustical insulation. Aerogels have the lowest thermal conductivity values of all solid or porous materials(1), which is a key property for insulation applications, e.g. for architectural purposes(37). While in the acoustic field, aerogels are used to adjust the acoustic impedance of ultrasonic devices to make them more efficient and to improve sound absorption(37).

AEROGEL INSULATOR

Aerogels are inert, non-toxic, environmentally friendly insulation materials(38), which, over time, becomes more relevant as production costs decrease due to research and development. The need for research on these materials is due to the fact that natural polymers are relatively cheap, readily available in our environment and can be used to produce biodegradable composites(28).

The thermal, and mechanical properties of the composite material improve with the use of fillers due to the reinforcement of hydrogen bonding between the -NH2 group of the matrix, for example with CS, and the -OH group of the filler(29) like fuctional groups of GO.

GO AND PVA INTERACTION

When GO suspensions and PVA solutions are mixed in water, as it is an ideal solvent for both PVA and GO(25), homogeneous mixtures can be obtained due to the hydrogen bonds(11) between the functional groups on the basal planes and edges of the GO with the PVA(32).

In the case of GO, due to the large number of hydrophilic groups on the surface, individual sheets can be dispersed in water(25); likewise, due to the presence of these groups on the surface, hydrogen bonds may form with the PVA molecule chains containing even more hydrophilic groups(25)(41), which could improve the interfacial adhesion(42) and charge transfer between GO with PVA and therefore the mechanical

performance of the resulting PVA/GO composite(25)(43). The interaction mechanism between GO and PVA is showing in Figure 1.

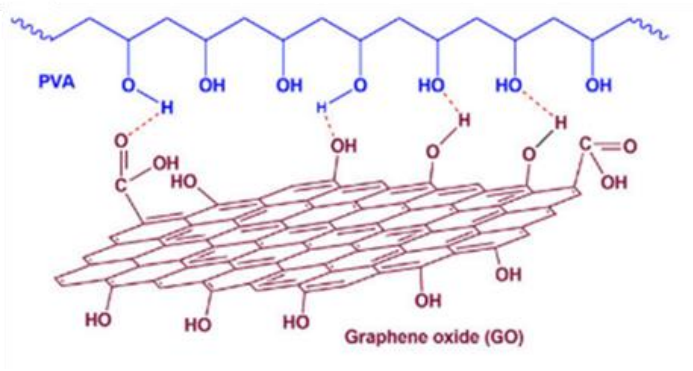

Figure 1. Interaction between GO and PVA (32)

CS AND PVA INTERACTION

The interactions of CS with PVA improve the mechanical and chemical properties(20) due the strong intermolecular hydrogen bonds between the CS and PVA(27) molecules, as well as weak molecular force interactions between the intramolecular structure of CS(44), as can be seen in Figure 2. Thus, through the aggregation of hydrophobic chains and the intermolecular and intramolecular hydrogen bonds(20)(44) of the mixture, ion exchange and electrostatic interactions(20) are achieved.

PVA and CS have hydroxyl groups(23) which improve miscibility in mixtures between them. However, the mixing behaviour of PVA with CS is related to the amount of PVA present. As these materials are partially miscible at the molecular level(23) and immiscible at high PVA concentrations (>50%); so miscibility can only occur at low PVA concentrations(44). Therefore, blends between PVA and CS could improve the properties of an aerogel.

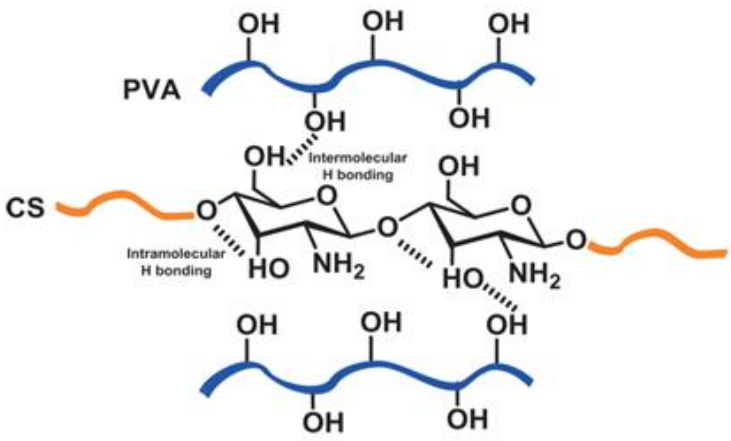

Figure 2. Interaction between PVA and CS (45)

CS AND GO INTERACTION

Due to its electronegativity, GO can easily interact with cationic polymers, such as CS(46). Since the interaction between CS and GO is enhanced by the hydrophilic nature of GO due the epoxy groups of GO react by addition with the primary amino groups of CS(47), which would facilitate its dispersion in aqueous CS solutions and simplifies the formation of composites(47).

Multiple hydrogen bonds can form between GO sheets and CS chains, increasing the bonding strength in a suspension blend. Therefore a cross-linking between CS and GO is possible due to their chemical structure by amino and epoxy groups, respectively(48). Thus CS is an efficient crosslinking reagent for GO(13), just as GO can reinforce natural polymers such as CS(46).

Studies such as those of Moradi et al. have shown that 1 wt.% GO loading can improve the tensile strength from 43.2 MPa of pure CS to 104.2 MPa(46); due the formation of covalent bonds in the crosslinking of GO-CS, as well as the effective load transfer between GO and CS(48), which comes from the good interfacial properties of the mixture(46) and increases with GO loading.

Others important consideration for the interaction of CS and GO is pH and temperature. Firstly, at low pH values, the amino groups of CS are protonated so that the GO sheets are stably dispersed due to electrostatic repulsion between them(49). At pH values above 6, aggregation of GO appears in the suspension, this may be due to the deprotonation effect and the electrostatic repulsion between sheets decreases(9), and

the electrostatic interaction between these two species is weakened. Second at elevated temperatures the epoxy groups of GO and the amino groups of CS react to generate a cross-linking reaction(48).

It follows from the above that the CS aerogel as a skeleton and GO as a reinforcing phase are able to form a composite; where the flexible GO sheets can interact with the CS closely and form a variety of combinations to ensure good mechanical compression performance and shape stability(50) as shows in Figure 3.

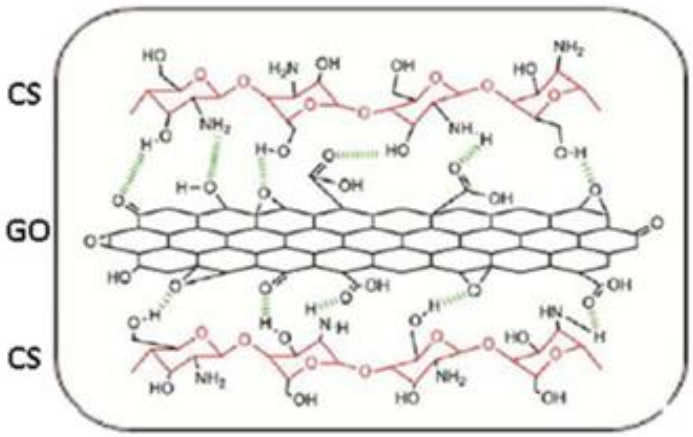

Figure 3. Interaction CS with GO (47)

CS AS MATRIX

For a stable base is required to be able to interact with reinforcements that improve both the mechanical and insulating properties of an aerogel, it is necessary to be compatible with substances that due to the available functional groups form a stronger structure. Also important is that the nanofiller is homogeneously dispersed in the polymer matrix and the interaction between the reinforcement and the matrix is strong(30). Therefore an excellent alternative are biopolymers that have more functional groups in their molecular chain and are able to form composites(34) and which are also environmentally friendly.

The structure of CS aerogels which can achieve up a high porosity up to ~97% has a great advantage in terms of mechanical toughness and flexibility(33), for the availability of amino groups to form electrostatic interactions with molecules such as GO and PVA to improve properties of a multifunctional composite such as the one investigated in

this work. So these aerogels have potential for use as insulators such as house windows, building glass walls(33) and many other applications.

GO AS FILLER

GO with oxygen functional groups on the basal planes and edges of graphene layers(32) can have a much lower Van der Waals interaction between its sheets and meet the desired characteristics of dispersibility and enhanced interfacial interaction with a polymer matrix through hydrogen bonding(32). It is also important to note that with a small addition of GO to the matrix it is possible to improve the thermal insulation and flame resistance(51). Therefore, by combining the mechanical properties and dispersibility of GO in a polymeric matrix, this filler is attractive for the production of nanocomposites(32).

A factor to be considered for the improvement of the composite properties is the interaction between the GO and the CS-PVA matrix(30), since the objective of GO loading is improve the mechanical strength, whereby with 2.5 wt.% GO loading it is possible to increase up to 60% in compressive strength, 152% in Young's modulus, and 69% in tensile strength(29).

The main reason for combining CS, PVA and GO into an aerogel is modification of the aerogel stability, thermal and insulating properties, as well as mechanical properties; with maintaining the existing positive properties such as high surface area, lightweight, density, porosity and thermal conductivity.

TYPES OF SYNTHESIS

The synthesis and drying methods by which aerogels are produced are listed below.

Sol–gel processes(35)**.** Described by Brinker and Scherer, the aerogel synthesis is divided into three steps, gel preparation, ageing, and drying. This is a process in which solid nanoparticles dispersed in a liquid agglomerate to form a continuous three-dimensional network that extends throughout the liquid. In the gel preparation the nanoparticles are grown directly in a liquid; while in the ageing the sol reaches the gel point, and finally in the drying the fluid is removed from the pores, the most critical step

in the production process as shrinkage and fracturing may occur due to the small pore size(35). A crucial step in ultra-light porous materials formation is the removal of the fluid within the gel without damaging the structure of the solid phase, the drying, as is critical to keep the morphology as much intact as possible. For this purpose, different methods have been developed.

- **Supercritical drying (SCD).** Refers to the liquid inside the pore being drawn out above the critical temperature and pressure to avoid capillary stress(35). The process is as follows: first, the aged gel is placed in an autoclave half-filled with the same solvent retained in the pores of the gel(35). The vessel is then sealed and slowly heated to above the critical temperature and pressure of the solvent. Secondly, the fluid is isothermally depressurised(35). Finally, at ambient pressure, the autoclave is cooled to room temperature(35).

- **Ambient pressure drying (APD).** Depends on the replacement of the original solvent used for gel formation by organic solvents with low surface tension(3). Is generally carried out in two steps: first, replacing the current solvent with a water-free solvent; secondly, drying which is carried out in three steps: after a heating period, the first drying period occurs, in which the volume loss of the gel balances that of the evaporated liquid; then in the second drying period, diffusive vapour transport occurs, allowing the liquid to slowly escape to the outside(35).

- **Freeze drying (FD).** The freeze-drying method uses sublimation of ice crystals in a high vacuum environment without destroying the matrix and forming the pore structure by ice crystal growth, thus preserving the pore structure obtained by the original ice crystal growth(52). The aerogel prepared by the freeze-drying technique has high porosity and good mechanical properties(52).

3. MAIN BODY

3.1 EXPERIMENTAL METHODOLOGY

The aim of this work is to prepare an aerogel of CS and PVA reinforced with GO by following the process described in the Figure 4:

- Synthesis of GO by the modified Hummers method
- Characterisation of GO
- Dissolution of CS
- Dissolution of PVA
- Preparation of CS, PVA and GO blends for aerogels
- Preparation of aerogel by freeze-drying method
- Characterisation of samples aerogel properties

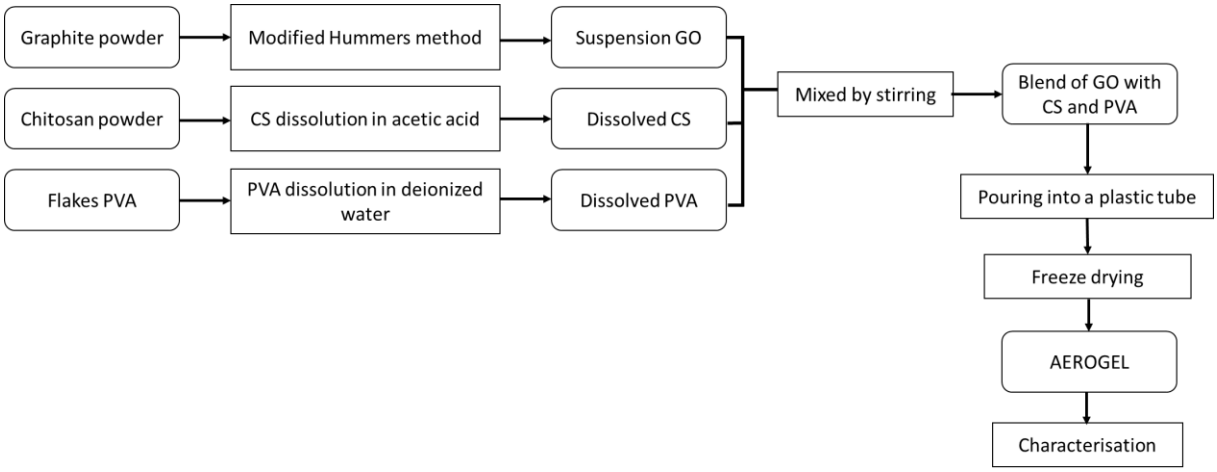

Figure 4. Experimental methodology

Using the following materials:

- GO synthesised in the laboratory under patent reg: MX-a-2018-014101
- CS powder by Sigma-Aldrich ≥75% (deacetylated)
- PVA powder (Mw 89,000-98,000, 99+% hydrolyzed)

3.1.1 GO SYNTHESIS

The graphite powder was oxidised by the modified Hummers method(15):

- A 3:1 mixture of concentrated sulphuric and nitric acid (H_2SO_2/HNO_3) was added to a mixture of graphite and potassium permanganate ($KMnO_4$), resulting in an exothermic reaction at around 40°C.
- The concentrated mixture was then heated to 85°C and stirred for 24 hours.
- Finally, the appropriate amount of water and peroxide (H_2O_2) was added to stop the reaction.
- After the air quenching process was completed, the mixture was purified by multiple washes until a neutral pH (7) was reached.

3.1.2 CS SOLUTION

To prepare a solution of CS at 1 %(w/v) in acetic acid at a concentration of 2.5 %(v/v) with stirring(13):

- Firstly 2.5 ml of acetic acid is dissolved in 100 ml of water at a temperature of 60°C,
- After that 1 g of CS is added
- Finally, the solution remains stirring at approximately 250 rpm by 1 hour until complete dissolution

3.1.3 PVA SOLUTION

For a homogeneous PVA solution of concentration 1%(w/v) the following steps were followed(53):

- 0.5 g of PVA powder was dissolved in 50 ml of water at 90°C
- keeping it under continuous stirring for 2-3 hours until complete dissolution

3.1.4 BLENDS

Once the GO, CS and PVA substances have been dissolved, certain quantities are taken for mixing. To obtain the aerogel it is possible to combine CS, PVA and GO by ultra-high shear mixing (IKA Ultra-Turrax T25) at 20.000 rpm for 5 minutes, to optimise the final porosity(11), and finally made freeze-dried for approximately 48 hours to obtain the material for characterisation.

The blends were made according to the Table 1, where it is indicated that the concentration of both CS and PVA is kept at 1% wt./v, while for GO it is 1 wt.%, taking different amounts in millilitres of these substances.

Table 1. Blends for freeze drying

Blends	CS (ml)	PVA (ml)	GO (ml)
A	4	2	4
B	1	3	6
C	5	2.5	2.5
D	2		8
E		2	8
F	8	2	
I	8		2

The process to form the aerogel is mainly in four steps described below:

1. In a flask on a bath on the heating plate at 70°C, depending on the blend, the substances are added, starting with the one with the highest ratio, while keeping it under magnetic stirring for 10 minutes.
2. To introduce bubbles to enhance aerogel formation, the blend is then ultra-high sheared with Ultra-Turrax T25 at 20,000 rpm for 5 minutes.
3. Finally, unidirectional freeze-drying(54) is carried out, so the blend is poured into a plastic tube, with the bottom surface exposed, and once filled, it is quickly immersed vertically in a container with liquid nitrogen for 5 minutes.
4. Then the solidified sample is freeze-dried for 48 hours under vacuum.

Finally, a porous foam is extracted from the tubes and stored in a dry place.

3.2 CHARACTERIZATIONS METHODS

To know and compare the characteristics of the synthesised material, different characterisation techniques are performed. Using the following equipment and methods.

3.2.1 X-RAY PHOTOELECTRON SPECTROSCOPY (XPS)

X-ray Photoelectron Spectroscopy (XPS) analysis of the sample was conducted using a XPS Escalab 250Xi (Thermofisher). With a monochromatic aluminium X-ray source (1486.68 eV, WF: 4.2eV) was used in the experiment. The binding energies were calibrated against C1s peak at 284.8 eV.

3.2.2 ATOMIC FORCE MICROSCOPY (AFM)

The sample topography was evaluated through Atomic Force Microscopy (AFM) observations. The standard AC-mode scanning was employed in an Asylum MFP 3D-SA AFM microscope. The GO samples were analysed after being centrifuged and deposited on a silicon nitride grid. Where Gwyddion software was used for data processing.

3.2.3 FOURIER TRANSFORM INFRARED SPECTROSCOPY (FTIR).

The Fourier Transform Infrared Spectroscopy (FTIR) was carried out on a spectrometer (Bruker Tensor 27 IR). The spectral range was 4000-400 cm^{-1} with a resolution of 4 cm^{-1}.

3.2.4 FIELD EMISSION SCANNING ELECTRON MICROSCOPY (FESEM).

The samples were gold-coated in a Gold Sputter Coating, and a Field Emission Scanning Electron Microscope (INSPECT F50, FEI) was used for the observation of the samples. The structural and morphological characterization of GO sheets was carried out using Field Emission Scanning Electron Microscopy system (FE-SEM) model Nova 200 (FEI Company) with a STEM detector.

3.2.5 BRUNAUER-EMMETT-TELLER (BET)

The specific surface area analysis was performed using Gemini VII 2390p equipment. The samples were analysed under nitrogen atmosphere (adsorption isotherms at 77 K) in a volumetric working device. The moisture content in the samples was removed by drying them at 200°C for 3 h prior to the analysis.

3.2.6 THERMOGRAVIMETRIC ANALYSIS (TGA)

The Thermogravimetric Analysis was performed on the TGA 5500 (TA instruments) thermogravimetric analyser. The samples of raw materials and the blends were carried out under a nitrogen atmosphere from 30°C to 600°C at a heating rate of 10°C/min.

3.2.7 DIFFERENTIAL SCANNING CALORIMETRY (DSC)

A Differential Scanning Calorimeter DSC25 (TA instruments) was used to study the curing behaviours of the blank materials and blends. The samples were carried out at 10°C/min from 40 up to 400°C. Experiments were performed below 400°C to prevent any possible degradation reactions inside the chamber.

3.3. RESULTS

To describe the relationship between the different materials that make up the blends, the following characterisations were made, both of the starting materials and of each of the blends that were tested. Firstly, are analysed the morphology, topography, functional groups present and the chemical structure of the raw material to be used, GO, CS and PVA. Next, for the different samples obtained to compare the influence of their components.

3.3.1. CHARACTERIZATION OF GO

3.3.1.1 STEM for GO

To determine the morphology of GO, a STEM analysis was first performed, as shown in imagens below.

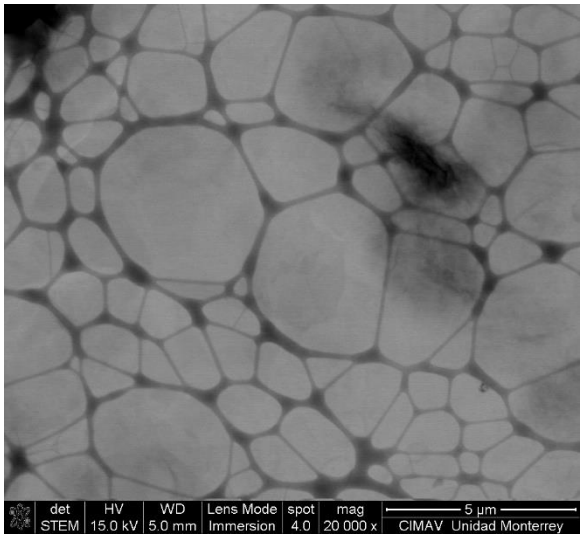

Figure 5. GO at 20,000x magnification

The Figure 5 shows a low contrast of the GO sheets because there are only a few layers stacked.

While in Figure 6, it's possible see the characteristic wrinkles and folds of GO, due to the force of interaction between the sheets. The thin sheets have a length of approximately 2 μm, there are previous reports where the length can reach 10μm (15).

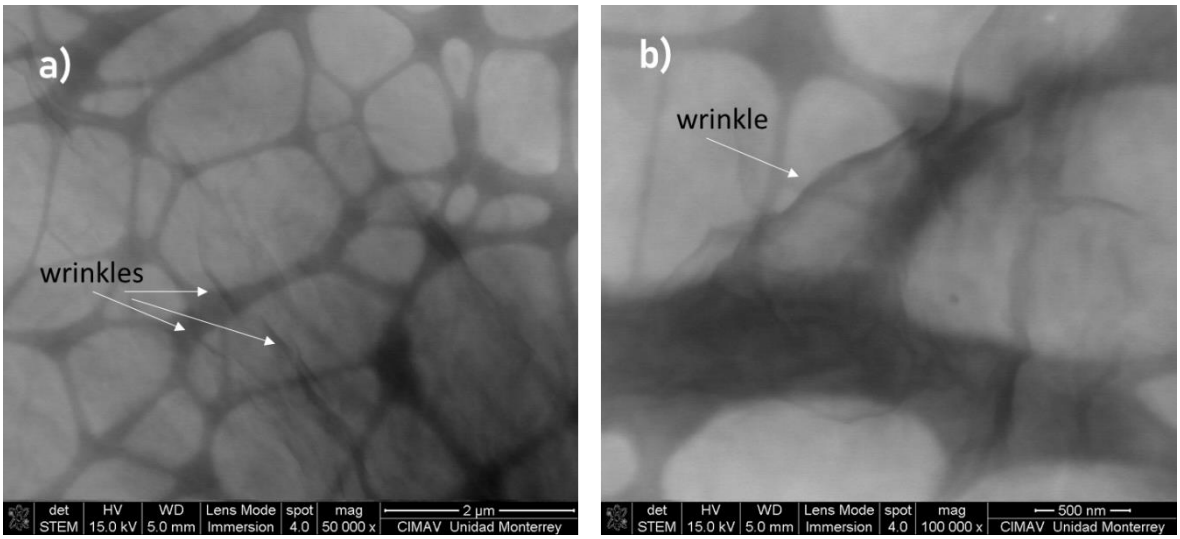

Figure 6. GO magnification: a) at 50,000x b) at 100,000x

The wrinkles in the micrographs are present due to the interaction of the functional groups on the surface of the GO, which causes increased attraction between the sheets. This is in agreement with the literature since, according to Rattana, T. *et al*.(55), GO consists of thin, crumpled and randomly aggregated sheets where surface wrinkles and folds are also observed. Also the literature points out that due to the sp^3 hybridization of the material, there is more interaction between the sheets which causes the wrinkles(56).

3.3.1.2. AFM for GO

The method to characterise morphology, roughness and thickness is AFM which is shown in the Figure 7. Where the morphology of the analysed samples and its thickness are shown.

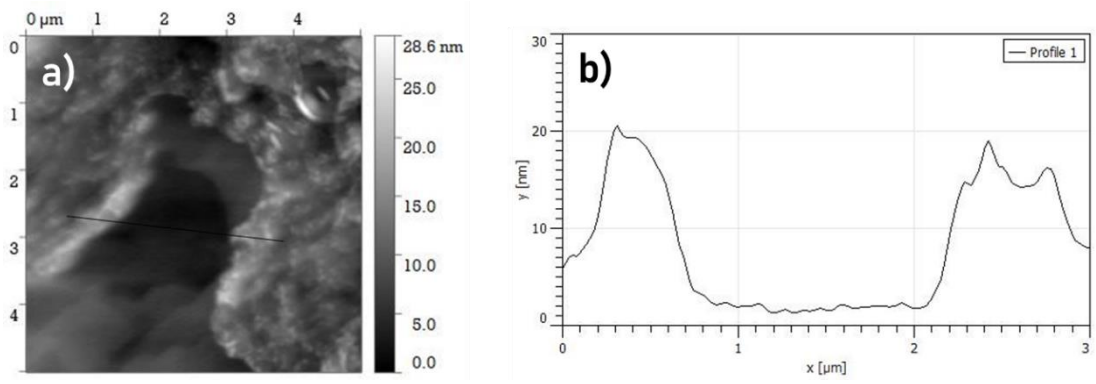

Figure 7. Analysis of GO roughness: a) surface, b) profile

The dimensions of the sample profile (Figure 7b) show that the thickness is approximately up to 20 nm indicating the presence of stacked layers of GO. According to previous research, Xiaoming Yang, *et. al*., describes the thickness of the GO sheets is 0.851 nm(57), however, due to the interaction of functional groups on the surface of GO sheets, these can be up to 1.2 nm high. In this way, the GO sheets are stacked approximately 16 times.

The thickness of the GO layers is due to the stacking of the sheets and the distance between them generated by the presence of the functional groups on the surface, which is why the surface of the material is rough due to the accumulation of layers.

3.3.1.3 XPS for GO

XPS analysis was performed to identify functional groups present in the samples, these XPS spectra in Figure 8 were deconvoluted for both carbon and oxygen bonding to study the chemical structure.

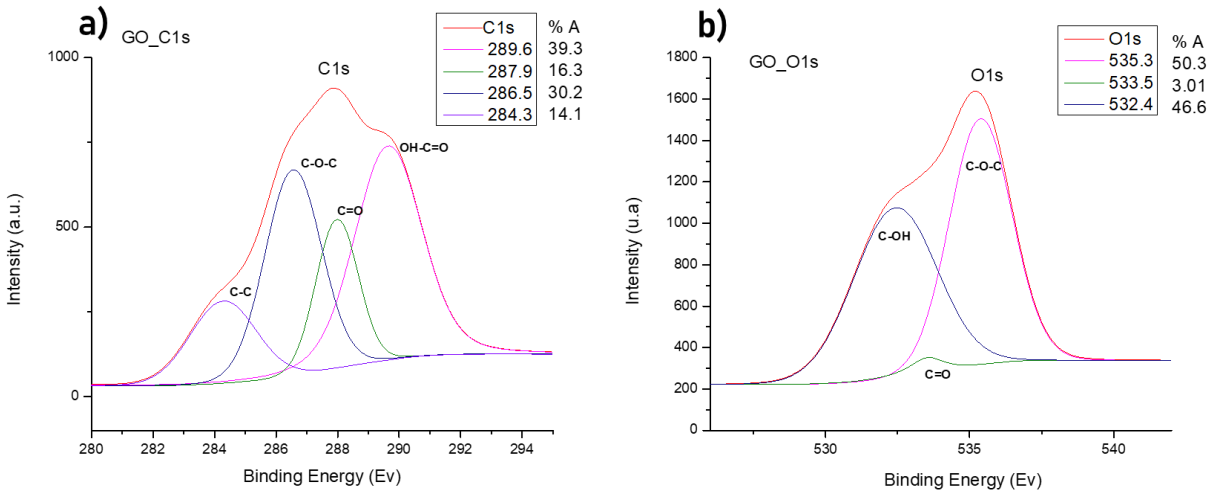

Figure 8. XPS spectrum of GO. a) XPS C1 spectrum of GO and b) XPS of GO O1 spectrum

In the XPS spectrums for C1s (Figure 8a) it is possible observe the presence of four peaks corresponding to carbon bonding, of which one corresponds to carbon-carbon bonds and the rest to carbon-oxygen bonds. The peak at 284.3 eV corresponds to the C-C bond where the energy corresponding to C sp^2 and C sp^3 is overlaps(58). The peak at 286.5 eV corresponds to interaction between C-O of the epoxy group (58),(59),(60). The peak with the energy of 287.9 eV corresponds to carbon double

bond oxygen (C=O) of the carbonyl group (58),(59). Finally the peak at 289.6 eV is due to carbon-oxygen bond of the carboxyl group (OH-C=O) (60).

While the XPS spectrum for O1s (Figure 8b) shows peaks corresponding to the oxygen groups found at the edges and on the surface of GO. The peak at 532.4 eV is due to carbon-oxygen bond of the hydroxy group (-OH) (58),(60) which have an area under the curve of 46.6%. The peak at 533.5 corresponding to carbon double bond oxygen of carbonyl groups (C=O) (60). Finally, the peak at 535.3 corresponding to carbon-oxygen interaction of epoxy group (C-O-C) (61) with an area under the curve of 50.3%. These results show a higher presence of both epoxy groups and hydroxyl groups, confirming the correct synthesis of GO.

3.3.1.4. FTIR for GO

The FTIR is used to characterize the presence of specific chemical groups in GO as show in Figure 9.

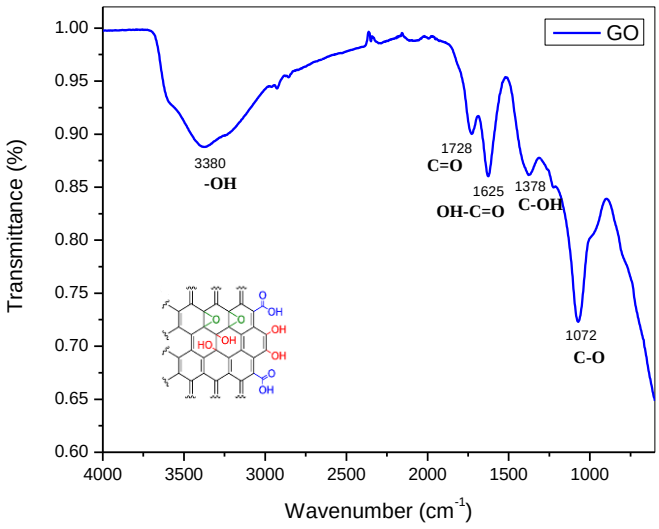

Figure 9. FTIR spectrum of GO

FTIR spectrum of GO shown a broadband at 3380 cm^{-1} is ascribed to O-H stretching, from the hydroxyl functional groups on the surface and edges. The peak at 1728 cm^{-1} is assigned to C=O asymmetric stretching while the peak at 1625 cm^{-1} is due the symmetric stretching and peak at 1378 cm^{-1} are ascribing C=O of carboxyl groups. Finally the bands at 1072 cm^{-1} are ascribing C-O stretching of epoxy groups. (60) (9).

In summary bands related to the hydroxyl (-OH), epoxy (C-O-C), and carboxyl (OH-C=O) functional groups that are present on the surface and at the edges of the GO are observed. These results correlate with XPS results, suggesting the existence of the

mentioned groups. Therefore, these functional groups are key to improve the interaction with the other materials that will form the blend of the aerogel.

3.3.1.5 SEM for GO

On the Figure 10 SEM is used to examine the morphology of GO foam formed by freeze-drying.

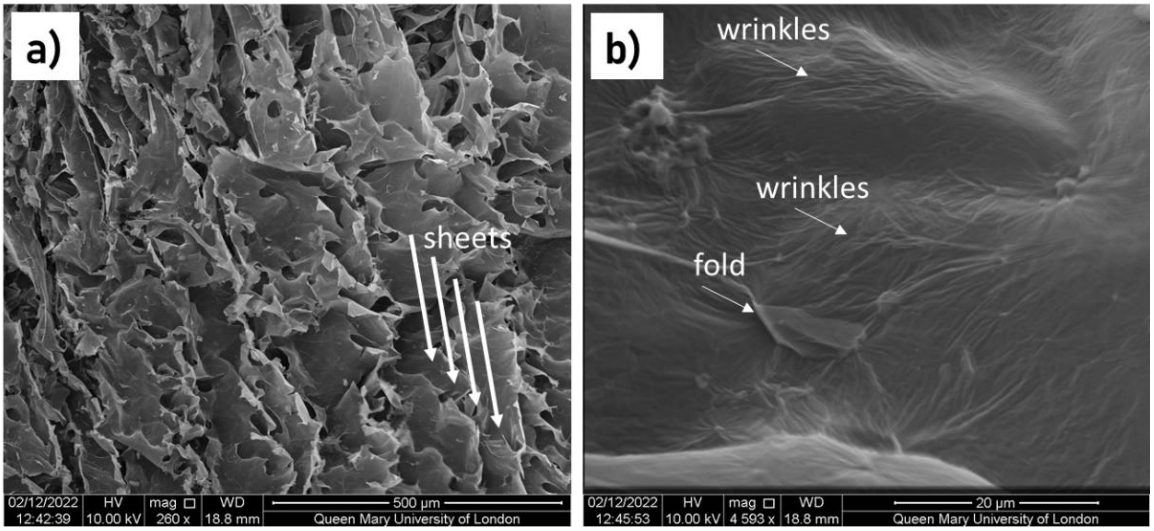

Figure 10. GO micrographs (a) at 260x magnification, (b) at 4600x magnifications

GO foam shows smooth, wrinkled, and folded regions due to functional groups adhering to and modifying the surface. The roughness on the surface of the GO sheets can be seen, as well as the arrangement that occurs between them after freezing in one direction only, which can be seen in the Figure 10a with the sheets stacked in one direction. In addition, the specific surface area was determined by BET method resulting in 328.8942 m^2/g.

3.3.1.6 TGA for GO

This analysis thermogravimetric shows the main weight losses of the GO with respect to temperature (Figure 11), which is caused by different events.

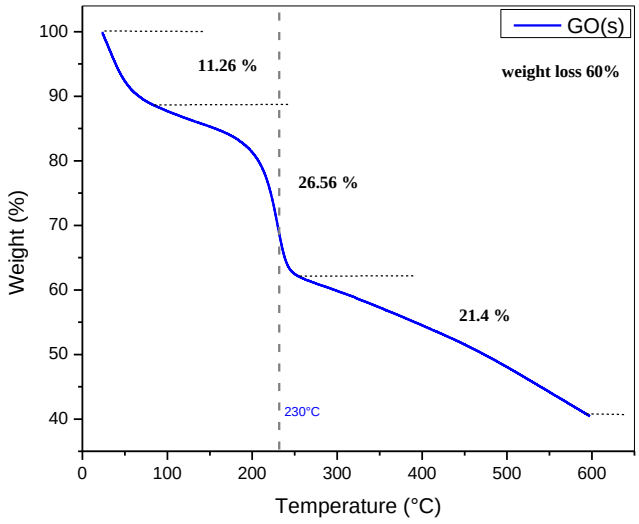

Figure 11. TGA curve for GO

In the first step, there is a weight loss of 11.26% due to moisture inside the polymer (adsorbed water) (62). At the second step, the main weight loss, is 26.5% resulting decomposition of oxygen functional groups (63), with the highest point at 230°C, where the decomposition of GO begins. Finally, in the third and last step, the weight loss is about 21.4% after the 250°C which is due to the transformation and elimination of epoxy groups and the whole degradation of the sheets of GO (63). Resulting in a total loss of approximately 60%.

3.3.1.7 DSC for GO

The DSC shows the behaviour of GO foam to evaluate the thermal properties in the Figure 12.

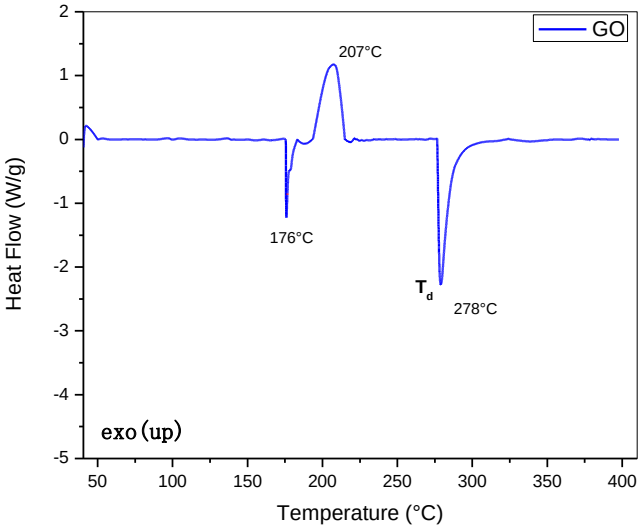

Figure 12. DSC curves of GO

According to some references, there should be only one endothermic peak in the GO samples due to humidity, which is usually present at temperatures below 100°C (64). However, there are also two endothermic peaks. The first one appears at 176°C due to moisture while the second one at 278°C, is due to the decomposition of GO nanosheets. While the exothermic peak at 207°C is the due transformation of epoxy groups in the surface of GO at CO and CO_2 (64).

3.3.2 CHARACTERIZATION OF CS

3.3.2.1 FTIR for CS

The FTIR is used to characterize the presence of specific chemical groups in CS, Figure 13, to evaluate possible interactions with other materials.

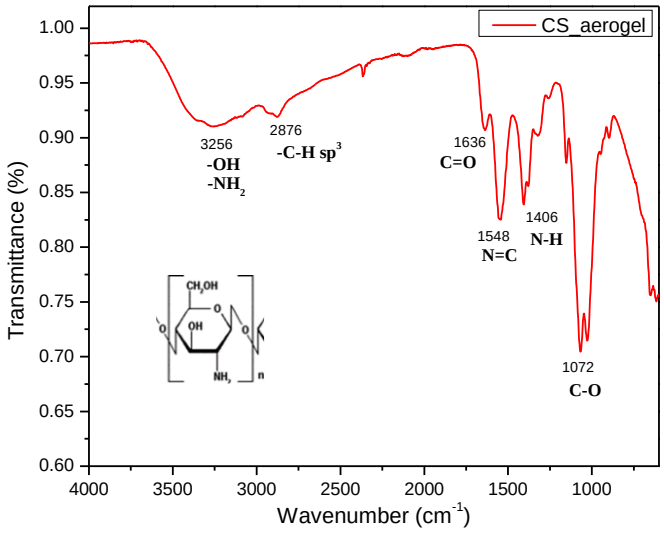

Figure 13. FTIR spectra of CS

FTIR spectrum of CS shown a broadband at 3256 cm^{-1} is ascribed to O-H and $–NH_2$ stretching (65), bands at 2876 cm^{-1} are assigned to C-H of sp^3 stretching (33), the peak at 1636 cm^{-1} are ascribing C=O stretching (33), the peaks at 1548 cm^{-1} and 1406 cm^{-1} are assigned to N-C and N-H stretching by amino groups in the structure (63)(66), and the bands at 1072 cm^{-1} are assigned C-O stretching (63). Therefore, this groups present in CS are important for the formation of hydrogen bonds.

3.3.2.2 SEM for CS

The SEM is used to examined the morphology and porosity of CS foam formed by freeze-drying which is shown in the figures below.

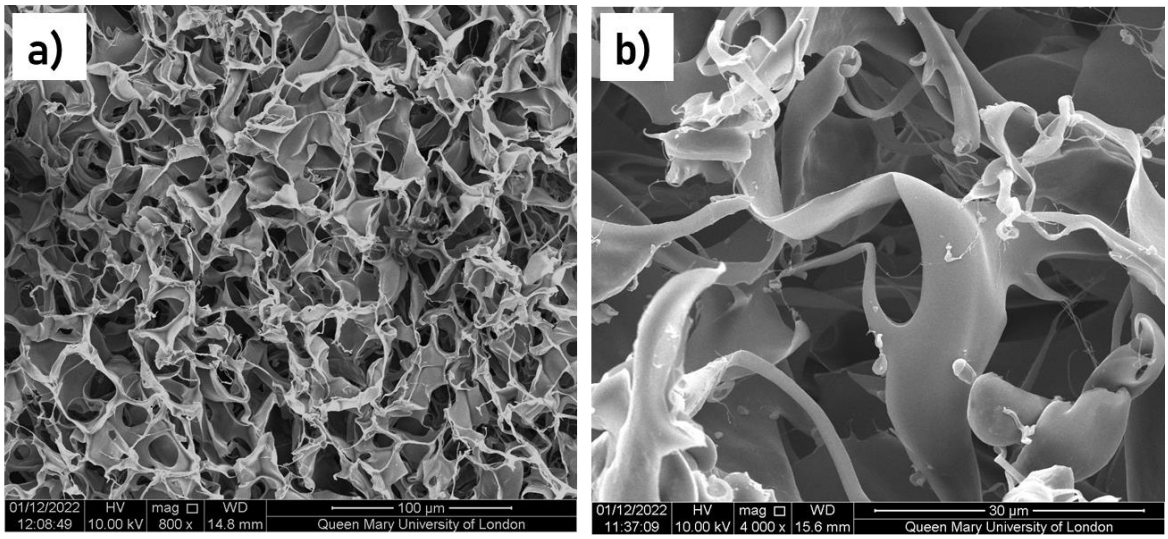

Figure 14. SEM for CS at magnification a) 100μm b) 30μm

The Figure 14 present different magnifications of CS foam, in the first one (a) at 100 μm and the second one (b) at 30 μm where it's possible to observe the porous network formed during freeze-drying, which has small cavities formed by the sublimation of ice crystals within the aerogel structure. The average size of these pores is around 10 μm extending over the surface of the material.

3.3.2.3 BET for CS

The method developed by Brunauer, Emmett and Teller (BET) is used to characterise the surface of a solid, based on gas adsorption on the surface, so in this case is possible to evaluate the surface area of CS foam in diagram of the Figure 15.

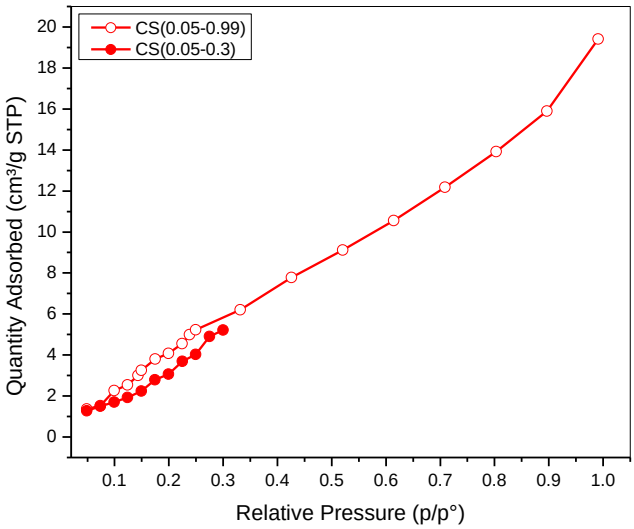

Figure 15. BET for CS

For this analysis, first was measured the density of the CS foam sample, which was 0.87 g/cm^3. An isotherm with slight curves was obtained, so it is possible to deduce that it is a type II isotherm, related to macroporous materials, was obtained, with a surface area of 11.2003 m²/g.

3.3.2.4 TGA for CS

This analysis thermogravimetric shows the main weight losses of the CS with respect to temperature, which is caused by different events shows in Figure 16.

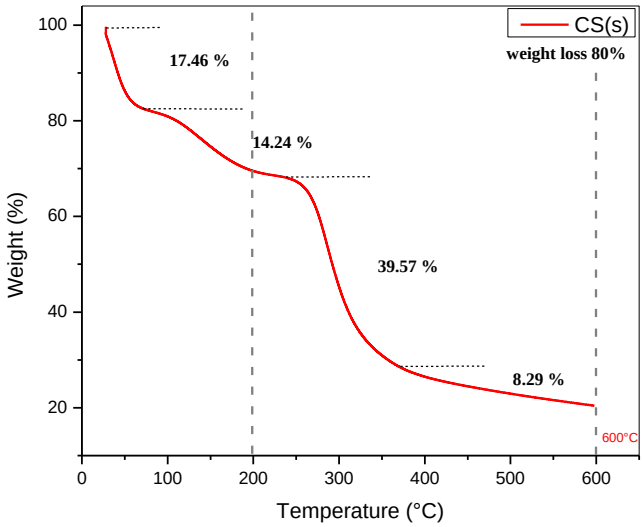

Figure 16. TGA for CS

The diagram shows in the first step, there is a weight loss of 17.46% due to the loss of water (67). Then a two-step degradation occurs, with the main weight loss approx. 54%; firstly, loss of remaining water occurred, followed by degradation of the CS (68)(63). In the last step, the weight loss is about 8.3% after the 350°C which indicates the decomposition of CS, which is complete after 600°C (33)(67).

3.3.2.5 DSC for CS

Figure 17 shows a DSC diagram of the behaviour of CS foam to evaluate the thermal properties.

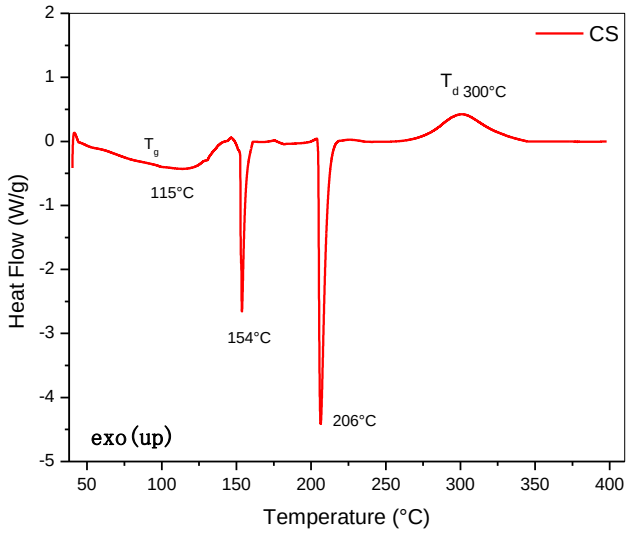

Figure 17.. DSC for CS

References by authors such as Arifin B. *et al.* (66), Zuñiga Rodriguez TD. *et al.* (67) show only two peaks for CS, one endothermic and one exothermic, at approximately 115°C and 300°C, attributed to dehydration and polymer decomposition. However, this sample of CS has an endothermic peak of around 115°C is attributed to the evaporation of water; another peak, this time an exothermic peak, is around 300°C is due to CS degradation. In addition to these two characteristic peaks of CS, there are two other endothermic peaks present, which can be attributed to by-products present in CS, which are found at 154°C and 206°C respectively.

3.3.3 CHARACTERIZATION OF PVA

3.3.5.1 FTIR for PVA

The FTIR in Figure 18 is used to characterize the presence of specific chemical groups in PVA.

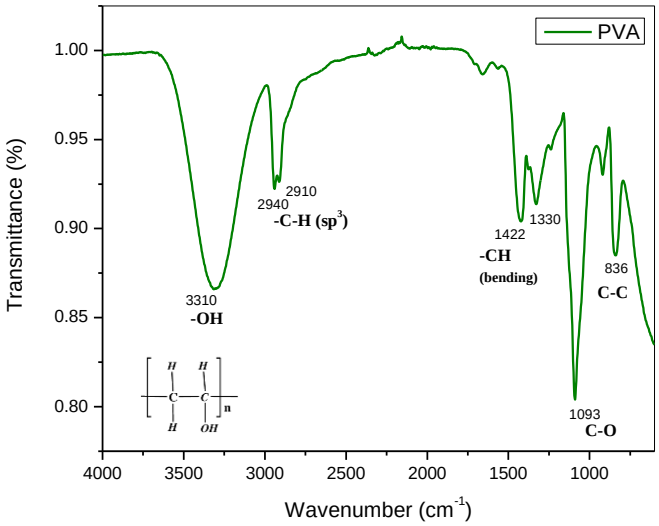

Figure 18. FTIR for PVA

This spectre show a broadband at 3310 cm^{-1} is ascribed to O-H stretching (69). Peaks at 2940 cm^{-1} and 2910 cm^{-1} are assigned to C-H of sp^3 asymmetric and symmetric stretching (69). Peak at 1422 cm^{-1} are ascribing –CH bending (70). The peak at 1093 cm^{-1} is characteristic of C-O stretching (70), and the peak at 836 cm^{-1} is ascribing C-C stretching (69).

3.3.3.2 SEM for PVA

The SEM is used to examine the morphology of freeze-dried PVA foam shown in Figure 19.

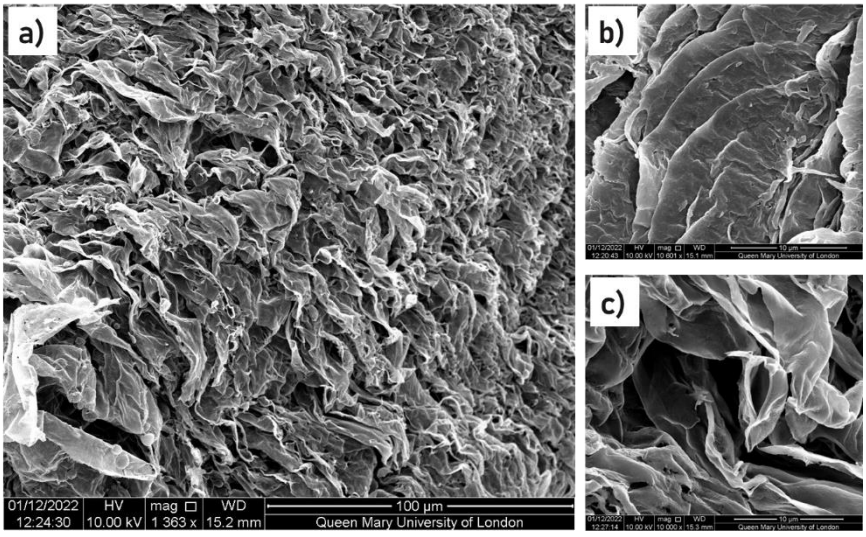

Figure 19. PVA micrographs at different magnifications a) at 100 µm, b) at 10 µm c) at 10 µm

The micrographs at magnification 100 µm (a) and 10 µm (b,c), show that the material is very stacked, with distances of less than 2 µm between the PVA layers. As well as a very rough surface of the material. This stacking is the reason for the fragility of the

material once it has been freeze-dried, as it is not possible to handle it without it breaking.

3.3.3.3 TGA for PVA

This TGA shows the main weight losses of the PVA with respect to temperature, which is caused by different events show below.

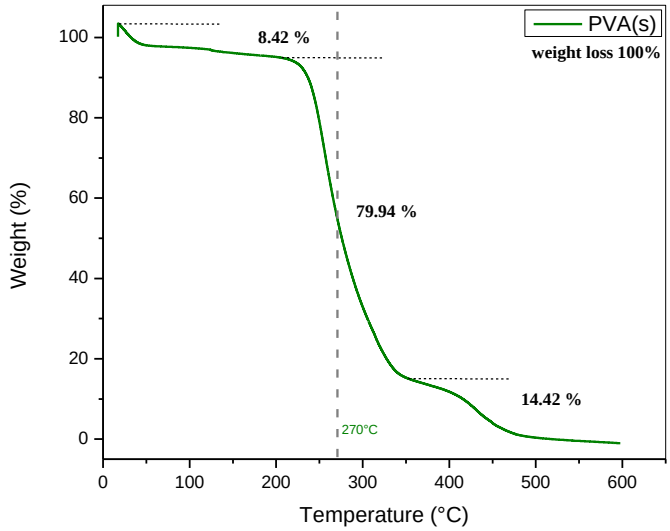

Figure 20. TGA for PVA

Figure 20 shows the degradation of the material in three main steps, characteristic of PVA (32)(41). First, there is a weight loss about of 8.4% due to absorbed water and the decomposition of oxygen groups (32). The largest PVA weight loss occurs in the second region due to the degradation of the PVA chain with approx. 80% of the total weight (32)(67), with 270°C like the temperature of maximum degradation of the PVA (41). Finally in the last step, the weight loss is approx. 12% for the complete decomposition of PVA (32).

3.3.3.4 DSC for PVA

The DSC shows the behaviour of PVA foam (Figure 21) to evaluate the thermal properties.

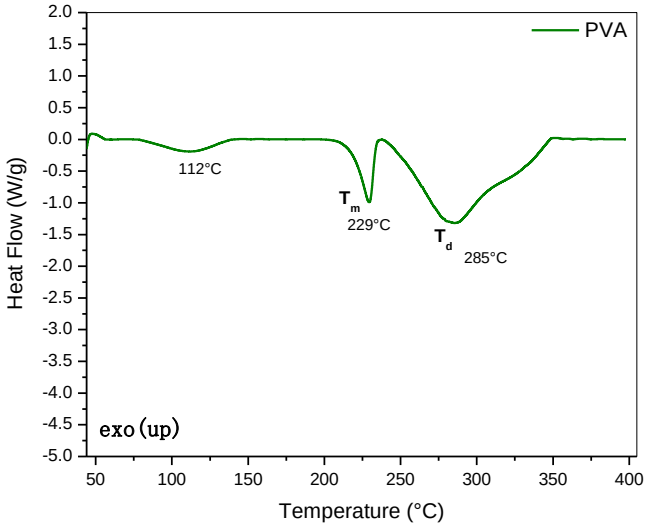

Figure 21. DSC for PVA

The diagram has three endothermic peaks, the first is a change in the baseline at 110°C is due to dehydration (41). The second one at 229°C, an endothermic peak, appears due melting point of PVA (67). Finally, the decomposition of PVA appears approx. at 285°C in the last endothermic peak (67).

3.3.4 BLENDS

Different combinations of CS (1 %w/v), PVA (1 %w/v), and GO (1 wt.%) were made to identify the interaction between them and then optimize this composition to obtain a stable aerogel, some of the blends are shown below.

3.3.4.1 BLEND A

This blend is composed of GO, PVA and CS in a 4:2:4 ratio respectively, as show in Table 2, with the intention to observe the behaviour of the components by keeping GO and CS in the same ratio and in a higher quantity than PVA.

Table 2. Composition of blend A

Blends	CS (ml)	PVA (ml)	GO (ml)
A	4	2	4

3.3.4.1.1 FTIR for A

The FTIR is used to characterize the behaviour and presence of functional groups after combining GO with CS and adding a smaller proportion of PVA. Since similar functional groups exist in these materials, in Figure 22 it is possible to observe the presence of the principal functional groups of both GO and CS.

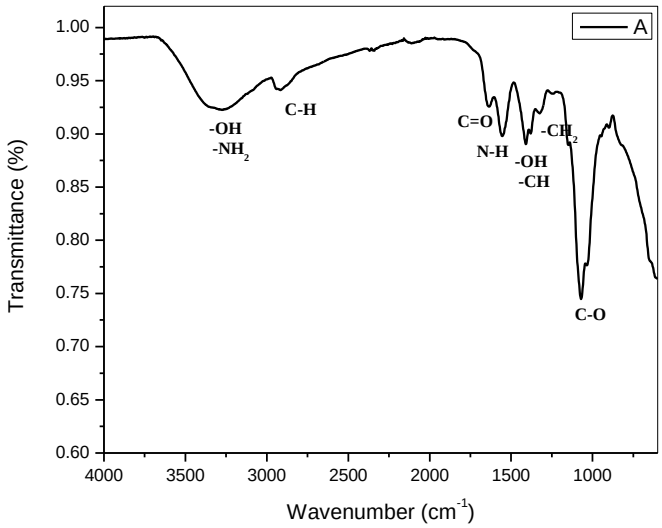

Figure 22. FTIR spectrum for blend A

The spectrum show a broadband absorbed at 3300 cm^{-1} was ascribed to O–H stretching of GO as well to NH_2 of CS, indicating different oxygen and amide containing functional group (9). While, the bands at 1644, 1560, 1409, 1312, and 1070 cm^{-1} were assigned to C-H bending, C=O stretching, N-H stretching, C–OH stretching, C–O–C stretching, and C–O stretching (epoxy) vibrations, respectively (30). Finally the bands at 2912 cm^{-1} were attributed to –CH stretching vibrations (9).

There is a similarity between this analysis and that of CS, so it is possible to deduce that the influence of CS is very strong in the blend, with the difference that there is a decrease in the intensity of the peaks corresponding to the interaction of the amide group for blend A compared to CS. In addition, the characteristic absorption bands of the oxygen groups decrease significantly compared to those of PVA and GO.

3.3.4.1.2 SEM for A

The SEM is used to examined the morphology and porous size of foam formed by freeze-drying in Figure 23.

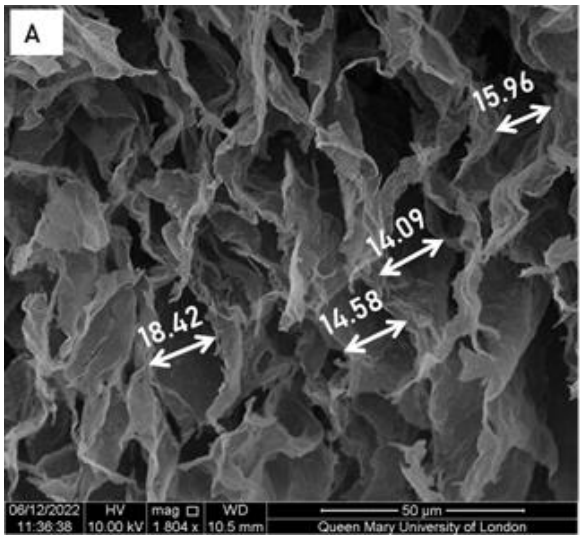

Figure 23. SEM for blend A at 50μm

The micrograph at 50 μm of the foam of blend A, shows the surface looks like sheets interacting with each other forming porosity in the material. The size of these pores formed by the crossing of the sheets appears to be under 20 μm.

3.3.4.1.3 BET for A

The method developed by Brunauer, Emmett and Teller (BET) is used to characterize the surface of a solid, in this case is possible to evaluate the surface area of this foam in Figure 24.

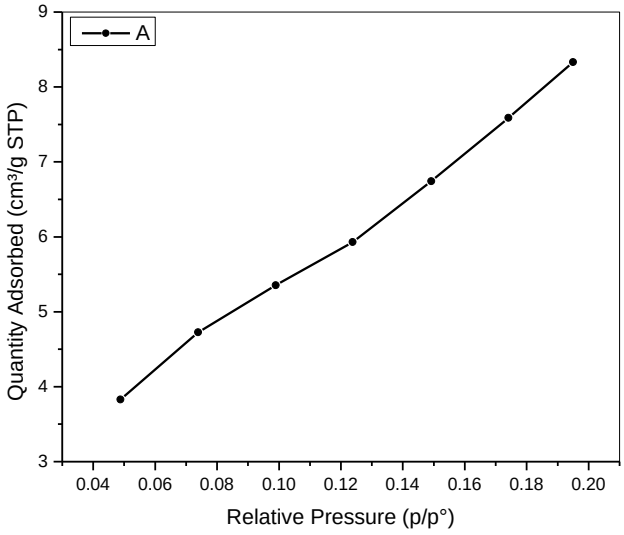

Figure 24. BET for blend A

Firstly, the measured density for this sample was 0.5537 g/cm^3. Then, with this information the BET surface area analysis was 37.1173 m²/g. In addition, the isotherm

obtained is type III, with constant adsorption, which corresponds to a macroporous material, confirmed by the micrographs above.

3.3.4.1.4 TGA for A

This TGA shows the main weight losses of the blend with respect to temperature (Figure 25), which the intention of observing how the mixture ratio influences the behavior.

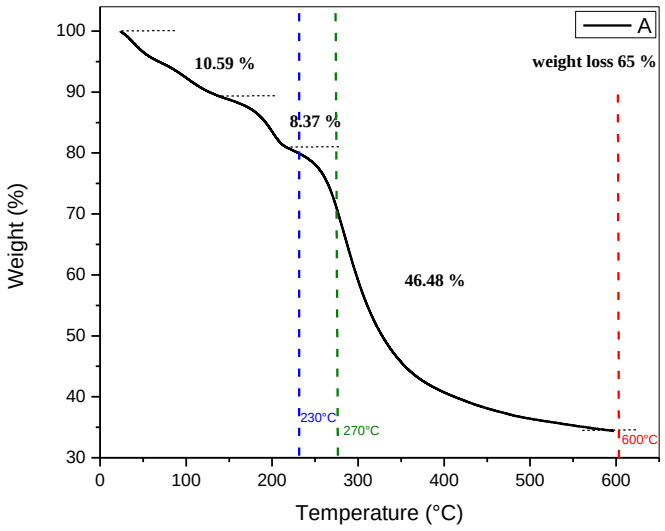

Figure 25. TGA for blend A

In the first step, there is a weight loss of 10.59% due to the loss of water, at temperatures below 100°C (63). Then a small degradation step occurs, the weight loss is about 8.37% due loss of remaining water and the degradation of the GO, between 150°C and 230°C (62). Finally in the last step, the main weight loss occurs, with 46.5%; after the 250°C which indicates the decomposition of CS, and continues to be completed after 600°C (33)(67).

3.3.4.1.5 DSC for A

The DSC shows the behaviour of foam made it in different rations of CS, PVA and GO to evaluate the thermal properties in Figure 26.

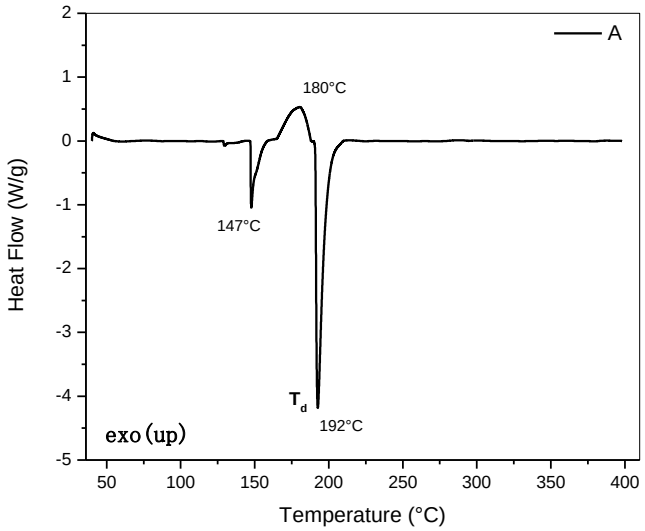

Figure 26. DSC for blend A

The graph is composed of two very large and sharp endothermic peaks and one exothermic peak. The behavior of graphic is similar to GO (Figure 12) with the second peak bigger, at the same time the behavior of the two endothermic peaks is similar to CS (Figure 17), which is logical since the largest amount of this blend is GO with CS with PVA being in smaller proportion.

The endothermic peak at 147°C is due to dehydration displaced from the common values due to the presence of functional groups that forming hydrogen bonds between PVA, CS and GO (71). The exothermic peak at 180°C could be due to the transformation of the epoxy groups of GO (72). Finally, the last one, it´s an endothermic peak at 192°C, due melting point of CS but with a shift to lower temperature (67).

3.3.4.2 BLEND B

This blend is composed of GO, PVA and CS of a 6:3:1 ratio respectively, Table 3, with the intention of observing the behaviour of GO with the addition of PVA and CS in lower proportions.

Table 3. Composition of blend B

Blends	CS (ml)	PVA (ml)	GO (ml)
B	1	3	6

3.3.4.2.1 FTIR for B

The FTIR is used to characterize the behaviour and presence of functional groups after combining GO with PVA and adding a smaller proportion of CS in the Figure 27.

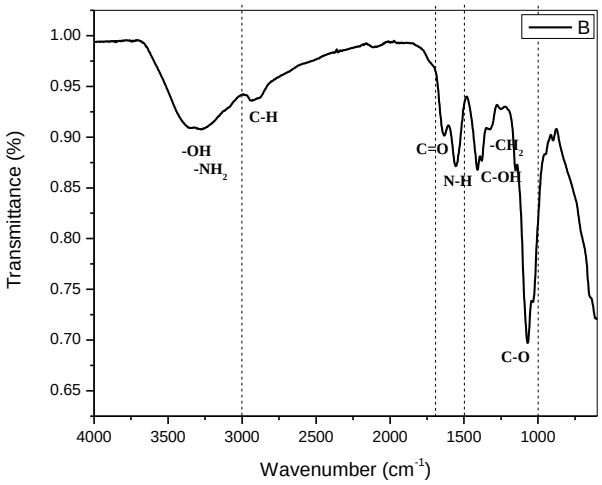

Figure 27. FTIR spectrum for blend B

The presence of the functional groups of GO, PVA and CS is observed. The spectrum shows a broadband ~3200 cm^{-1} is ascribed to O-H and $–NH_2$ stretching (63). The bands at 2932 cm^{-1} are assigned to C-H of sp^3 stretching (65)(68). The peaks at 1630 cm^{-1} are ascribing C=O stretching, and at 1555 cm^{-1} are assigned N-H stretching of the amide group of CS (57)(73). Finally the peaks at 1395 cm^{-1} for C-OH stretching, peak at 1319 cm^{-1} for C-H bending, and the bands at 1076 cm^{-1} are assigned C-O stretching (69).

3.3.4.2.2 SEM for B

The SEM in Figure 28 is used to examined the morphology and porous size of foam formed by freeze-drying.

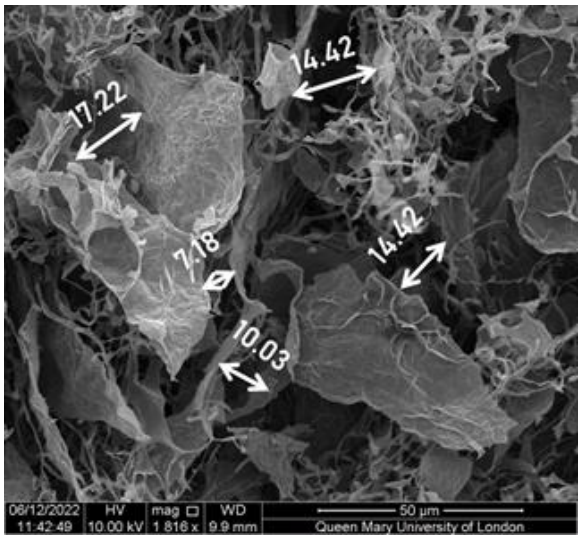

Figure 28. Micrography for blend B at 50μ

The imagen shows thin layers interacting with each other in disorder, forming tangled areas, where the size of gaps between the layers can be as large as 20 μm.

3.3.4.2.3 BET for B

The BET method is used to characterize the surface of a solid, based on gas adsorption on the surface, to evaluate the surface area of this foam see Figure 29.

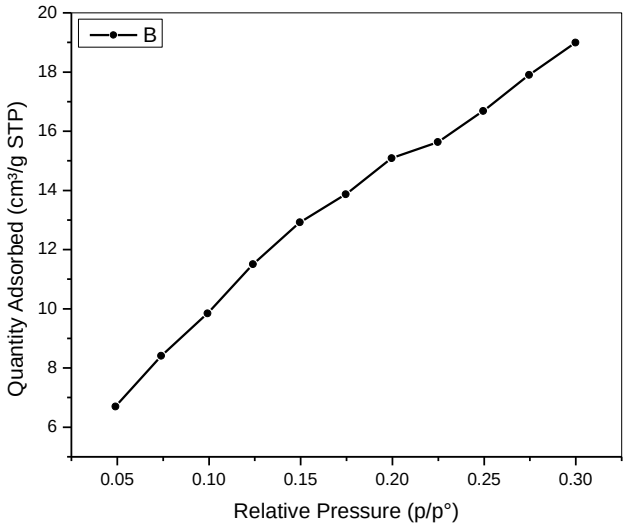

Figure 29. BET for blend B

The measured density for this sample was 0.1879 g/cm^3. While the analysis showed a BET surface area of 68.1355 m²/g. This isotherm looks like a type II isotherm, which is typical of a macroporous material, so the gape size is >50nm, which is consistent with the micrographs shown above.

3.3.4.2.4 TGA for B

This TGA (Figure 30) shows the main weight losses of the blend with respect to temperature, which the intention of observing how the components ratio of the blends influences the behavior.

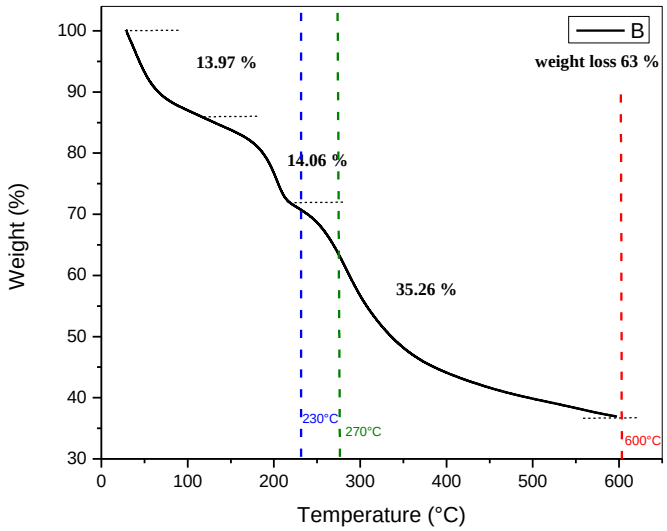

Figure 30. TGA for blend B

The diagram shows in the first step, there is a weight loss of 13.97% due to adsorbed water inside the polymer (62). The second step, weight loss is ~14% resulting detachment of oxygen functional groups, due to the decomposition of GO (62). In the third and last step, the weight loss is about 35.2% after the 230°C which is due to the transformation and elimination of epoxy groups and the degradation of the sheets of GO (63).

3.3.4.2.5 DSC for B

The DSC in Figure 31 shows the behaviour of foam made it in different rations of CS, PVA and GO to evaluate the thermal properties.

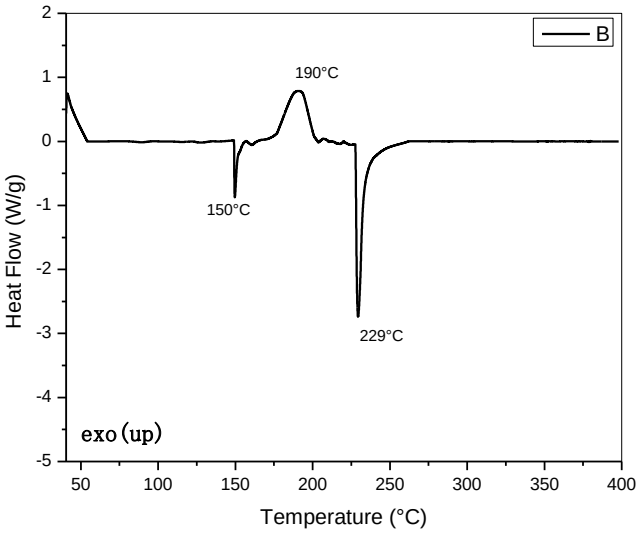

Figure 31. DSC for blend B

In general, the behavior of this blend is like that of GO alone (Figure 12), however, it is displaced at lower temperatures and this could be due to the decomposition temperature of the other two materials, mainly PVA (41), which in this case is more abundant than CS.

The endothermic peak at 150°C is due to dehydration (67). The exothermic peak at 190°C could be due to the transformation of the epoxy groups of GO (64). The endothermic peak at 229°C, could be due to the melting point of the PVA polymer (41), although this peak and in general the graph has a behaviour like that of GO (Figure 12); however, these values show the influence of the other components in the blend.

3.3.4.3 BLEND C

This blend is composed by a ratio of PVA and GO in the same proportion while the CS is at the double ratio, Table 4, this with the intention of observing the behaviour of the CS acting as a matrix with the addition of PVA and GO.

Table 4. Composition of blend C

Blends	CS (ml)	PVA (ml)	GO (ml)
C	5	2.5	2.5

3.3.4.3.1 FTIR for C

The FTIR is used to characterize the behaviour and presence of functional groups after combining PVA with GO on CS, as shown in Figure 32. FTIR spectrum for blend C

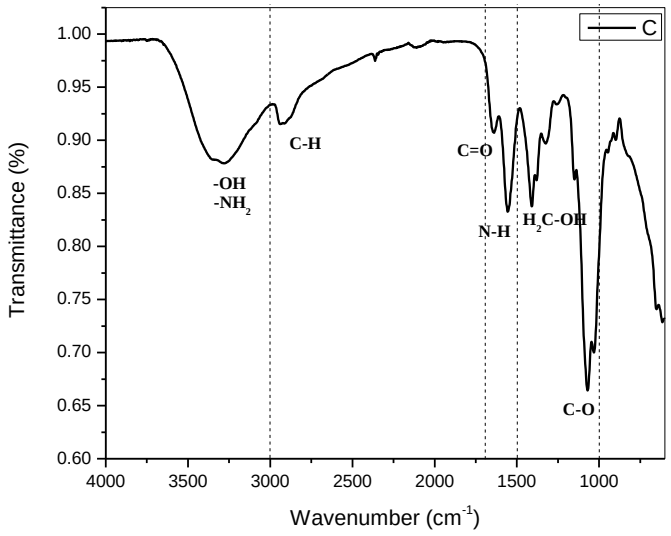

Figure 32. FTIR spectrum for blend C

The spectrum shows a broadband at ~3300 cm^{-1} that is ascribed to O-H and $–NH_2$ stretching (70). The bands at 2926 cm^{-1} are assigned to C-H of sp^3 stretching (9), and the peak at 1637 cm^{-1} are ascribing C=O stretching (9). Peak at 1555 cm^{-1} is due N-H stretching (30), peak at 1409 cm^{-1} are assigned C-OH stretching (30), and the peak at 1319 cm^{-1} are assigned C-H bending (30). Finally the bands at 1069 cm^{-1} are assigned C-O stretching (41).

3.3.4.3.2 SEM for C

The SEM is used to examined the morphology, porous size and interlayer spaces of foam formed by freeze-drying in Figure 33.

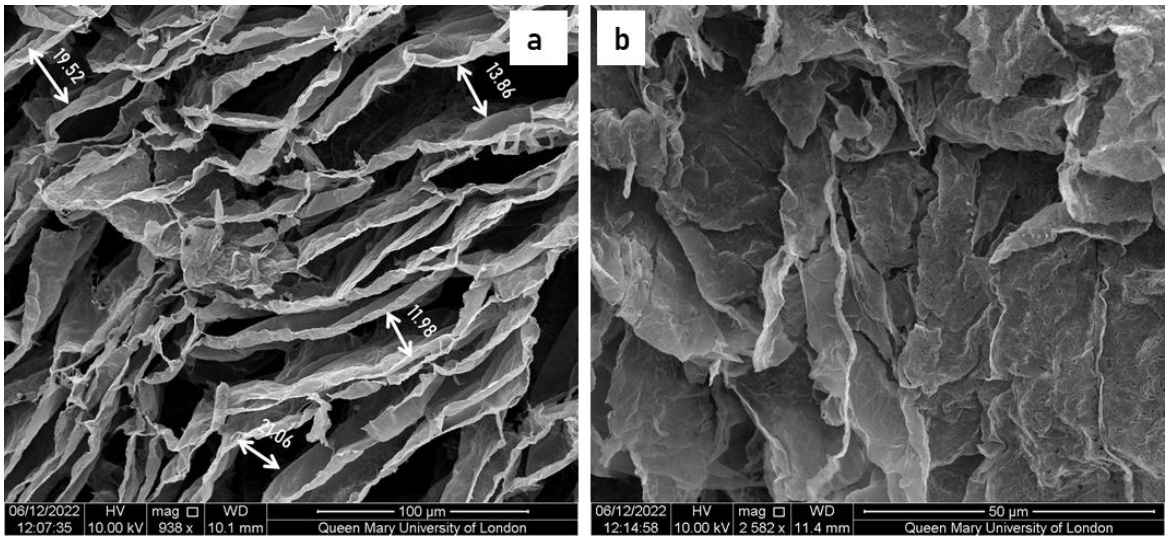

Figure 33. SEM for blend C at different magnification a) 100 µm b) 50µm

In the micrograph of blend C, at magnification of 100 μm and 50 μm, it is possible to observe the gaps between the layers that form during freeze-drying by sublimation of water inside of the sample, as well as the difference between the sample surface and the lower layers. The gaps between the layers are 10 and 40 μm. However, the layers resulting from freeze-drying show roughness and pilling which is easy to observe in the b micrograph.

3.3.4.3.3 BET for C

The BET method is used to characterize the surface of a solid, based on gas adsorption on the surface, so in Figure 34 is possible to evaluate the surface area of this foam.

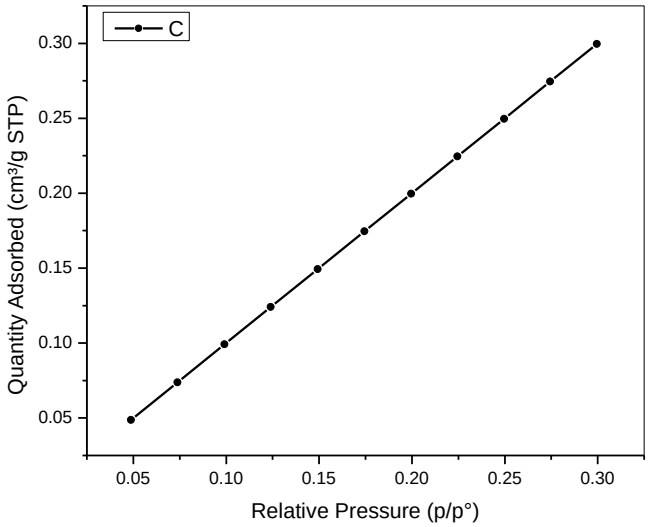

Figure 34. BET for blend C

The measured density for this sample was 0.6317 g/cm^3. While the analysis showed a BET surface area of 22.2599 m²/g.

The isotherm has a linear behavior, where the volume of adsorbed gas is directly proportional to the pressure, so it has the behavior of a type III isotherm; which is typical of a macroporous material, so the pore size is >50 nm, which is consistent with the micrographs shown above.

3.3.4.3.4 TGA for C

This TGA (Figure 35) shows the main weight losses of the blend with respect to temperature, which the intention of observing how the components ratio of the blends influences the behavior.

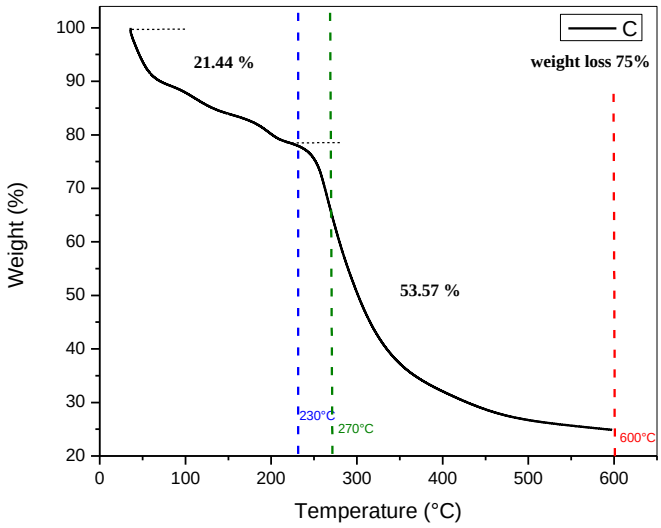

Figure 35. TGA for blend C

The diagram shows two main weight losses in the sample, for a total of 75%. In the first step, there is a weight loss of 21.44% due to moisture inside the polymer (33). In the second step, the weight loss is 53.57% resulting detachment of oxygen functional groups, which indicates the decomposition of chitosan approx. 300°C (63).

3.3.4.3.5 DSC for C

The DSC shows the behaviour of foam made it in different rations of CS with PVA and GO to evaluate the thermal properties in Figure 36.

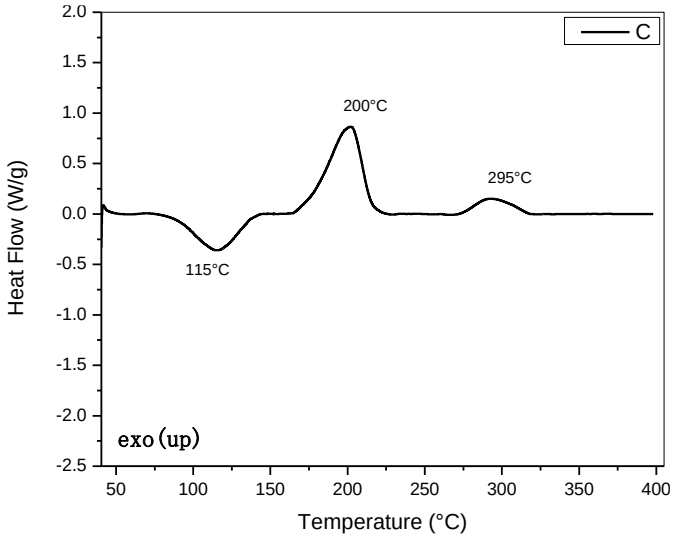

Figure 36. DSC for blend C

This graphic has three peaks, the first one is an endothermic peak at 115°C due to the moisture (67)(72). The second one is an exothermic peak at 200°C appears due transformation of epoxy groups (72), and the last one is an exothermic peak at 295°C due to the decomposition of CS chains (67).

The influence of the three components of the blend is noticeable as the values of the peaks coincide, for example, although the first endothermic peak is due to the loss of humidity in the sample (72), this value is very similar to that of CS, which is the most abundant element in this blend, as well as to that of PVA (67); also, the first exothermic peak has similar values to the exothermic peak of GO (72)(64), and finally, the last exothermic peak is similar to the CS decomposition peak (67).

3.3.4.4 BLEND D

This blend is composed of a ratio of GO to CS with the GO being maintained in greater quantity (Table 5), with the intention of observing the influence of CS on GO.

Table 5. Composition of blend D

Blends	CS (ml)	PVA (ml)	GO (ml)
D	2	0	8

3.3.4.4.1 FTIR for D

The FTIR in Figure 37 is used to characterize the behaviour and presence of functional groups after combining CS on GO.

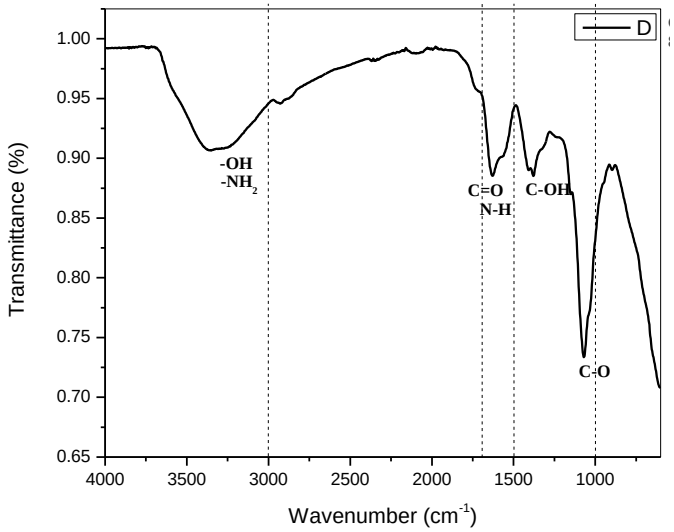

Figure 37. FTIR spectrum for blend D

The spectrum shows a broadband at ~3320 cm^{-1} is ascribed to O-H and $–NH_2$ stretching (70). Peak at 1630 cm^{-1} is ascribing C=O stretching and the peak at 1585 cm^{-1} is assigned N-H stretching of the amide functional groups present in the CS (73).

The peak at 1388 cm^{-1} is assigned C-OH stretching, peak at 1319 cm^{-1} is assigned C-H bending and the bands at 1069 cm^{-1} are assigned C-O stretching.

3.3.4.4.2 SEM for D

The SEM is used to examined the morphology and porous size of foam formed by freeze-drying, as shown in Figure 38.

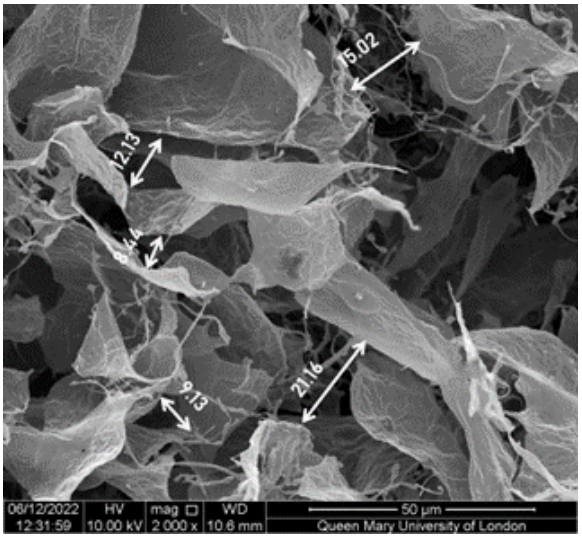

Figure 38. SEM for blend D at 50 μm

The micrography shows that there are very large leaves are observed crisscrossed but not stacked, with approximate size of 50 μm and forming non-uniform spaces between them of 10-20 μm.

3.3.4.4.3 BET for D

The BET method is used to characterize the surface of a solid, in Figure 39 is evaluate the surface area of this foam.

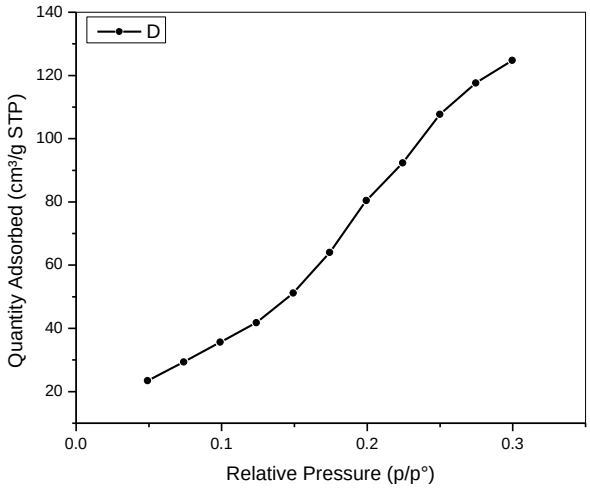

Figure 39. BET for blend D

The measured density for this sample was 1.0629 g/cm^3. While the analysis of the isotherm shows high gas absorption at low relative pressures, which corresponds to a type I isotherm for microporous materials, it also showed a BET surface area of 822.3278 m²/g, which is a large surface area that also indicates the presence of a microporous material.

3.3.4.4.4 TGA for D

This analysis thermogravimetric shows the main weight losses of the blend with respect to temperature, with the intention of observing how the components of the blends influences the behavior in Figure 40.

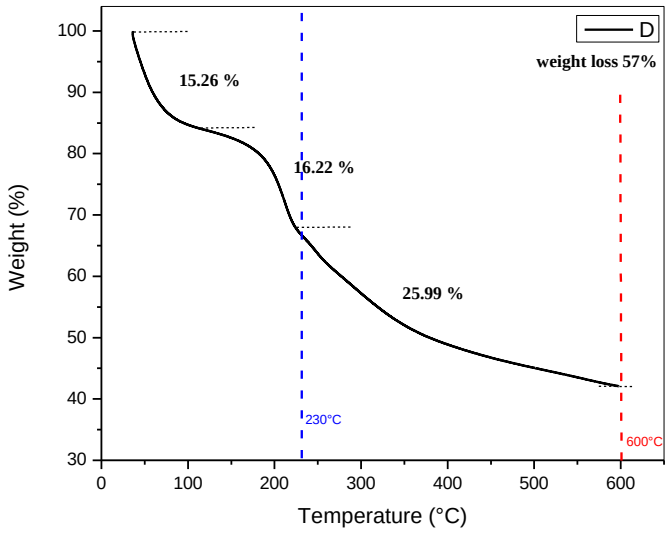

Figure 40. TGA for blend D

There are three main weight losses in the material, for a total of 57%. In the first step, there is a weight loss of 15.26% due to moisture inside the polymer at a temperature below 100°C (67). The second step, the weight loss is 16.22% resulting decomposition of oxygen functional groups (72), with the highest point at 230°C, where the principal decomposition of GO occurs. Finally in the third and last step, the weight loss is about ~26% after the 230°C which is due to the transformation and elimination of stable epoxy groups of sheets GO and the degradation of the CS (72).

3.3.4.4.5 DSC for D

The DSC shows the behaviour of foam made of CS on GO to evaluate the thermal properties in Figure 41.

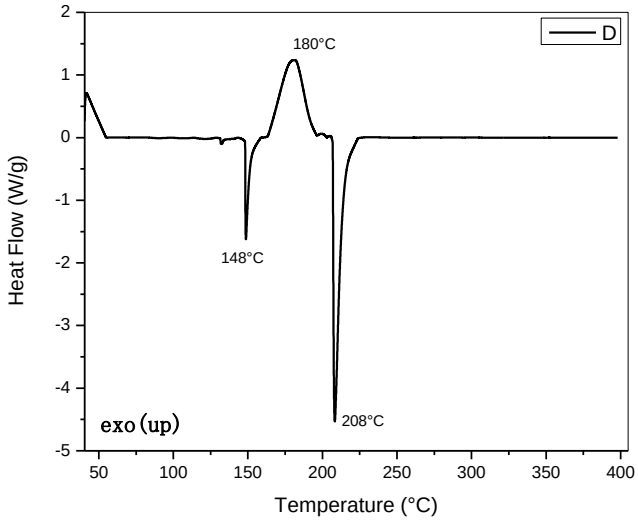

Figure 41. DSC for blend D

This graphic show three peaks, very similar to the GO graphic (Figure 12). The exothermic peak at 180° looks like the peak of GO at a lower temperature, so that means that this peak is due to the evaporation and transformation of oxygen groups of GO (62). While the two endothermic peaks at 148°C and 208°C look like the peaks of the CS (68) with a little difference in the temperature of the first peak, due to the interaction of the functional groups of both the GO and the CS.

3.3.4.5 BLEND E

This blend is composed of a ratio of GO to PVA, with a higher proportion of GO (Table 6), with the intention of observing how PVA influences GO.

Table 6. Composition of blend E

Blends	CS (ml)	PVA (ml)	GO (ml)
E	0	2	8

3.3.4.5.1 FTIR for E

The FTIR is used to characterize the behaviour and presence of functional groups after combining GO with PVA as shown in Figure 42.

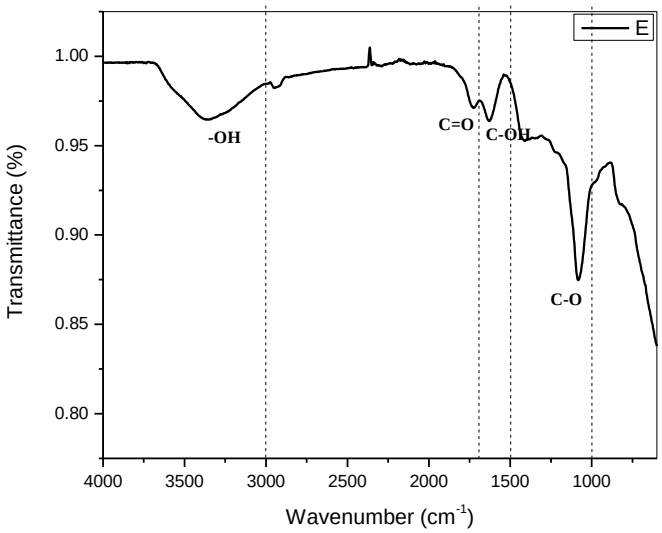

Figure 42. FTIR spectrum for blend E

The spectrum shows a broadband ~3375 cm^{-1} is ascribed to O-H stretching (69)(74). The peaks at 1728 cm^{-1} and 1630 cm^{-1} are ascribing C=O stretching and C-OH stretching respectively of the carboxyl group (55). Peak at 1430 cm^{-1} is assigned C-H bending, and bands at 1083 cm^{-1} are assigned C-O stretching (64).

Only the main peaks for the hydroxyl, epoxy and carboxyl functional groups are observed, as this blend contains only GO and PVA. However, the decrease of the intensity of the -OH band in the composite is noticeable, which confirms the formation of hydrogen bonds between GO and PVA (32).

3.3.4.5.2 SEM for E

The SEM is used to examined the morphology and porous size of foam formed by freeze-drying, as show in Figure 43.

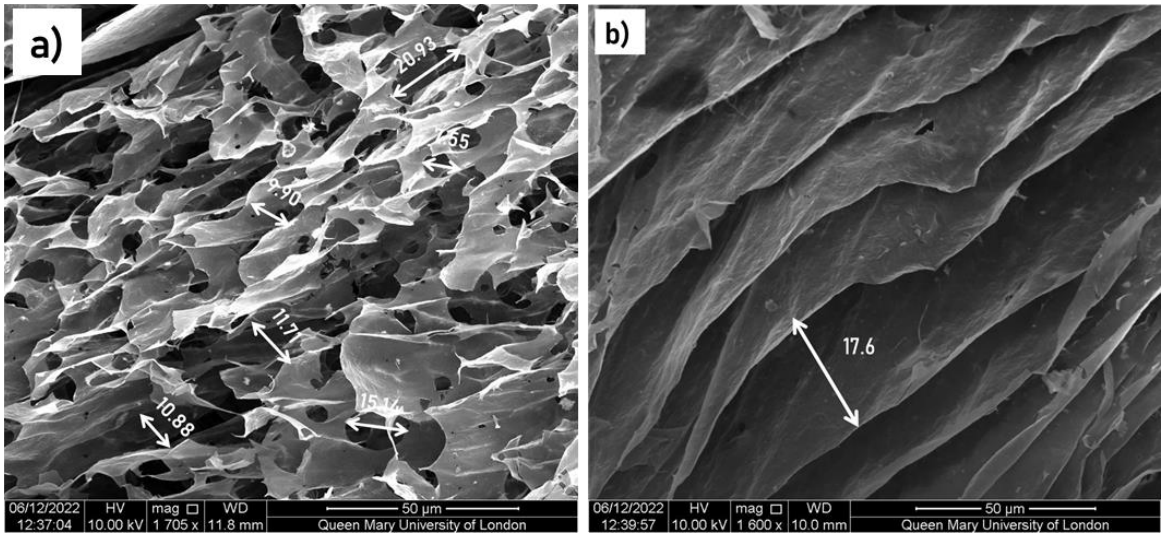

Figure 43. SEM for blend E at 50μm

Is observed the micrograph at 50 μm of two different areas, in which it can be seen that the surface is not uniform as in some areas. In Figure 43a the layers are closer together and with pores on their surface with a size of less than 10 μm; while in other areas (Figure 43b) the layers are very well stacked with spaces between them lower of 20 μm.

3.3.4.5.3 BET for E

The BET method is used to characterize the surface of a solid, in Figure 44 is evaluate the surface area of this foam.

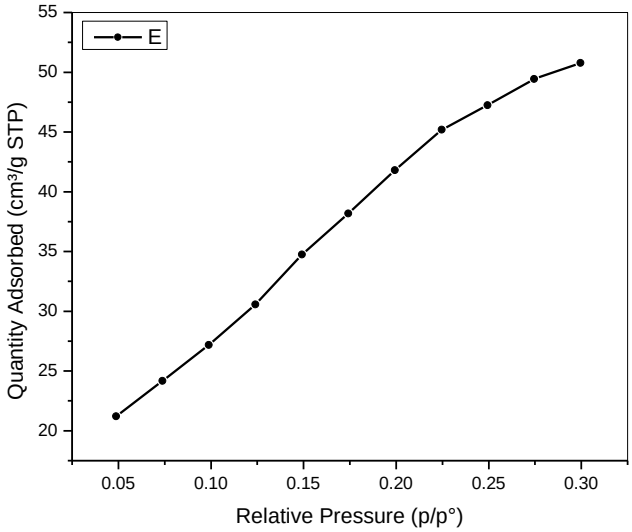

Figure 44. BET for blend E

The measured density for this sample was 0.0185 g/cm^3. While the isotherm shows a behaviour corresponding to a type II isotherm for macroporous materials, it also

showed a BET surface area of 183.4799 m²/g, which is a large surface area that also indicates the presence of a small porous material. These two characteristics, both low density and high surface area, are ideal characteristics of an aerogel.

3.3.4.5.4 TGA for E

The TGA (Figure 45) shows the three main weight losses of the blend with respect to temperature, with the intention of observing how components the blends influence the behavior.

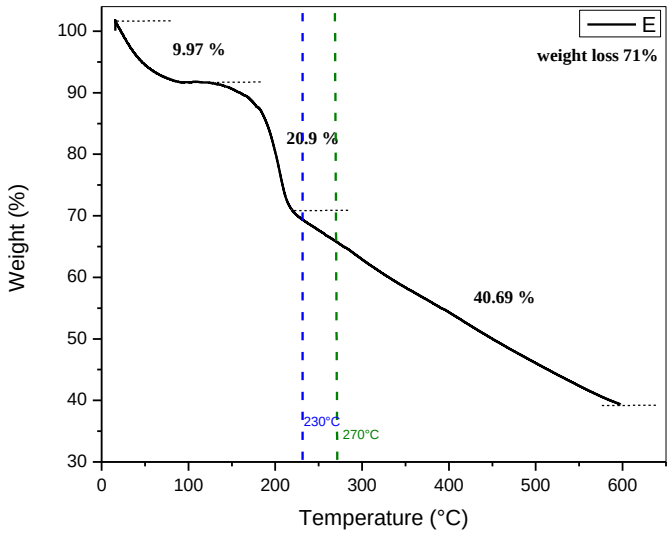

Figure 45. TGA for blend E

In the first step, there is a weight loss of ~10% due to moisture inside the blend (62).The second step between 120-230°C, is ~21%, due to the transformation of oxygen functional groups of GO(72). In the third and last step, the weight loss is about 40.7% after the 230°C which is due to the transformation and elimination of epoxy groups and the whole degradation of the sheets of GO (41,62).

3.3.4.5.5 DSC for E

The DSC shows the behaviour of foam made with a higher proportion of GO plus PVA to evaluate the thermal properties in Figure 46.

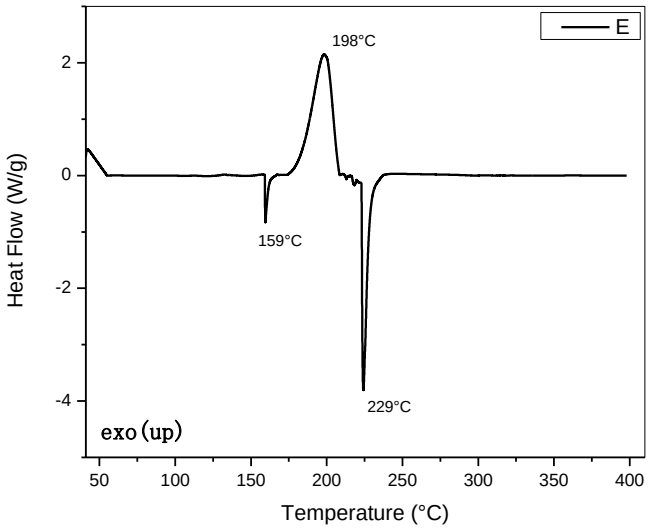

Figure 46. DSC for blend E

This graphic show three peaks, very similar to the GO graphic (Figure 12) (64). The exothermic peak at 198° looks like the peak of GO at a lower temperature, so that means that this peak is due to the transformation of oxygen groups of GO (72). While the two endothermic peaks at 159°C and 229°C look like the peaks of the GO with the difference that are shifted at a lower temperature which could be due to the amount of PVA in the blend (41). Since the melting point of PVA is ~229°C (41), which proves the shift of the second endothermic peak.

Contrary to the interaction of CS with GO, this interaction with PVA shifts the endothermic peaks which cause water loss and decomposition in the sample at higher temperatures, but not to the same scale as the original GO.

3.3.4.6 BLEND I

This blend is composed of a ratio of CS to GO with a higher proportion of CS (Table 7), with the intention of observing the influence of GO on CS.

Table 7. Composition of blend I

Blends	CS (ml)	PVA (ml)	GO (ml)
I	8	0	2

3.3.4.6.1 FTIR for I

In the Figure 47 the FTIR is used to characterize the behaviour and presence of functional groups after combining GO with CS.

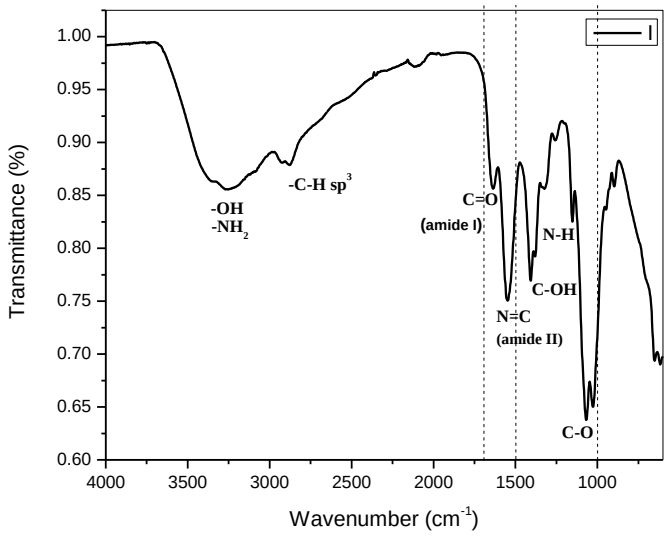

Figure 47. FTIR spectrum for blend I

The interaction of the functional groups of both GO and CS is observed. The peaks of spectra of blend I, shows a broadband ~3272 cm^{-1} is ascribed to O-H and $–NH_2$ stretching (65). Bands at 2905-2884 cm^{-1} are assigned to C-H of sp^3 stretching (33)(64). Peak at 1637 cm^{-1} are ascribing C=O stretching, while the peak at 1548 cm^{-1} are assigned N-C stretching (70). Peak at 1402 cm^{-1} are assigned C-OH bending (33), and the peak at 1319 cm^{-1} are assigned N-H stretching (65). Finally, the bands at 1069 and 1021cm^{-1} are assigned C-O stretching (65).

3.3.4.6.2 SEM for I

The SEM is used to examined the morphology and porous size of foam formed by freeze-drying in Figure 48.

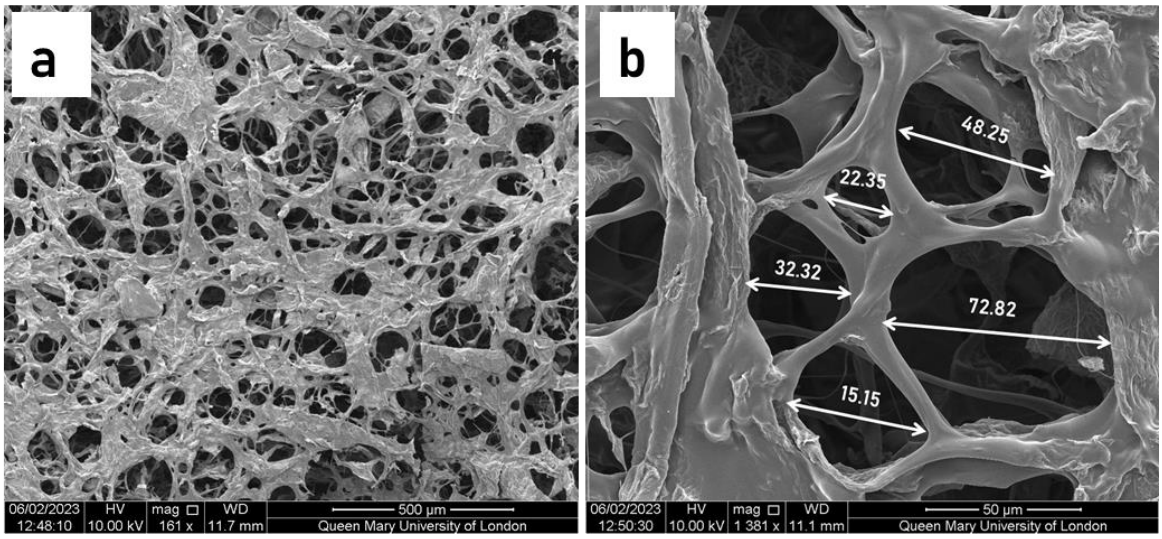

Figure 48. SEM for blend I at a) 500 µm and b)50 µm

The 500 μm micrograph (a) shows a very uniform surface of the material with pores of similar sizes, while at 50 μm magnification (b) it is possible to appreciate in better detail the morphology and size of the pores, as well as the fact that these pores are found in the different layers that form the foam. These images demonstrate the influence of CS when used as the aerogel matrix, as it provides stability and better pore distribution on its surface than the rest of the blends presented previously.

3.3.4.6.3 BET for I

The method developed by Brunauer, Emmett and Teller (BET) is used to characterize and evaluate the surface area of this foam in Figure 49.

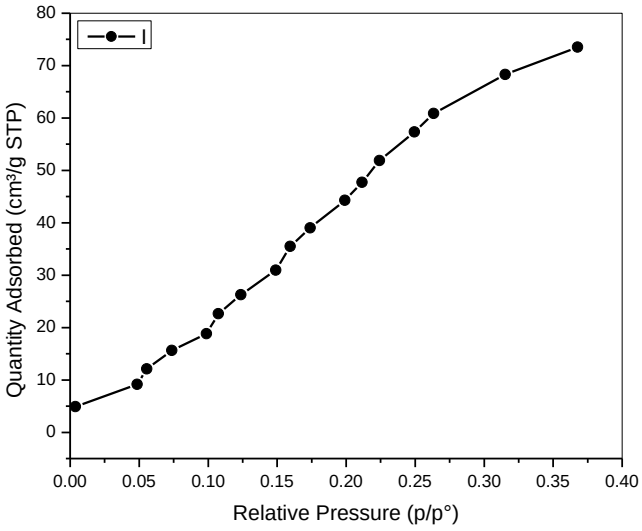

Figure 49. BET for blend I

The measured density for this sample was 3.7178 g/cm^3. While the analysis by BET method showed a surface area of 401.6190 m^2/g; with a type II isotherm for macroporous materials. This is consistent with the previous micrographs (Figure 48). However, although this sample has a large surface area, it also has a very high density, which is not expected for an aerogel.

3.3.4.6.4 TGA for I

This TGA shows the main weight losses with respect to temperature in Figure 50, with the intention of observing how the components influences the behavior.

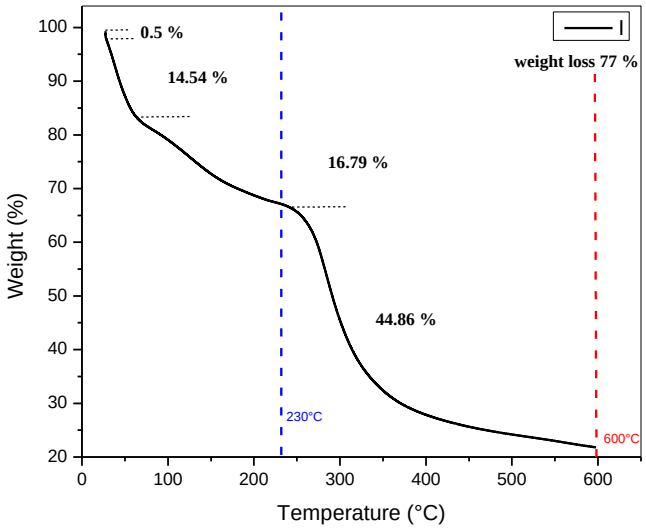

Figure 50. TGA for blend I

There are two small steps, with a weight loss of 15% due to the loss of water (67), then a degradation occurs, with a loss of approx. 16.79% by degradation of the CS (68), and in the last step, the weight loss is about 44.86% after the 260°C which indicates the decomposition of CS and the degradation of GO (67)(72).

It should be noted that, being a sample with low GO content, it is normal for it to present higher weight losses and therefore more degradation (30), as there are less functional groups to form hydrogen interactions, therefore the mobility of the polymer is greater and easier to degrade, even at lower temperatures.

3.3.4.6.5 DSC for I

The DSC shows the behaviour of foam made of CS and GO to evaluate the thermal properties in Figure 51.

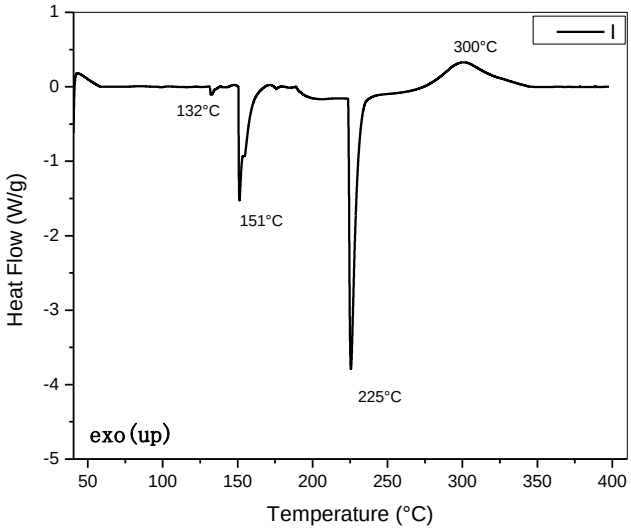

Figure 51. DSC for blend I

The diagram shows a small endothermic peak at 132°C due to water evaporation (67), indicating the influence of the GO by shifting the peak slightly to higher temperatures (64). Two endothermic peaks at 151°C and 225°C which could be due to the breaking of the polymer chains (68), while the first endothermic peak appears at the same temperature of CS, the second peak is shifted to a higher temperature and, finally, an exothermic peak at 300°C characteristic of CS degradation (68)(65).

Although the oxygen functional groups provided by the GO shift the peak values towards higher temperatures, due to interaction with the functional groups of the CS, to form hydrogen bonds; the low presence of oxygen functional groups that is represented in the exothermic peak intensity, indicates the low combustion of the material, and therefore higher resistance to degradation.

3.3.4.7 BLEND F

This blend is composed of a ratio of CS to PVA with a higher proportion of CS (Table 8), with the intention of observing how PVA influences CS.

Table 8. Composition of blend F

Blends	CS (ml)	PVA (ml)	GO (ml)
F	8	2	0

3.3.4.7.1 FTIR for F

The FTIR in Figure 52 is used to characterize the behaviour and presence of functional groups after combining CS with PVA.

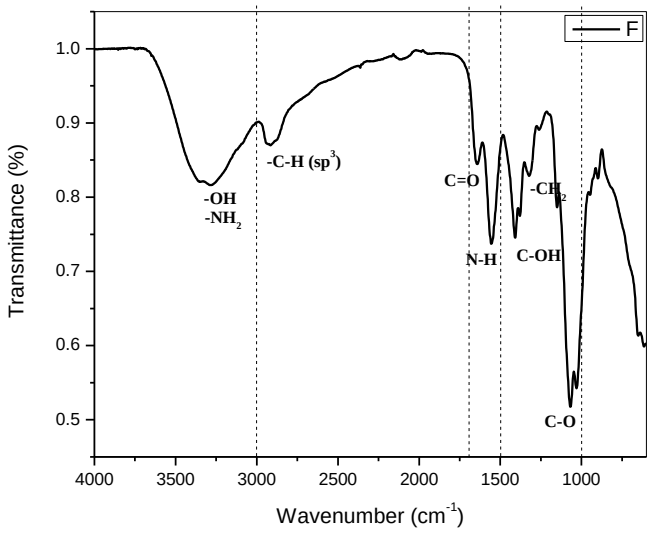

Figure 52. FTIR spectrum for blend F

The peaks of spectra of blend C show a broadband ~3306 cm^{-1} is ascribed to O-H and $–NH_2$ stretching (65). Bands at 2919 cm^{-1} are assigned to C-H of sp^3 stretching (33). The peak at 1644 cm^{-1} are ascribing C=O stretching, while the peak at 1555 cm^{-1} are assigned N-H stretching (70)(66), also the peak at 1409 cm^{-1} are assigned C-OH stretching. Peak at 1319 cm^{-1} are assigned C-H bending (70), and the bands at 1069 cm^{-1} are assigned C-O stretching (65).

3.3.4.7.2 SEM for F

The SEM is used to examined the morphology and porous size of foam by freeze-drying in Figure 53.

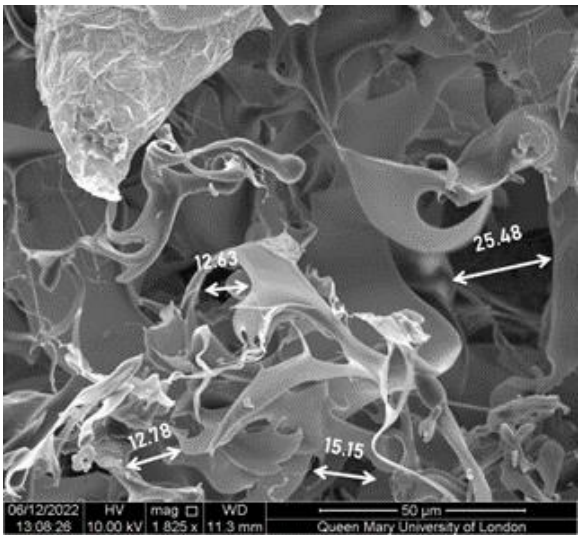

Figure 53. SEM for blend F

The micrograph at 50 μm shows that the foam formed during freeze-drying is cross-layered material with gaps of size of >50 μm between them, in addition to the fact that there is no uniform surface, and some of these sheets show wrinkles and folds.

Therefore, although CS had proved to be a very good material to be used as a matrix with the addition of GO, in this sample with the addition of PVA, the behavior is very different to that presented in the previous blend.

3.3.4.7.3 BET for F

The method developed by Brunauer, Emmett and Teller (BET) is used to characterize the surface area of this foam, Figure 54 ,composed mostly of CS with a part of PVA.

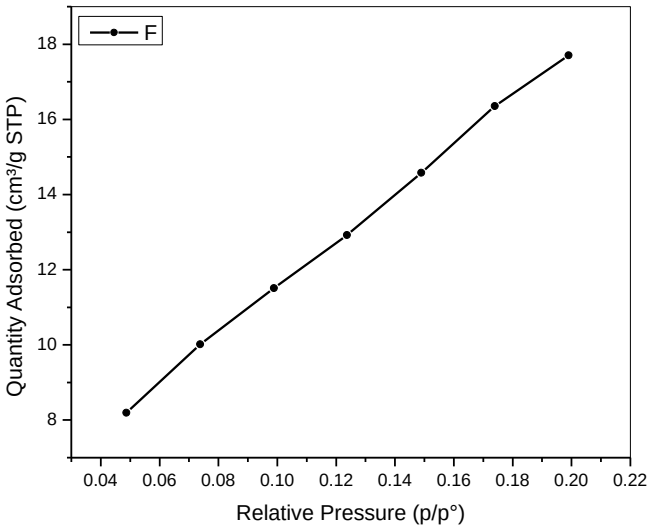

Figure 54. BET for blend F

The measured density for this sample was 0.787 g/cm^3. The diagram shows a linear behaviour corresponding to a type II isotherm for macroporous material; with a BET surface area of 79.0043 m²/g. Although it does not have a high surface area, it is the sample with the best relationship between surface area and density.

3.3.4.7.4 TGA for F

This TGA (Figure 55) shows the main weight losses of the blend with respect to temperature, with the intention of observing how the components of the blends influences the behavior.

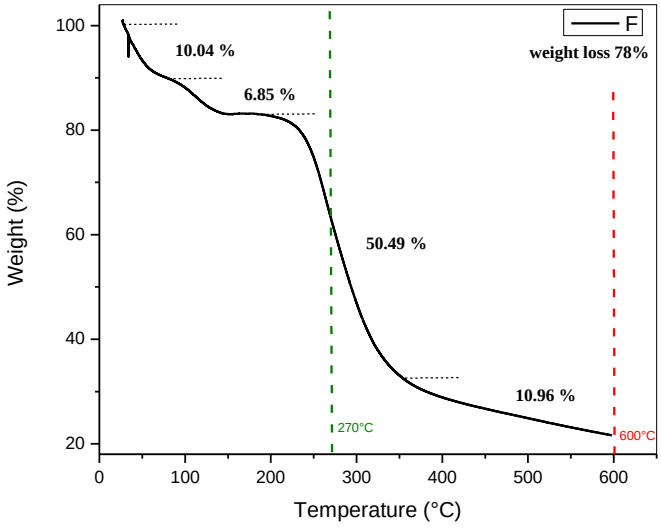

Figure 55. TGA for blend F

There are three main weight losses, in the first step, there is a weight loss of 10% due to the loss of water (67)(75). Then a two-step degradation occurs, with the main weight loss approx. 50.5%; firstly, loss of remaining water occurred, followed by degradation of the CS and PVA (68). In the last step, the weight loss is about 10.96% after the 350°C which indicates the decomposition of cs and PVA (68).

3.3.4.7.5 DSC for F

The DSC shows the behaviour of foam made of CS and PVA to evaluate the thermal properties in Figure 56.

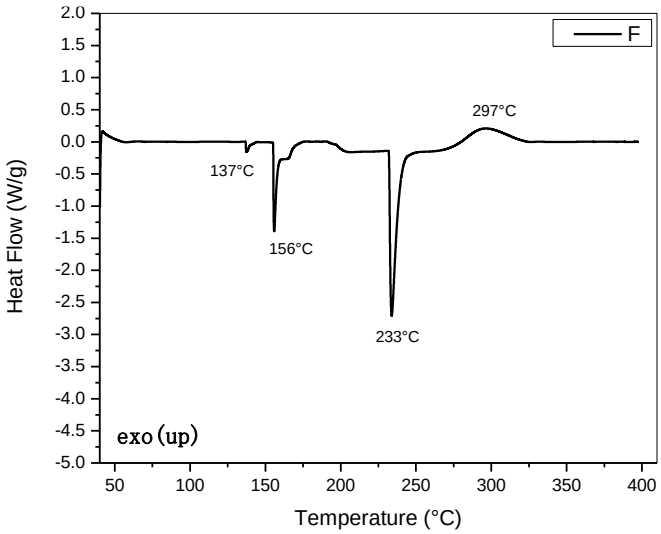

Figure 56. DSC for blend F

The diagram shows a little endothermic peak at 137°C due to evaporation of water and the melting point of CS (67). Two endothermic peaks at 156°C and 233°C that could be due to the breaking of polymeric chains (68), while the first endothermic peak

appears at the same temperature the second peak is shifted at a higher temperature (68) with respect to the CS (Figure 17). Finally, an exothermic peak appear at 297°C characteristic of CS degradation (65) as is the temperature of degradation of PVA (67). However, the shift of the second peak may be due to the PVA content in the blend as low concentrations improve the stability of the compound at high temperatures (71).

Although the oxygen functional groups provided by the PVA shift the endothermic peak values towards higher temperatures, due to interaction with the functional groups of the CS, to form hydrogen bonds; is logical that it presents a similar behaviour to sample I, however due to the fact that there is a difference in the proportion of functional groups present in PVA and GO, as PVA contains only hydroxyl groups and in much smaller amounts compared to GO, the exothermic peak intensity is much less intense.

3.3.5 MATRIX OF CS WITH PVA

According to the results obtained from the previous blends, with the best thermal results of the blends F and I, whose major component is CS, in addition to very good values of density and surface area; and since according to previous research (30) where the combination of CS with PVA to be used as a matrix for aerogel presents the best behavior, these two components are chosen for the next step of the project.

In order to identify the ratio of CS to PVA to find the one with the best properties as a matrix for the aerogel, different amounts of CS were mixed with PVA without exceeding half the proportion of PVA with respect to CS, since, as some articles indicate (42), the lower the amount of PVA, the higher the miscibility in the blend, due to the functional groups present in both substances.

The interactions that were made are shown in the Table 9. Where the concentrations for CS and PVA are 1 %w/v for each.

Table 9. Different combinations of CS with PVA

Blends	CS (ml)	PVA (ml)
CP1	10	1
CP2	10	2
CP3	10	3
CP4	10	4
CP5	10	5

The same process was followed to freeze-dry these samples and then characterisation by FTIR, SEM and DSC was performed, in order to identify the morphology of the pores formed and the thermal properties.

3.3.5.1 SAMPLE CP1

This blend identified as sample CP1 is composed of a ratio of 10 ml CS to 1 ml PVA, with the intention of observing how the small amount of PVA influences on CS.

3.3.5.1.1 FTIR for CP1

In Figure 57 FTIR is used to characterise the behaviour and presence of functional groups when combining CS with PVA.

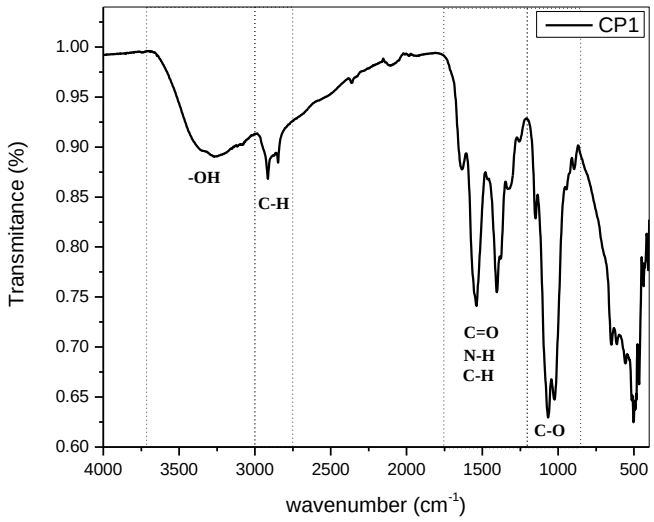

Figure 57. FTIR spectrum of CS and PVA at 10:1 ratio

The peaks of spectrum show a broadband ~3257 cm^{-1} is ascribed to O-H stretching, related to the functional groups of PVA as well as of CS (30)(65) and the formation of hydrogen bonds between them. The peaks between 2917 cm^{-1} and 2849 cm^{-1} are assigned to C-H of sp^3 asymmetric and symmetric stretching respectively due to PVA molecules (33). The peak at 1625 cm^{-1} is ascribing C=O stretching (70) while the peak at 1546 cm^{-1} is assigned N-H stretching (66), also the peak at 1319 cm^{-1} are assigned C-H wagging coupled with OH (30)(70), and finally the peaks at 1070 cm^{-1} are assigned C-O stretching (65).

This spectrum confirms the interaction of the functional groups of PVA with those of CS to form hydrogen bonds; however, due to the low ratio of PVA to CS there is little interaction between them demonstrated by the C-H peaks.

3.3.5.1.2 SEM of CP1

The SEM is used to examined the morphology and porous size of foam formed by freeze-drying in Figure 58.

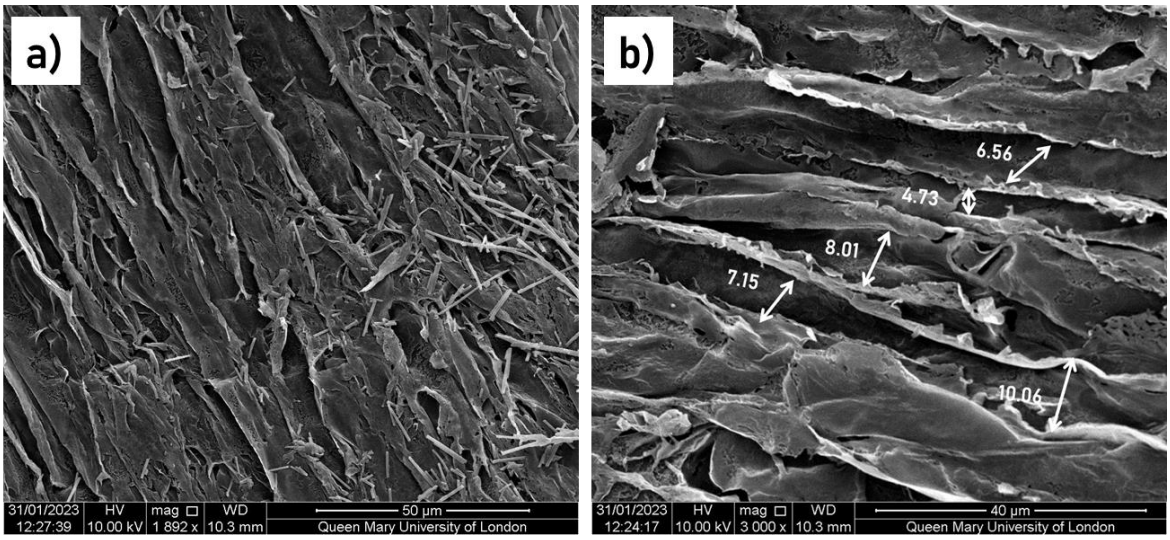

Figure 58. SEM of CS and PVA at 10:1 ratio at a) 50 μm b) 40 μm

Two micrographs are presented at 50 μm and 40 μm where the direction of the stacked sheets of CS blended with a small portion of PVA can be observed, also it can be seen that on the surface of the sample the spacing between the layers is approximately 10 μm, and shows small folds.

Compared to the CS-only foam (Figure 14), where small pores are observed on the thin layers formed during freeze-drying, this behaviour is not present in this sample, this may be due to the low distribution of PVA on the CS, as the folds observed are similar to those presented in the PVA micrographs (Figure 19).

3.3.5.1.3 DSC for CP1

DSC shows the behaviour of the freeze-dried foam obtained by combining CS with PVA in Figure 59.

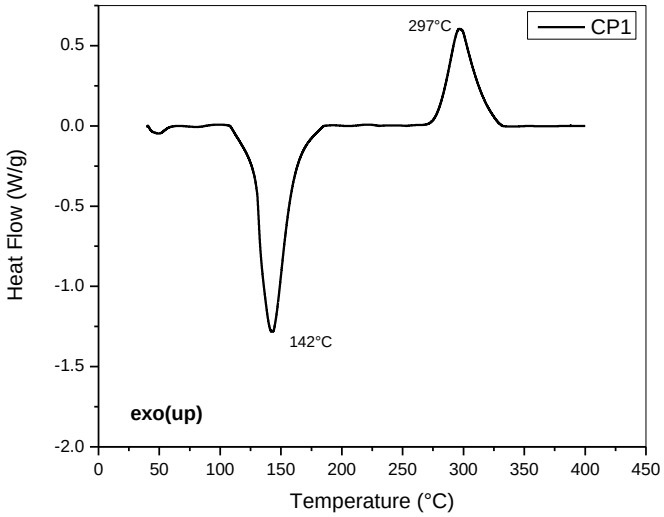

Figure 59. DSC spectrum of CS and PVA at 10:1 ratio

Two peaks are observed, an endothermic one at 142°C, and an exothermic one at 297°C, which is associated with the decomposition of both CS and PVA.

3.3.5.2 SAMPLE CP2

This blend is composed of a ratio of 10 ml CS to 2 ml PVA, with the intention of observing how PVA influences CS.

3.3.5.2.1 FTIR for CP2

FTIR is used to characterise the behaviour and presence of functional groups when combining CS with PVA in Figure 60.

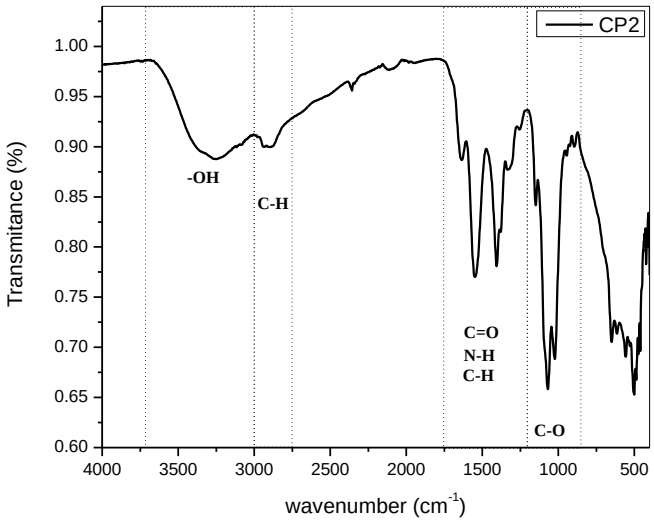

Figure 60. FTIR spectrum of CS and PVA at 10:2 ratio

The peaks of spectrum show a broadband ~3291 cm^{-1} is ascribed to O-H stretching, related to the functional groups of PVA as well as of CS (30)(65). The peak at 2906 cm^{-1} is assigned to C-H of sp^3 stretching (33). The peak at 1648 cm^{-1} are ascribing C=O stretching (70) while the peak at 1546 cm^{-1} are assigned N-H stretching (66), also the peak at 1308 cm^{-1} are assigned C-H wagging (70), and the peaks at 1082 cm^{-1} are assigned C-O stretching (65).

3.3.5.2.2 SEM of CP2

The SEM is used to examined the morphology and porous size of foam formed by freeze-drying in Figure 61.

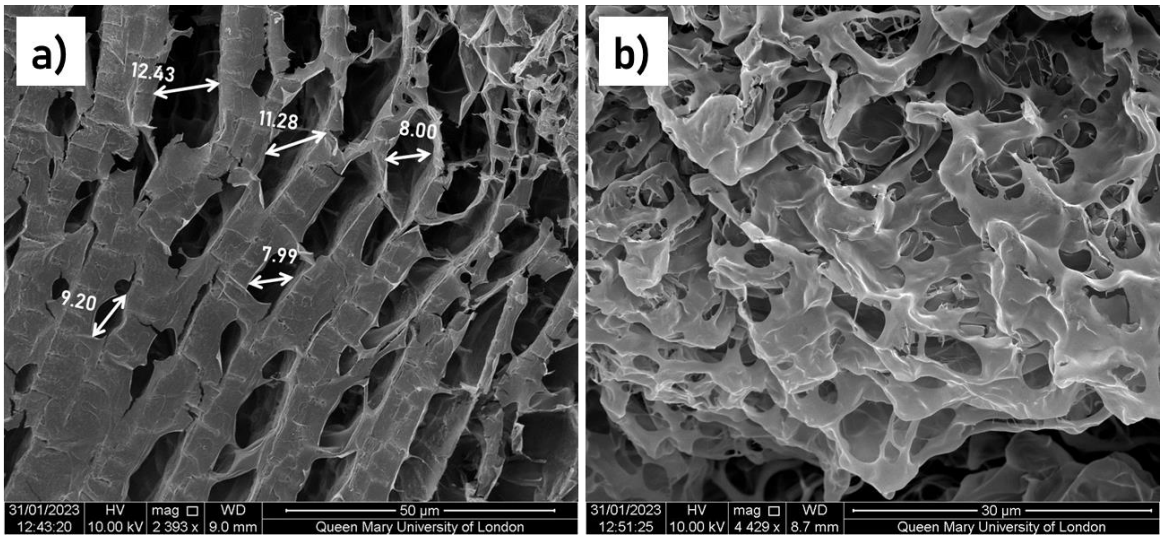

Figure 61. SEM of CS and PVA at 10:2 ratio at a) 50 µm, b) 30 µm

The formation of layers in the material with small pores of heterogeneous sizes of less than 20 µm between them is observed (Figure 61a). More homogeneously distributed pores are also observed in what appear to be stacked sheets (Figure 61b), which is consistent with the behavior presented above in the pure CS foam (Figure 14), which makes sense as CS is still present in higher amounts.

3.3.5.2.3 DSC for CP2

DSC shows the behaviour of the freeze-dried foam obtained by combining CS with PVA in Figure 62.

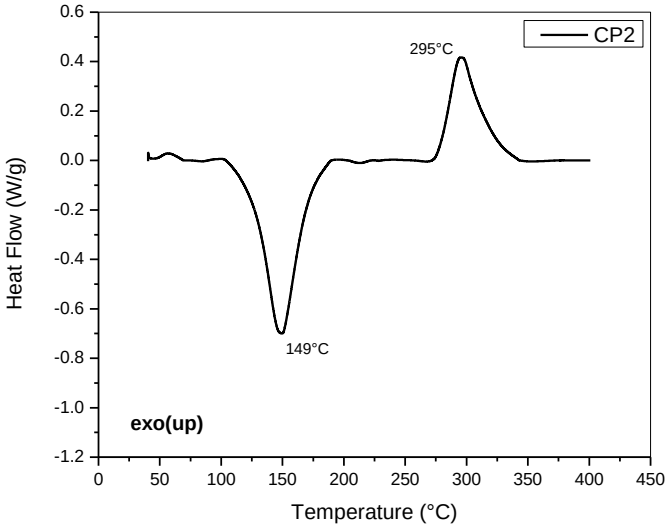

Figure 62. DSC spectrum of CS and PVA at 10:2 ratio

Two peaks are observed, an endothermic one at 149°C, and an exothermic one at 295°C, which is associated with the decomposition of both CS and PVA. A small shift of the peaks towards lower temperatures is observed compared to the first sample with less PVA (Figure 59).

3.3.5.3 SAMPLE CP3

This blend is composed of a ratio of 10 ml CS to 3 ml PVA, with the intention of observing how PVA influences CS.

3.3.5.3.1 FTIR for CP3

FTIR is used to characterise the behaviour and presence of functional groups when combining CS with PVA as show in Figure 63.

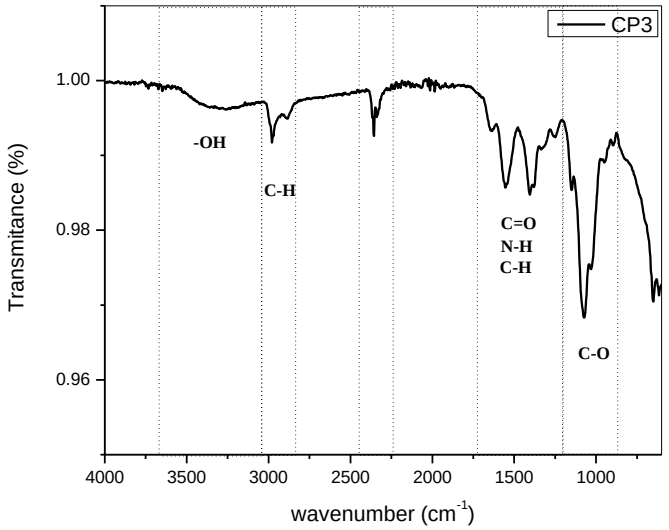

Figure 63. FTIR spectrum of CS and PVA at 10:3 ratio

The peaks of spectrum show a broadband ~3319 cm^{-1} is ascribed to O-H stretching (65), which is less broad compared to previous samples (Figure 57 and Figure 60). The peak at 2977 cm^{-1} is assigned to C-H of sp^3 stretching (33), while the peak at 1640 cm^{-1} is ascribing C=O stretching (70). The peak at 1545 cm^{-1} is assigned N-H stretching (66), also the peak at 1393 cm^{-1} is assigned C-H stretching (70), and the peak at 1062 cm^{-1} are assigned C-O stretching (65).

3.3.5.3.2 SEM of CP3

The SEM is used to examined the morphology and porous size of foam formed by freeze-drying in Figure 64.

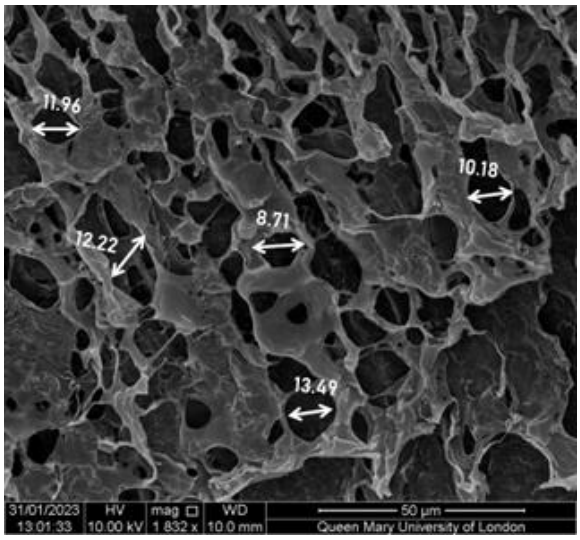

Figure 64. SEM of CS and PVA at 10:3 ratio at 50 µm

There are layers of material with pores randomly distributed in the layers, with size less than 20 µm, however, the layers with more pores are the upper ones, as it is possible to identify larger leaves at more depth.

3.3.5.3.3 DSC for CP3

DSC shows in Figure 65 the behaviour of the freeze-dried foam obtained by combining CS with PVA.

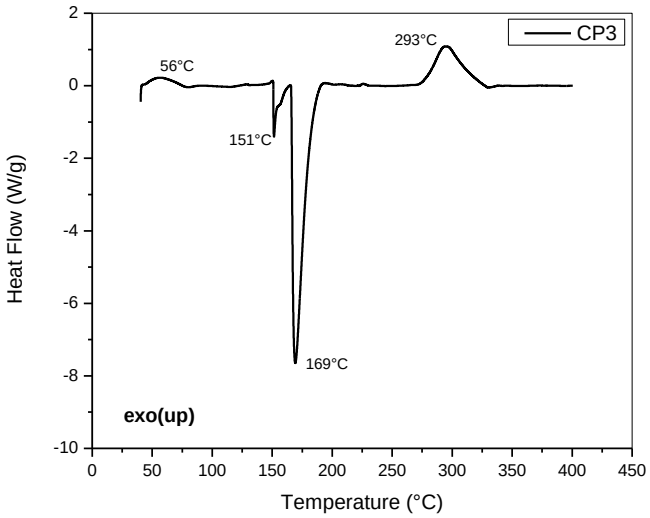

Figure 65. DSC spectrum of CS and PVA at 10:3 ratio

Three peaks are observed, firstly tow endothermic peaks, one at 151°C and 169°C; related to the behavior presented by the CS, with a notable difference in the intensity of the second peak with respect to the first peak. After that an exothermic peak appear at 293°C, which is associated with the decomposition of both CS and PVA. A small shift of the exothermic peak towards lower temperatures is observed.

3.3.5.4 SAMPLE CP4

This blend is composed of a ratio of 10 ml CS to 4 ml PVA, with the intention of observing how PVA influences CS.

3.3.5.4.1 FTIR for CP4

FTIR is used to characterise the behaviour and presence of functional groups when combining CS with PVA as show in Figure 66.

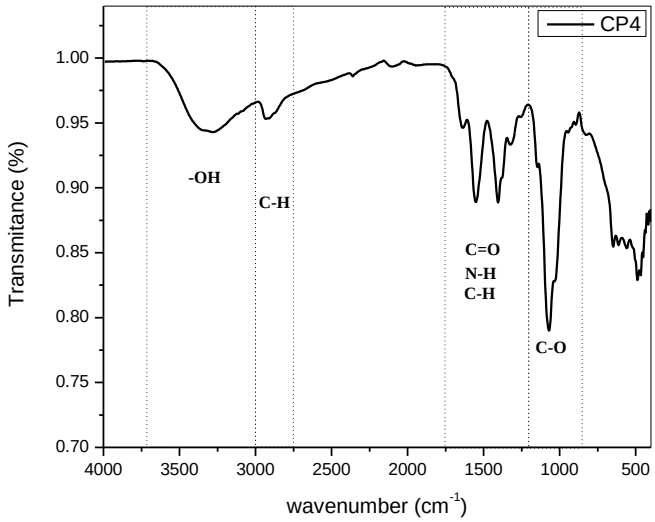

Figure 66. FTIR spectrum of CS and PVA at 10:4 ratio

The peaks of spectrum show again a broadband ~3313 cm^{-1} is ascribed to O-H stretching (65). The small peak at 2929 cm^{-1} is assigned to C-H of sp^3 stretching (33), while the peak at 1648 cm^{-1} is ascribing C=O stretching (70). The peak at 1546 cm^{-1} is assigned N-H stretching (66), also the peak at 1398 cm^{-1} are assigned C-H stretching (70), and the peak at 1059 cm^{-1} are assigned C-O stretching (65).

3.3.5.4.2 SEM for CP4

SEM shows, Figure 67, the behaviour of the freeze-dried foam obtained by combining CS with PVA.

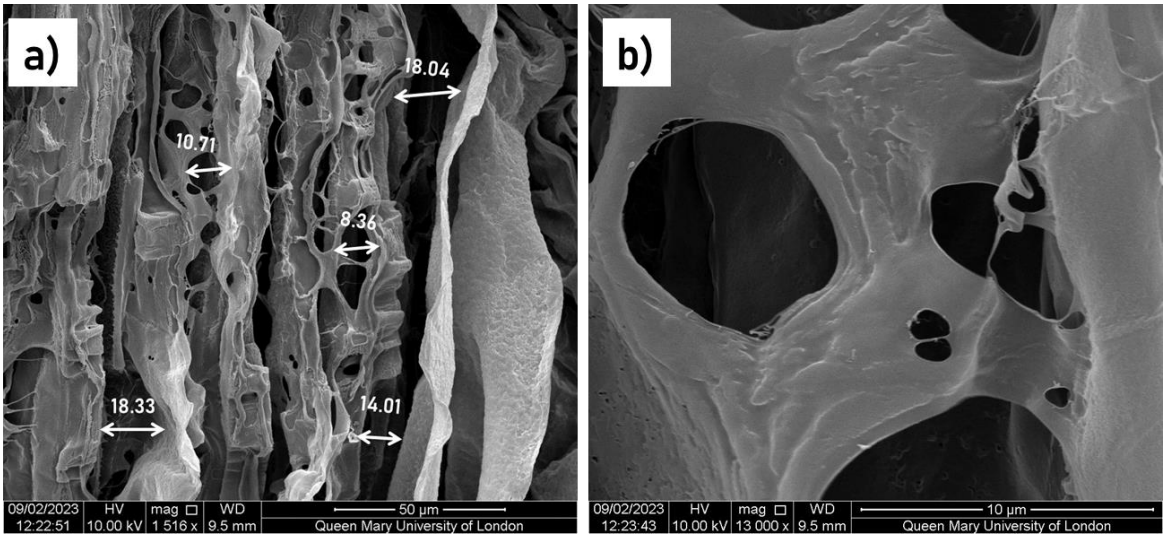

Figure 67. SEM of CS and PVA at 10:4 ratio at a) 50 µm and b) 10 µm

The formation of layers stacked in one direction only, with folds and pores in them is observed (Figure 67a). A close-up view of the pores shows that they are well formed with an approximate pore size of 10 μm (Figure 68b). It is important to note that in this sample a uniformity in the appearance of the pores and the distribution of the layers formed is starting to be noticed.

3.3.5.4.3 DSC for CP4

DSC shows the behaviour of the freeze-dried foam obtained by combining CS with PVA in Figure 68.

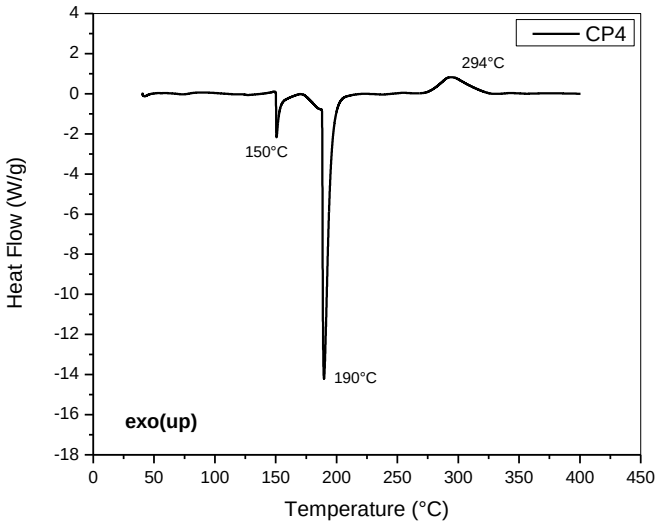

Figure 68. DSC spectrum of CS and PVA at 10:4 ratio

Three peaks are observed, firstly two endothermic peaks, one at 150°C and 190°C; related to the behavior presented by the CS, with the second peak very intense compared to the first one. Then an exothermic peak appears at 294°C, which is associated with the decomposition of both CS and PVA.

3.3.5.5 SAMPLE CP5

This blend is composed of a ratio of 10 ml CS to 5 ml PVA, with the intention of observing how PVA influences CS.

3.3.5.5.1 FTIR for CP5

FTIR in Figure 69 is used to characterise the behaviour and presence of functional groups when combining CS with PVA.

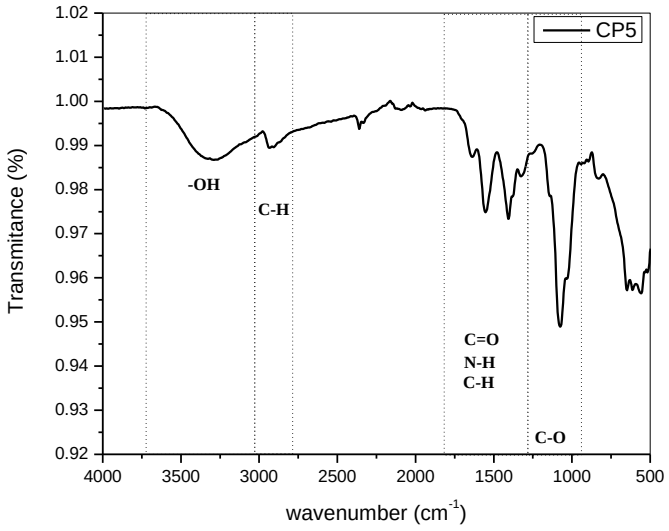

Figure 69. FTIR spectrum of CS and PVA at 10:5 ratio

The peaks of spectrum show a broadband ~3311 cm^{-1} is ascribed to O-H stretching (65), a small peak at 2914 cm^{-1} is assigned to C-H of sp^3 stretching (33), while the peak at 1614 cm^{-1} is ascribing C=O stretching (70). The peak at 1548 cm^{-1} is assigned N-H stretching (66), also the peak at 1405 cm^{-1} is assigned C-H stretching (70), and the peak at 1075 cm^{-1} are assigned C-O stretching (65).

3.3.5.5.2 SEM for CP5

SEM shows, Figure 70, the behaviour of the freeze-dried foam obtained by combining CS with PVA.

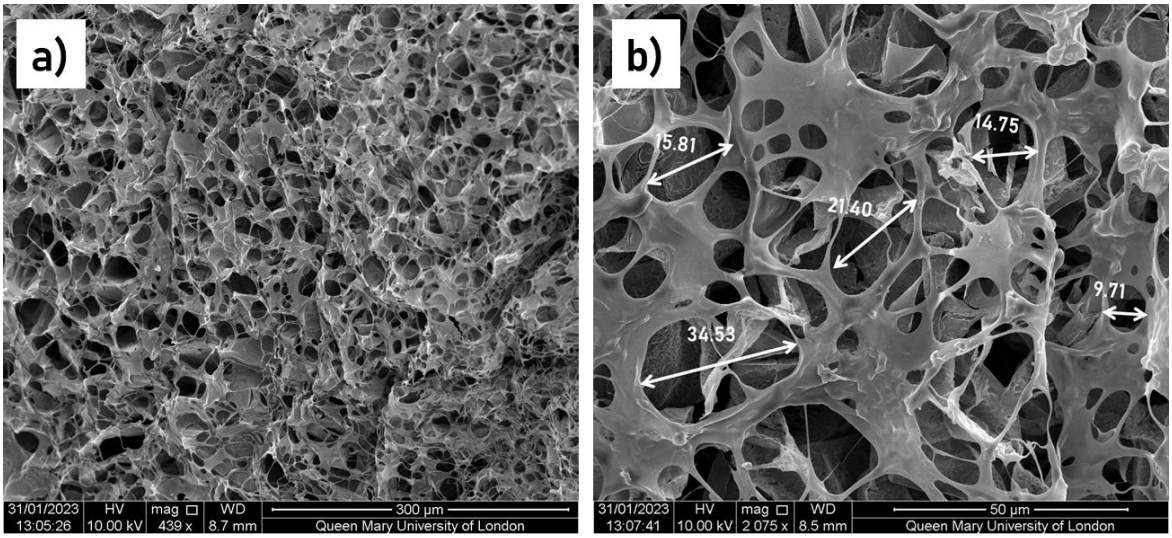

Figure 70. SEM of CS and PVA at 10:5 ratio at a) 300 µm and b) 50 µm

Is possible observe a surface full of homogeneously distributed pores, Figure 70a, in a close up in Figure 70b a variety of sizes is evident being smaller than 35 μm, very close to each other.

It can therefore be deduced that, although they still maintain the structure of the original CS (Figure 14), there is a greater distribution of holes in the structures as the amount of PVA increases.

3.3.5.5.3 DSC for CP5

DSC shows in Figure 71 the behaviour of the freeze-dried foam obtained by combining CS with PVA.

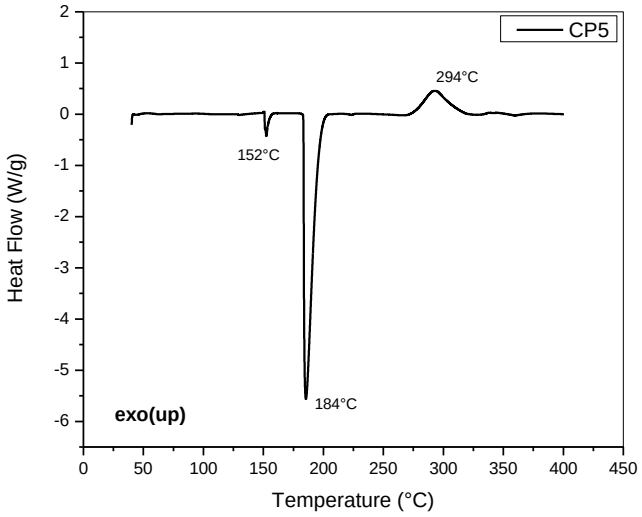

Figure 71. DSC spectrum of CS and PVA at 10:5 ratio

Three peaks are observed, firstly tow endothermic peaks, one at 152°C and 184°C; related to the behavior presented by the CS, with the second peak very intense compared to the first one. Finally, an exothermic peak appears at 294°C, which is associated with the decomposition of both CS and PVA.

3.3.6 GO AS FILLER IN THE MATRIX OF CS WITH PVA

As the CP4 sample showed the most uniform morphology (Figure 67), as well as the highest values in thermal properties (Figure 68), this combination is chosen to add GO and observe the behaviour of the material, considering also that the GO is kept at low concentrations to avoid agglomeration and promote a better dispersion in the chosen solution.

The interactions that were made are shown in the following table.

Table 10. Different variation of GO in the combination of CS with PVA

Blends	CS (ml)	PVA (ml)	GO (ml)
CPG1	10	4	1
CPG2	10	4	2
CPG3	10	4	3
CPG4	10	4	4
CPG5	10	4	5

The same process was followed to freeze-dry these samples and then characterisation by FTIR, SEM and DSC was performed.

3.3.6.1 SAMPLE CPG1

This blend is composed of 10 ml of CS, 4 ml of PVA and 1 ml of GO with the intention of observing how GO influences the CS with PVA matrix.

3.3.6.1.1 FTIR for CPG1

FTIR is used to characterise the behaviour of functional groups when GO is added to the combining of CS with PVA, as show in Figure 72.

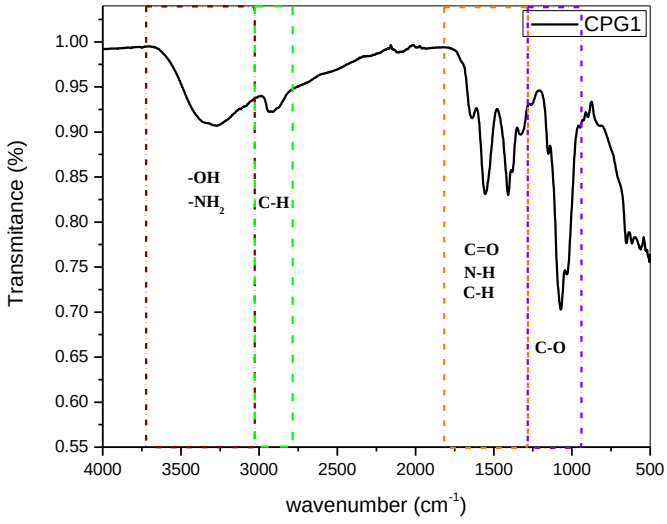

Figure 72. FTIR spectrum of CS and PVA with GO at 10:4.1 ratio

The spectrum shows a broadband at ~3311 cm^{-1} that is ascribed to O-H and $–NH_2$ stretching, the bands at 2925 cm^{-1} are assigned to C-H stretching, the peak at 1647 cm^{-1} are ascribing C=O stretching, peak at 1570 cm^{-1} is assigned N-H stretching, peak at 1406 cm^{-1} is assigned C-H stretching and the peak at 1075 cm^{-1} is assigned C-O stretching.

3.3.6.1.2 SEM for CPG1

SEM in Figure 73 shows the behaviour of the freeze-dried foam obtained by adding GO to the combination of CS with PVA.

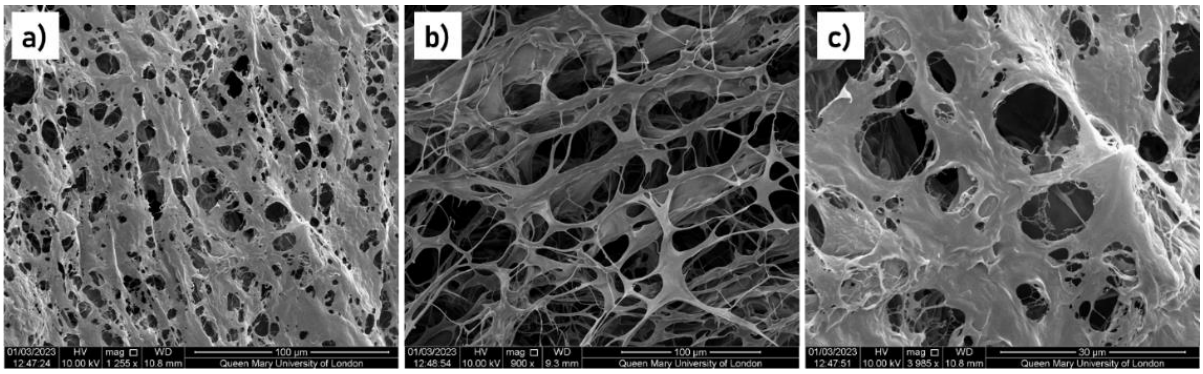

Figure 73. SEM of CS and PVA with GO at 10:4:1 ratio at a) 100 μm b) 100 μm and c) 30 μm

In image a) and b) different structures can be observed although both are micrographs at 100 μm; although in both images pores are uniformly distributed, in image a) the layer covers a larger surface, keeping the pores separated at a greater distance; while in image b) a very thin network is formed on the surface that extends towards the bottom, and finally in image c) a close-up of the well-formed pores is made to identify the size that remains smaller than 10 μm, however it is also possible to identify the formation of much smaller pores in some areas of the layers.

3.3.6.1.3 DSC for CPG1

DSC shows in Figure 74 the behaviour of the freeze-dried foam obtained when the GO ratio is varied in the combination of CS with PVA.

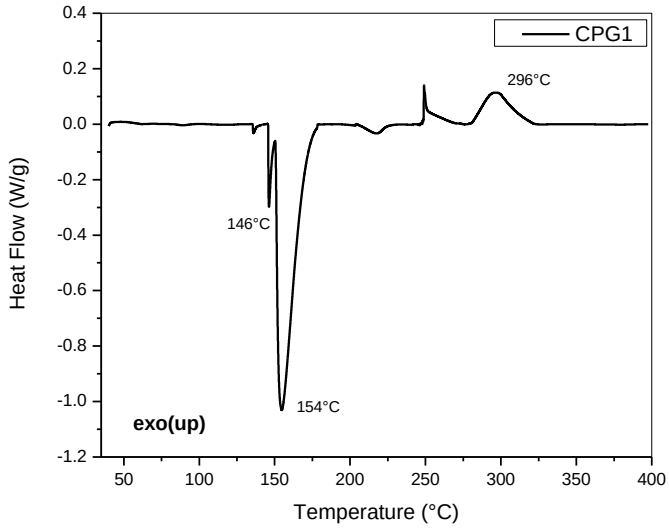

Figure 74. DSC spectrum of CS and PVA with GO at 10:4.1 ratio

Two peaks are clearly visible, firstly an endothermic peak, which appears to split into two peaks at different temperatures, at 146°C and 154°C; related to the behavior presented by the CS. Finally, an exothermic peak appears at 296°C, which is associated with the decomposition of CS, PVA and GO.

3.3.6.2 SAMPLE CPG2

This blend is composed of 10 ml of CS, 4 ml of PVA and 2 ml of GO with the intention of observing how GO influences the CS matrix with PVA.

3.3.6.2.1 FTIR for CPG2

FTIR is used to characterise the behaviour of functional groups when GO is added to the combining of CS with PVA as show in Figure 75.

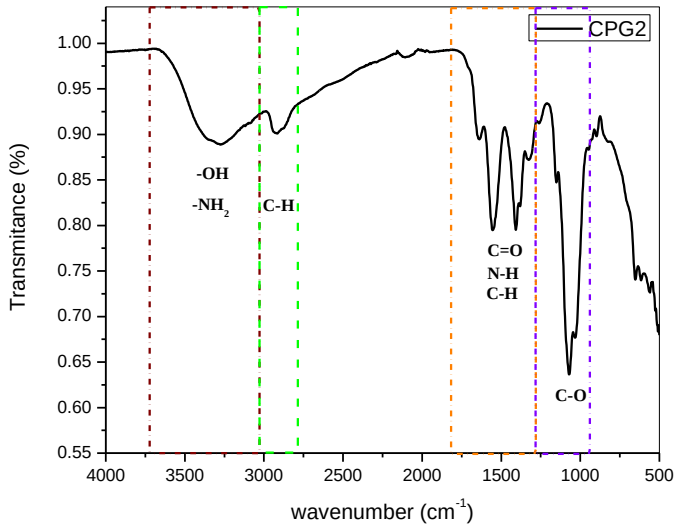

Figure 75. FTIR spectrum of CS and PVA with GO at 10:4.2 ratio

The spectrum shows a broadband at ~3299 cm^{-1} that is ascribed to O-H and $–NH_2$ stretching, the bands at 2925 cm^{-1} are assigned to C-H stretching, the peak at 1635 cm^{-1} are ascribing C=O stretching, peak at 1559 cm^{-1} is assigned N-H stretching, peak at 1405 cm^{-1} is assigned C-H stretching and the peak at 1076 cm^{-1} is assigned C-O stretching, being more intense than in the previous sample (Figure 72).

3.3.6.2.2 SEM for CPG2

SEM shows in Figure 76 the behaviour of the freeze-dried foam obtained by combining CS with PVA.

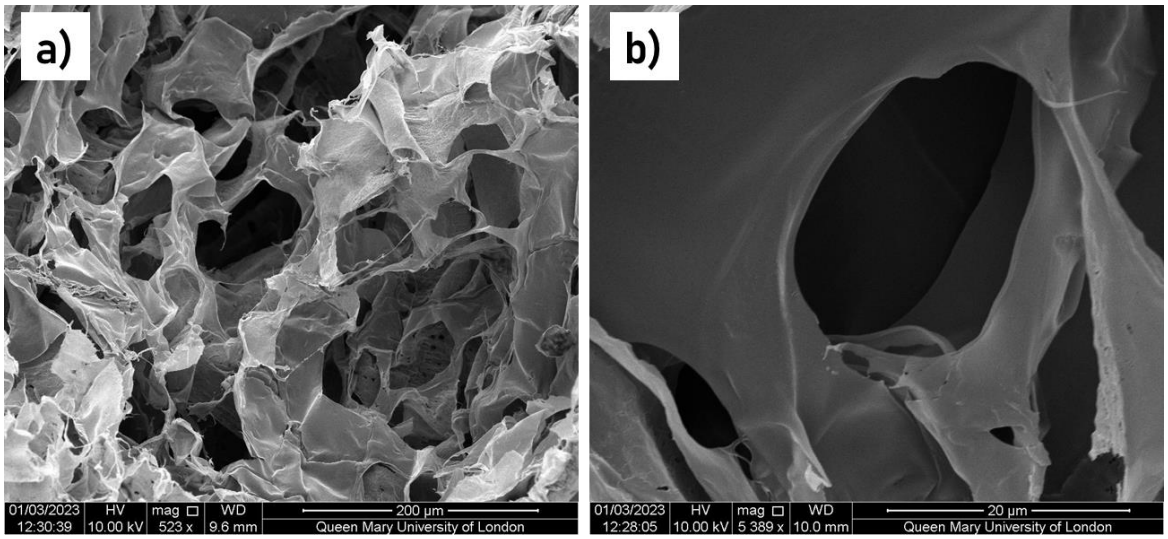

Figure 76. SEM CS and PVA with GO at 10:4:2 ratio at a) 200 µm b) 20 µm

The first image (a) shows the formation of pores in the sample due to the separation of the sheets, which wrinkled and folded together, making it difficult to distinguish the direction in which they are stacked, while the Figure 76b shows one of the pores formed by the cavities left between the leaves, which has an approximate size of 20 µm.

3.3.6.2.3 DSC for CPG2

DSC shows, Figure 77, the behaviour of the freeze-dried foam obtained when the GO ratio is varied in the combination of CS with PVA.

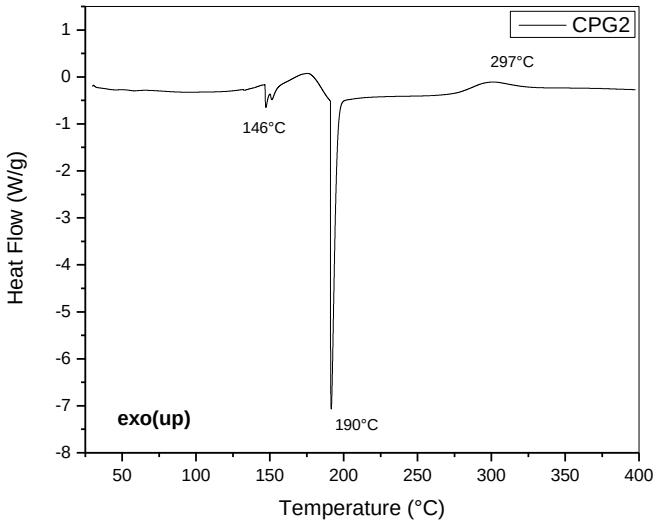

Figure 77. DSC spectrum of CS and PVA with GO at 10:4.2 ratio

Three peaks are visible, firstly an endothermic peak, which appears to split into two peaks at 146°C, the second one is a thin and very intense peak which appear at 190°C; related to the behavior presented by the PVA respect to the melting point (Figure 21). Finally, an exothermic peak appears at 297°C, which is associated with the decomposition and transformation of the oxygen groups of CS, PVA and GO to CO and CO_2.

3.3.6.3 SAMPLE CPG3

This blend is composed of 10 ml of CS, 4 ml of PVA and 3 ml of GO with the intention of observing how GO influences the CS with PVA matrix.

3.3.6.3.1 FTIR for CPG3

FTIR in Figure 78 is used to characterise the behaviour of functional groups when GO is added to the combining of CS with PVA.

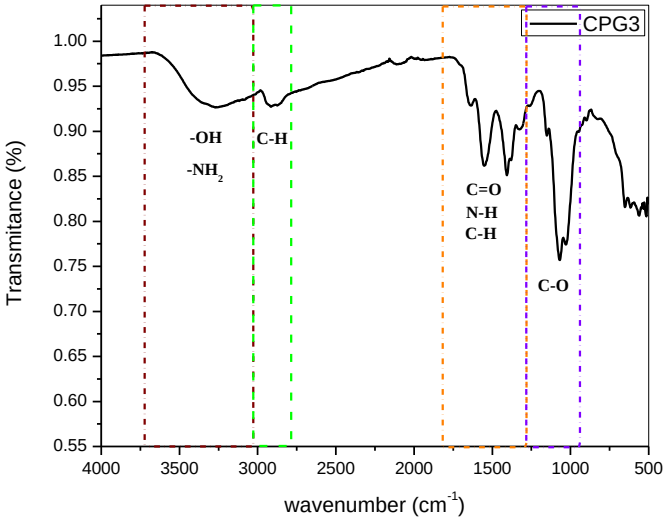

Figure 78. FTIR spectrum of CS and PVA with GO at 10:4.3 ratio

The spectrum shows a broadband at ~3299 cm^{-1} that is ascribed to O-H and $–NH_2$ stretching, being more intense. The bands at 2914 cm^{-1} are assigned to C-H stretching, the peak at 1636 cm^{-1} is ascribing C=O stretching, peak at 1548 cm^{-1} is assigned N-H stretching, peak at 1405 cm^{-1} is assigned C-H stretching and the peak at 1075 cm^{-1} is assigned C-O stretching.

3.3.6.3.2 SEM for CPG3

SEM shows the behaviour of the freeze-dried foam obtained by combining CS with PVA in Figure 79.

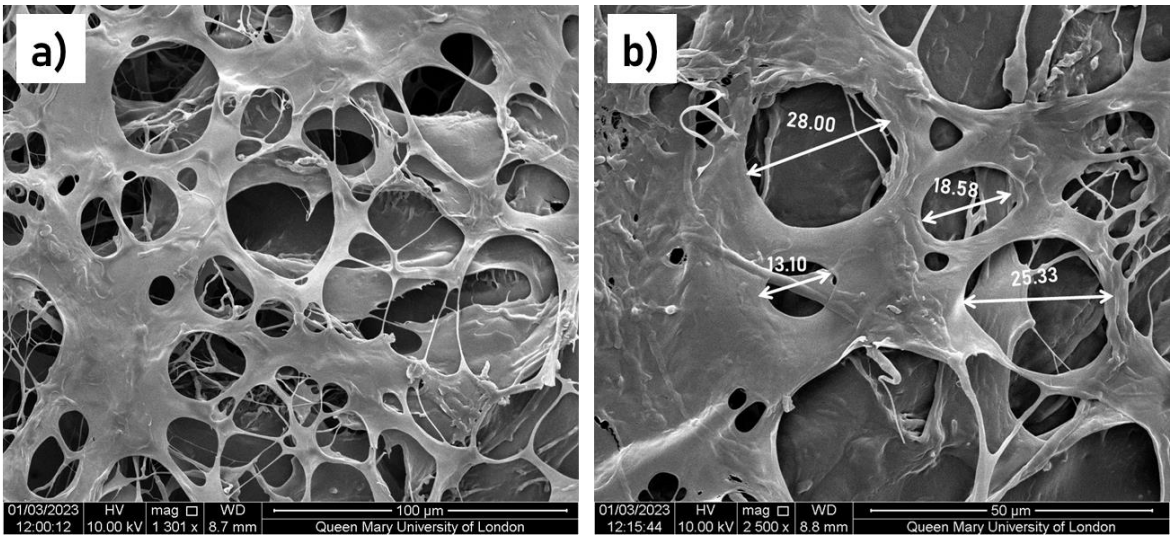

Figure 79. SEM of CS and PVA with GO at 10:4:3 ratio at a) 100 µm b) 50 µm

The pores on the surface are very close together, distributed in the upper layers, while in the lower layers there are larger sheets without so many pores on them however well-formed and well-distributed pores are visible. The pore size is found to be less than 30 µm (Figure 79b).

3.3.6.3.3 DSC for CPG3

DSC shows in Figure 80 the behaviour of the freeze-dried foam obtained when the GO ratio is varied in the combination of CS with PVA.

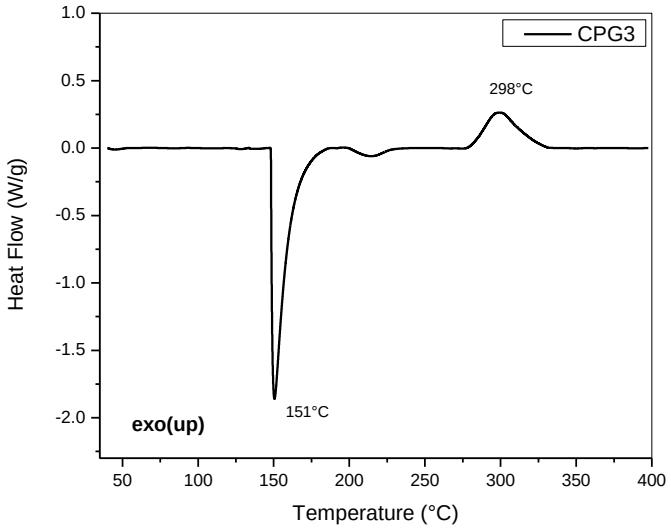

Figure 80. DSC spectrum of CS and PVA with GO at 10:4.3 ratio

Two peaks are visible clearly, firstly an endothermic peak, at 151°C, which is a thin and intense peak; matching with one of the peaks associated with the CS (Figure 17).

Finally, an exothermic peak appears at 298°C, which is associated with the decomposition and transformation of the oxygen groups of CS, PVA and GO.

3.3.6.4 SAMPLE CPG4

This blend is composed of 10 ml of CS, 4 ml of PVA and 4 ml of GO with the intention of observing how GO influences the CS matrix with PVA.

3.3.6.4.1 FTIR for CPG4

FTIR is used to characterise the behaviour of functional groups when GO is added to the combining of CS with PVA in Figure 81.

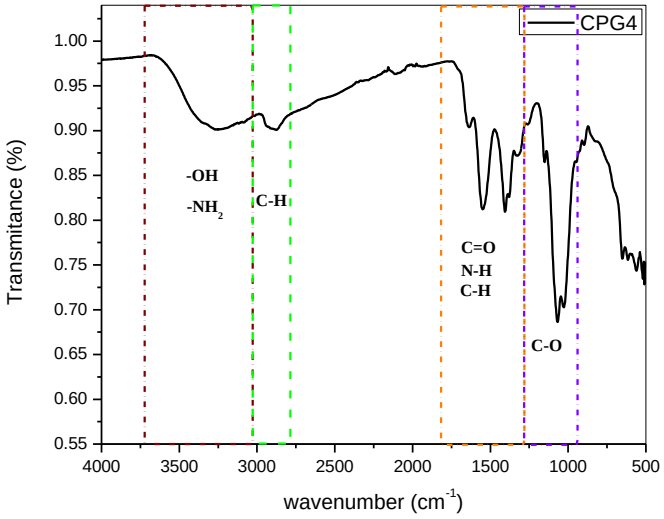

Figure 81. FTIR spectrum of CS and PVA with GO at 10:4.4 ratio

The spectrum shows a broadband at ~3266 cm^{-1} that is ascribed to O-H and $–NH_2$ stretching, being more intense. The bands at 2914 cm^{-1} are assigned to C-H stretching, the peak at 1636 cm^{-1} is ascribing C=O stretching, peak at 1548 cm^{-1} is assigned N-H stretching, peak at 1405 cm^{-1} is assigned C-H stretching and the peak at 1063 cm^{-1} is assigned C-O stretching.

3.3.6.4.2 SEM for CPG4

SEM shows in Figure 82 the behaviour of the freeze-dried foam obtained by combining CS with PVA.

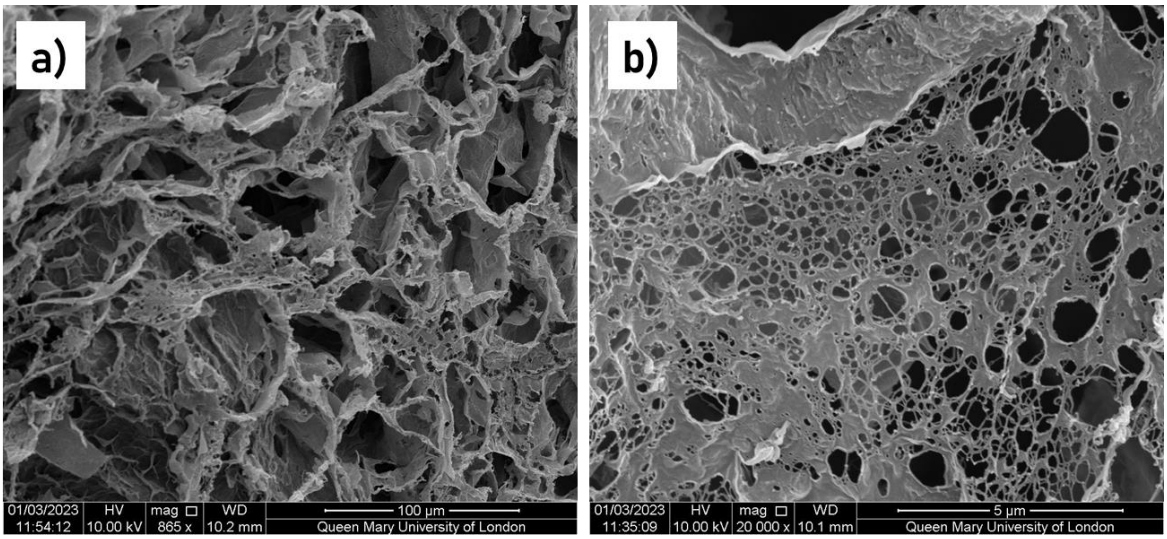

Figure 82. SEM of CS and PVA with GO at 10:4:4 ratio at a) 100 µm b) 5 µm

A honeycomb pore distribution between the leaves has been observed, and in addition to this, between the narrow gap between the leaves there are also much smaller pores as shown in image b) with pore sizes of less than 1 µm. It is due to this that the final structure of this sample is much fluffy than the rest, which at the same time decreases its stability.

3.3.6.4.3 DSC for CPG4

DSC shows in Figure 83 the behaviour of the freeze-dried foam obtained when the GO ratio is varied in the combination of CS with PVA

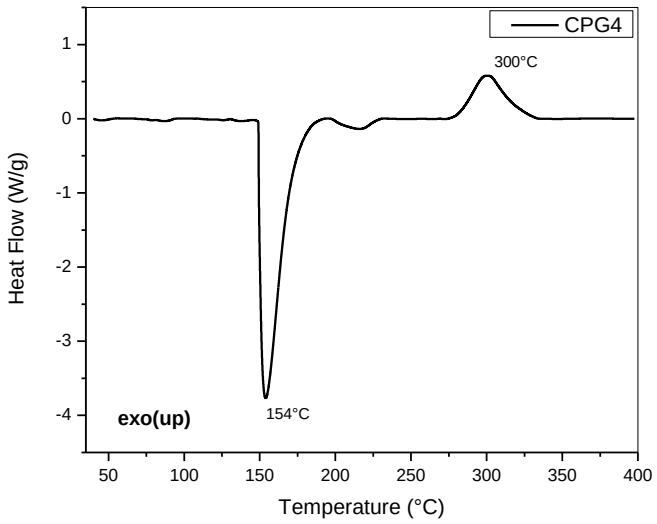

Figure 83. DSC spectrum of CS and PVA with GO at 10:4.4 ratio

Two peaks are visible clearly, firstly an endothermic peak, at 154°C, which is a thin and intense peak; matching with one of the peaks associated at CS (Figure 17). Finally,

an exothermic peak appears at 300°C, which is associated with the decomposition and transformation of the oxygen groups of CS, PVA and GO.

3.3.6.5 SAMPLE CPG5

This blend is composed of 10 ml of CS, 4 ml of PVA and 5 ml of GO with the intention of observing how GO influences the CS matrix with PVA.

3.3.6.5.1 FTIR for CPG5

FTIR is used to characterise the behaviour of functional groups when GO is added to the combining of CS with PVA as show in Figure 84.

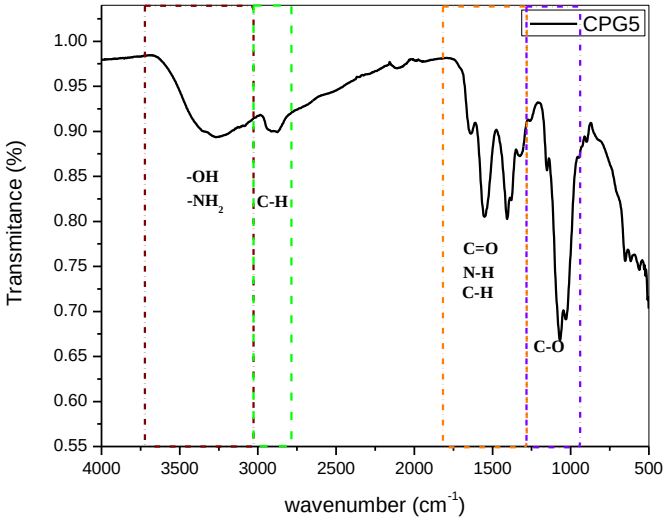

Figure 84. FTIR spectrum of CS and PVA with GO at 10:4.5 ratio

The spectrum shows a broadband at ~3255 cm^{-1} that is ascribed to O-H and $–NH_2$ stretching, being more intense. The bands at 2903 cm^{-1} are assigned to C-H stretching, the peak at 1636 cm^{-1} is ascribing C=O stretching, peak at 1548 cm^{-1} is assigned N-H stretching, peak at 1405 cm^{-1} is assigned C-H stretching and the peak at 1063 cm^{-1} is assigned C-O stretching.

3.3.6.5.2 SEM for CPG5

SEM shows in Figure 85 the behaviour of the freeze-dried foam obtained by combining CS with PVA.

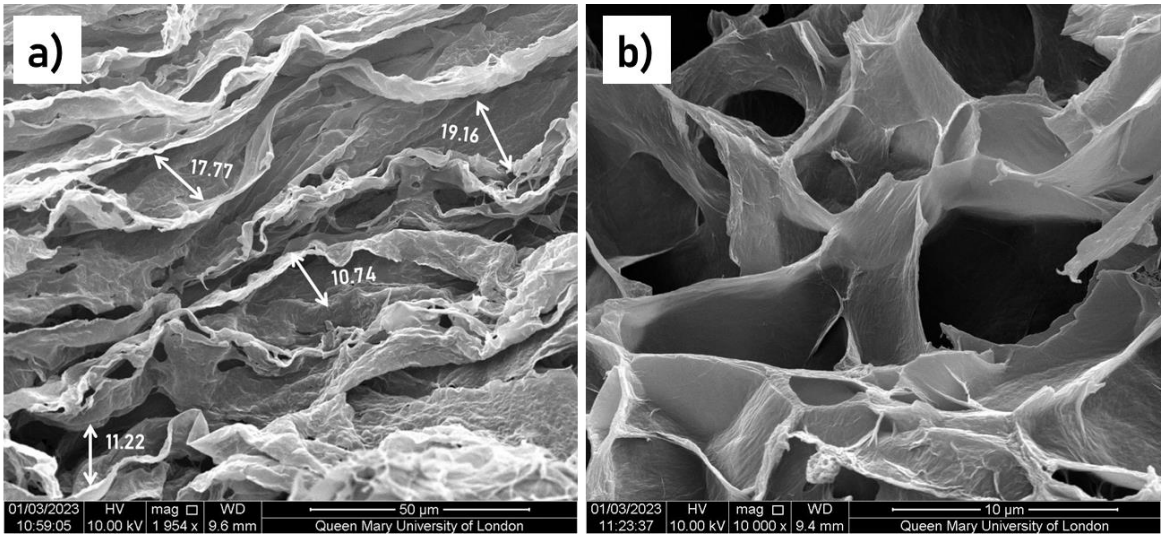

Figure 85. SEM of CS and PVA with GO at 10:4:5 ratio at a) 50 µm b) 10 µm

The layers forming the structure (Figure 85a) can be seen stacked in one direction, while image b) shows the formation of pores between these layers, whose size is approximately 10µm. In addition, these sheets are observed with wrinkles and folds between them, which may be due to the interaction of the substances in the formation of the foam.

3.3.6.5.3 DSC for CPG5

DSC shows in Figure 86 the behaviour of the freeze-dried foam obtained when the GO ratio is varied in the combination of CS with PVA.

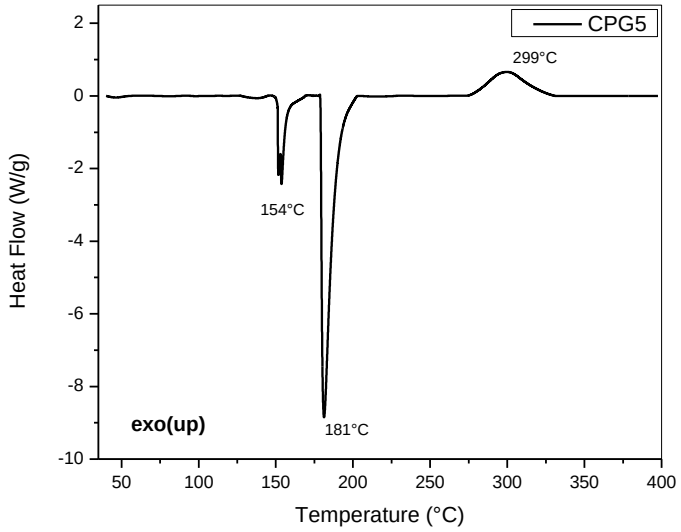

Figure 86. DSC spectrum of CS and PVA with GO at 10:4.5 ratio

Three peaks are visible, firstly an endothermic peak, which appears to split into two peaks at 154°C, the second one is a thin and very intense peak which appear and 181°C; related to the behavior presented by CS (Figure 17). Finally, an exothermic peak appears at ~299°C, which is associated with the decomposition of the oxygen groups of CS, PVA and GO.

3.3.7 THERMOGRAPHIC CAMERA TESTS

Finally, after obtaining all the samples, with the thermal camera FLIR TG165-X, the behavior of the material when exposed to temperatures up to 300°C was analyzed. For this procedure, these steps were followed:

Firstly, samples of approximately 1cm^3 were taken and placed on the heating plate, which was slowly raised in temperature, the temperature of the heating plate was recorded with the thermal camera, and then the temperature of the sample surface was recorded.

- Firstly, samples of 1 cm^3 were cut
- The temperature of hotplate is raised, keeping it below 300°C.
- Samples are placed on the hotplate
- The temperature of the heating plate was recorded with the thermal camera
- Finally, the temperature of the surface of the samples was recorded

The results obtained on samples that only contain CS and PVA are described below in the Figure 87.

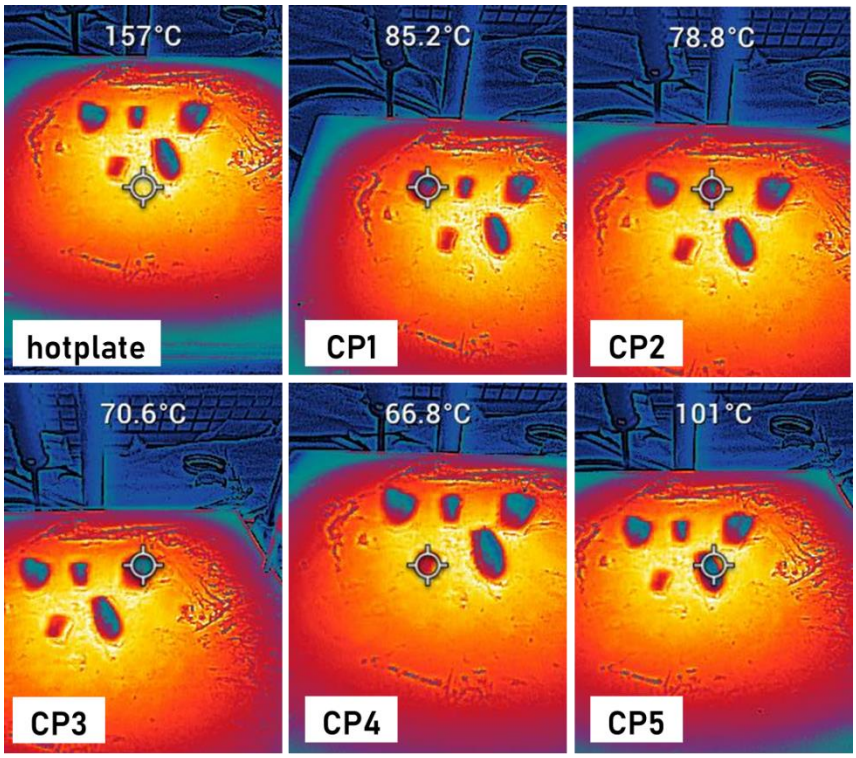

Figure 87. Thermographic tests of CS with PVA

The hotplate is at 157°C, while the samples of the combinations of CS with PVA at different ratios are on it. The temperatures recorded on the surface of the samples are:

- CP1 = 85.2°C
- CP2 = 78.8°C
- CP3 = 70.6°C
- CP4 = 66.8°C
- CP5 = 101°C

The results obtained on samples that of CS and PVA with GO are described below in the Figure 88.

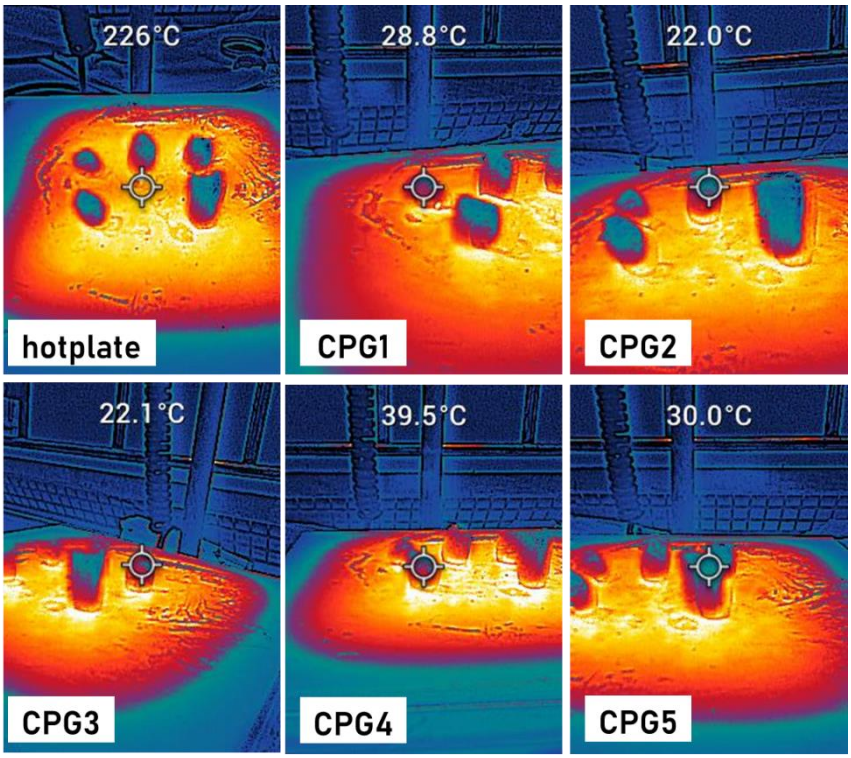

Figure 88. Thermographic tests of CS and PVA with GO

The hotplate is at 226°C, while the samples of the CS and PVA combinations with different GO ratios are on it. The temperatures recorded on the surface of the samples are:

- CPG1 = 28.8°C
- CPG2 = 22°C
- CPG3 = 22.1°C
- CPG4 = 39.5°C
- CPG5 = 30°C

A considerable decrease in the surface temperature of the samples is observed, this due to the improvement of the GO to the blend, due the strong interfacial interaction between GO and PVA which improves the thermal properties of the compound by the dispersion of GO in matrix(41).

Where CPG2 and CPG3 showed the lowest temperatures, indicating that they are the ones that best withstood the heat transfer.

3.4 DISCUSSION

In order to determine the blend with the best aerogel performance, a comparison of the properties obtained during characterisation is made below.

3.4.1 FTIR COMPARISON OF BLENDS

To identify the functional groups, present for the interaction in each blend, the FTIR analysis comparison of each sample was performed, as is shown in Figure 89.

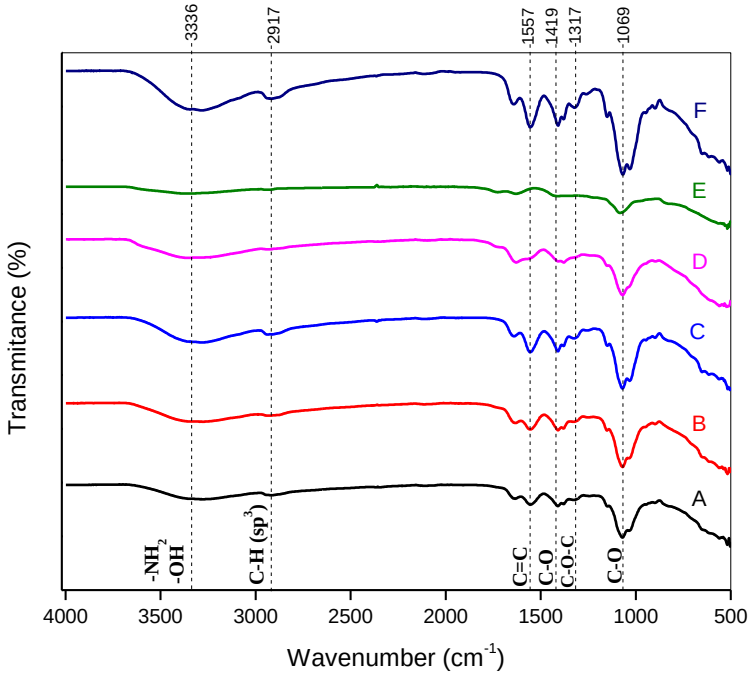

Figure 89. FTIR for blends A, B, C, D, E, F

In samples A and B, the peak corresponding to the C-H interaction is barely perceptible, this is because when CS, PVA and GO are present there are interactions between the functional groups. While for samples C and F this band appears without a problem, since they contain a greater abundance of CS and therefore more amino and hydroxyl groups are available in the mixture; so, it is possible that more H-bonds are formed between these functional groups resulting in broader bands in this area.

On the other hand, this band decreases in intensity in blends D and E, which contain more GO in the blend, and the hydroxyl and carbonyl groups being the most abundant, do not generate a large amount of hydrogen bonds.

The interactions corresponding to the double bond of the carboxyl group in the blend F appear as intense peaks while these disappear in E, this could also be due to the number of amino groups corresponding to CS in the mixture, since it is the largest

component in F and are not present in E, so the absence of these amino groups causes a decrease in the intensity of the OH band and also confirms the formation of H-bonds between GO and PVA, which are the main components of this blend.

Finally, what this comparison highlights are the strong presence of CS in the blends and how the amino and hydroxyl groups are related to each other forming hydrogen bonds, in order to correctly identify the presence of compatible functional groups. To improve the stability of the compound and thus improve the mechanical and thermal properties

3.4.2 FTIR COMPARISON OF MATRIX WITH FILLER

Now the interaction of the functional groups in blends of CS with PVA as matrix with the addition of GO as filler is observed below in Figure 90.

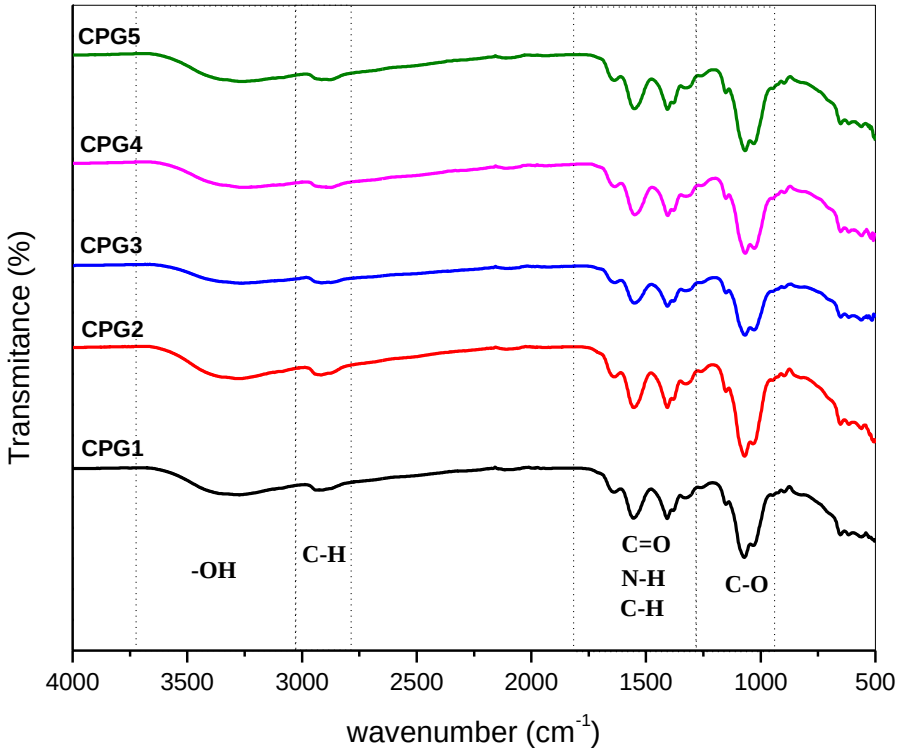

Figure 90. FTIR for CS and PVA with GO

There is no a big difference in the presence of functional groups in these blends, except for the decrease in the intensity of the peak corresponding to the C-O, interaction in the single bond region for the CPG3 sample. Furthermore, this sample shows a different behaviour with respect to the rest, since there is a notable decrease in the signal corresponding to OH, which indicates that there are no interactions that form H

bonds between the available functional groups, despite the fact that in the rest this signal decreases as the amount of PVA increases.

3.4.3 SEM COMPARISON OF PORE SIZE

In order to identify the pore size in the foams made by freeze drying, the following Table 11 shows the difference in the dimensions of the samples, that were observed in the micrographs taken of each sample.

Table 11. Pore size of samples

Blends	Pore size (μm)	Type of pore
A	<50	macro
B	40	macro
C	10-40	macro
D	50	macro
E	10	macro
F	>50	macro
I	50	macro
CP1	10	macro
CP2	30	macro
CP3	10	macro
CP4	10	macro
CP5	20	macro
CPG1	10	macro
CPG2	20	macro
CPG3	30	macro
CPG4	1	macro
CPG5	10	macro

According to the table, the dimensions of the pores are in the order of micrometers, so that the blend until now with the procedure carried out for the manufacture of aerogels, macropores are obtained in the structure, which although they are good, they are still far from being the most optimal. Since, as reported in previous papers, decreasing the pore size improves the thermal properties in the aerogel by decreasing the thermal conductivity and at the same time making them lighter; therefore, these dimensions should be further reduced.

3.4.4 BET COMPARISON

Another of the important characteristics of aerogels is related to the surface area, which is measured through the BET method, the data obtained is shown in Table 12.

Table 12 BET for samples

Blends	BET surface area (m^2/g)	Density ($g/cm^{3)}$
A	37.1173	0.5537
B	68.1355	0.1879
C	22.2599	0.6317
D	822.3278	1.0629
E	183.4799	0.0185
F	79.0043	0.787
I	401.619	3.7178

According to research, the BET surface areas of aerogels range from 200–1000 m^2/g (38). Therefore, only a couple of the samples carried out meet this criterion. For example, the blend with the highest surface area is D (822 m^2/g) followed by sample I (401 m^2/g); although these are the blends with the highest densities at 1.06 g/cm^3 and 3.71 g/cm^3 respectively, which for an aerogel are relatively high. However, blend F has a surface area of 79 m^2/g and a density of 0.787 g/cm^3 being the one with a balance between these properties, which is ideal for the lightness and stability properties of an aerogel o be used as an insulator.

3.4.5 TGA AND DSC COMPARISON

Finally, to identify the thermal properties, TGA and DSC measurements were performed and the results are compared in the following two tables, Table 13 and Table 14.

Table 13. TGA for samples

Sample	region of decomposition	Temperature range (°C)		Weight loss (%)	
		start	end	partial	total
A	1st	24.87	132.85	10.59	65
	2nd	132.85	218.35	8.37	
	3rd	218.35	600	46.48	
B	1st	26.81	118.56	13.97	63
	2nd	118.56	218.35	14.06	
	3rd	218.35	600	35.26	
C	1st	35	218.35	21.44	75
	2nd	218.35	600	53.57	
D	1st	39.17	110.36	15.26	57
	2nd	110.36	224.46	16.22	
	3rd	224.46	600	25.99	
E	1st	18.76	108.43	9.97	71
	2nd	108.43	218.35	20.9	
	3rd	218.35	600	40.69	
F	1st	28.89	81.92	10.04	78
	2nd	81.92	175.6	6.85	
	3rd	175.6	354.78	50.49	
	4rd	354.78	600	10.96	
I	1st	25.87	30.98	0.5	77
	2nd	30.98	65.53	14.54	
	3rd	65.53	242.78	16.79	
	4rd	242.78	600	44.86	

It is observed that the blend that loses less material is D, while the one that degrades the most is F and I. Both blends F and I are the ones with the highest weight loss, being the ones with the lowest GO content, while the blend with the highest GO content is the one with the lowest weight loss with only 57%. Therefore, the influence of GO to improve the decomposition of the material and therefore the thermal resistance is observed.

In the comparison with the results obtained in DSC, the degradation values of the samples are very similar as show in Table 14.

Table 14. DSC values of blends.

Sample	Thermic process	Temperature (°C)		Description
			Td	
CS	endo	115		evaporation of water
	endo	154		waste of CCS
	endo	206		waste of CS
	exo		300	CS degradation
PVA	endo	112		dehydration
	endo	229		melting point
	endo		285	decomposition
GO	endo	176		moisture
	exo	207		transformation of oxigen groups
	endo		278	decomposition fo GO
A	endo	147		dehydration
	exo	180		transformation of oxigen groups
	endo		192	decomposition of CS
B	endo	150		dehydration
	exo	190		transformation of oxigen groups
	endo		229	melting point of PVA
C	endo	115		moisture
	exo	200		tranformation of oxigen groups
	exo		295	decomposition of CS
D	endo	148		waste of CS
	exo	180		transformation of oxygen groups of GO
	endo		208	waste of CS
E	endo		159	degradation of GO shifted by PVA
	exo	198		transformation of oxygen groups of GO
	endo		229	degradation of GO shifted by PVA
F	endo	137		meltinng of CS
	endo	156		breaking of the polymer chains
	endo	233		breaking of the polymer chains
	exo		297	degradation of CS and PVA
I	endo	132		melting point of CS
	endo	151		breaking of the polymer chains
	endo	225		breaking of the polymer chains
	exo		300	degradation of CS

In all samples the total degradation temperature is approximately 300°C, which indicates that the samples cannot be used at temperatures higher than this.

Also in all samples, the first peak is attributed to water loss inside, however the temperatures at which these peaks appear is slightly higher than would be expected due to moisture loss, so it may also be due to the beginning of the loss of the polymer

chains of some of the sample components, so this peak shifts to higher temperatures than expected.

A comparison was also made between the temperature at which the degradation of the total material appears in the samples where the behaviour of the combination of CS with PVA, Figure 91, chosen to be the aerogel matrix is observed, and later with the addition of GO to observe how this influences the thermal behaviour (Figure 91,).

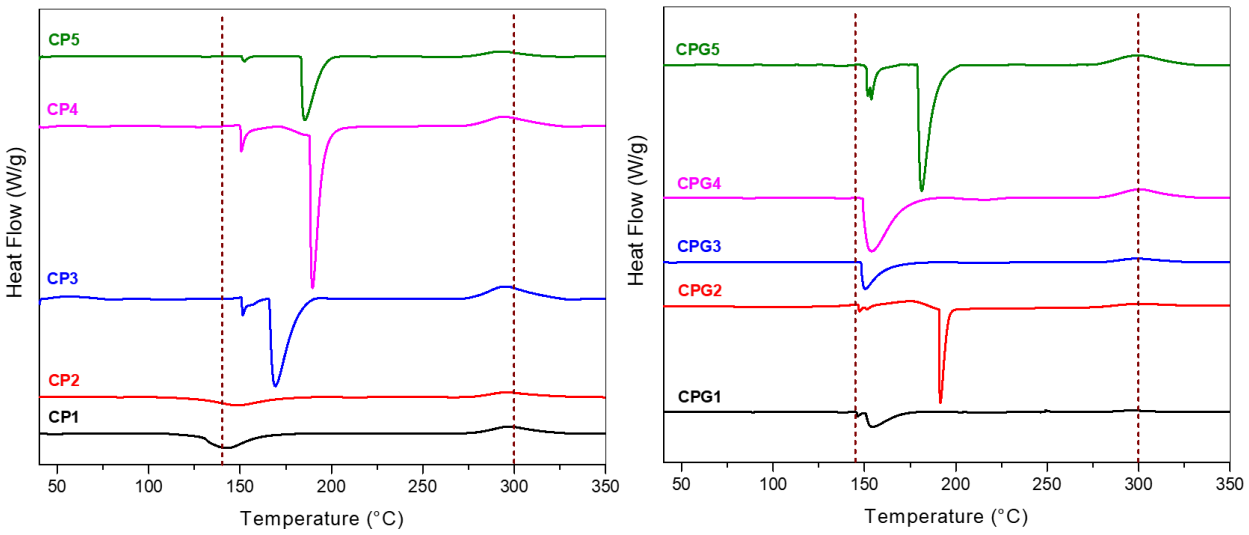

Figure 91. Comparison between matrix and matrix with filler

The difference in the intensity of the CS-related endothermic peaks is clearly observed, especially in sample CP4. There is a shift of the endothermic peaks towards higher values as the amount of PVA increases, being sample CP4 the one that shifts to higher temperature. Finally, in the exothermic peak there is no variation in the temperature at which it occurs. For this reason, the CP4 combination is chosen to add GO as a filler and observe the behaviour.

The main PVA-related endothermic peak in the CS samples with PVA was ~190°C; however, with the addition of GO there was a shift towards lower values in three of the samples. CPG5 and CPG2 showed the highest temperatures at approximately 180°C and 190°C respectively, so it is considered that CPG2 is the sample with the best temperature resistance.

4. CONCLUSIONS

Regarding the synthesis of GO, it was correctly implemented by the modified Hummers method, as was verified by XPS. It could be observed that GO sheets show wrinkles and folds due to the interaction of functional groups on their surface. Also, according to the STEM analysis, the sheets are about 2μm length, while AFM shows that the sheets remain stacked to a thickness of about 20 nm.

The behavior of the samples whose main material is CS showed the best pore distribution and surface area, as well as the best stability. For example, the Blend I presented a uniform surface with pores of 50 μm size, surface area of 401.61 m^2/g and density of 3.71 g/cm3. As well as a degradation starting at 230°C. While the Blend F presented stacked sheets with 50 μm sized spaces, with a surface area of 79.01 m^2/g and a density of 0.787 g/cm^3. As well as a degradation starting at 200°C due to the presence of PVA on CS. So was chosen like the best option to be used as a matrix for aerogel formation.

Regarding thermal behaviour the GO freeze-drying foam does not fully degrade when exposed to 600°C, however, it starts to degrade significantly from ~278°C. CS shows lower resistance to degradation than GO due to a higher weight loss when exposed to temperatures higher than 300°C. The samples CPG2 and CPG3 showed the best thermal behavior, as well as good pore distribution and pore formation, so it was found that add of GO to the matrix of CS with PVA improve the foam made by freeze-drying.

REFERENCES

1. Han X, Ding S, Zhu L, Wang S. Preparation and characterization of flame-retardant and thermal insulating bio-based composite aerogels. Energy Build. 2022 Jan;112656.

2. Dervin S, Lang Y, Perova T, Hinder SH, Pillai SC. Graphene oxide reinforced high surface area silica aerogels. J Non Cryst Solids [Internet]. 2017;465:31–8. Available from: http://dx.doi.org/10.1016/j.jnoncrysol.2017.03.030

3. Cakmak OK, Hassan KT, Wang J, Han X, Šiller L. Synthesis of sodium silicate-based silica aerogels with graphene oxide by ambient pressure drying. J Porous Mater [Internet]. 2021;28(5):1545–52. Available from: https://doi.org/10.1007/s10934-021-01103-2

4. Linn Berglund, Tuukka Nisssilä, Deeptanshu Sivaraman, Sanna Komulainen, Vill-Veikko Telkki and KO. Seaweed Derived Alginate Cellulose Nanofiber Aerogel for Insulation Applications.pdf. ACS Appl Mater Interfaces. 2021;13:34899–909.

5. Koebel M, Rigacci A, Achard P. Aerogel-based thermal superinsulation: An overview. Vol. 63, Journal of Sol-Gel Science and Technology. 2012. p. 315–39.

6. Buratti C, Merli F, Moretti E. Aerogel-based materials for building applications: Influence of granule size on thermal and acoustic performance. Energy Build [Internet]. 2017 Oct 1 [cited 2022 May 12];152:472–82. Available from: http://dx.doi.org/10.1016/j.enbuild.2017.07.071

7. Han X, Hassan KT, Harvey A, Kulijer D, Oila A, Hunt MRC, et al. Bioinspired Synthesis of Monolithic and Layered Aerogels. Adv Mater. 2018;30(23):1–7.

8. Lei Y, Hu Z, Cao B, Chen X, Song H. Enhancements of thermal insulation and mechanical property of silica aerogel monoliths by mixing graphene oxide. Mater Chem Phys [Internet]. 2017;187:183–90. Available from: http://dx.doi.org/10.1016/j.matchemphys.2016.11.064

9. Liu Y, Park M, Shin HK, Pant B, Choi J, Park YW, et al. Facile preparation and characterization of poly(vinyl alcohol)/chitosan/graphene oxide biocomposite nanofibers. J Ind Eng Chem [Internet]. 2014 Nov 25 [cited 2022 Apr 25];20(6):4415–20. Available from: http://dx.doi.org/10.1016/j.jiec.2014.02.009

10. Hu WH, Shang X, Han GQ, Dong B, Liu YR, Li X, et al. MoSx supported graphene oxides with different degree of oxidation as efficient electrocatalysts for hydrogen evolution. Carbon N Y [Internet]. 2016;100:236–42. Available from: http://dx.doi.org/10.1016/j.carbon.2016.01.019

11. Rapisarda M, Malfense Fierro GP, Meo M. Ultralight graphene oxide/polyvinyl alcohol aerogel for broadband and tuneable acoustic properties. Sci Rep. 2021 Dec 1;11(1).

12. Sitko R, Musielak M, Zawisza B, Talik E, Gagor A. Graphene oxide/cellulose membranes in adsorption of divalent metal ions. RSC Adv. 2016;6(99):96595–605.

13. Chen Y, Chen L, Bai H, Li L. Graphene oxide-chitosan composite hydrogels as broad-spectrum adsorbents for water purification. J Mater Chem A. 2013;1(6):1992–2001.

14. Marcano DC, Kosynkin D V, Berlin JM, Sinitskii A, Sun Z, Slesarev A, et al. Improved Synthesis of Graphene Oxide. Am Chem Soc. 2010;4(8).

15. Alejandra Huitrón Segovia E, Torres- Torres D, Raúl Pérez Higareda J, García-García A. Indentation size effects in graphene oxide under suspended nanoindentation. Mech Mater. 2021;158(April).

16. Figueroa T, Carmona S, Guajardo S, Borges J, Aguayo C, Fernández K. Synthesis and characterization of graphene oxide chitosan aerogels reinforced with flavan-3-ols as

hemostatic agents. Colloids Surfaces B Biointerfaces [Internet]. 2021 Jan 1 [cited 2022 Apr 25];197. Available from: https://doi.org/10.1016/j.colsurfb.2020.111398

17. Krishnamoorthy K, Mohan R, Kim SJ. Graphene oxide as a photocatalytic material. Appl Phys Lett. 2011;98(24):2013–6.

18. Lee SP, Ali GAM, Algarni H, Chong KF. Flake size-dependent adsorption of graphene oxide aerogel. J Mol Liq [Internet]. 2019 Mar 1 [cited 2022 Apr 15];277:175–80. Available from: https://doi.org/10.1016/j.molliq.2018.12.097

19. Croisier F, Jérôme C. Chitosan-based biomaterials for tissue engineering. Eur Polym J. 2013;49:780–92.

20. Jin L, Bai R. Mechanisms of lead adsorption on chitosan/PVA hydrogel beads. Langmuir. 2002;18(25):9765–70.

21. Pal K, Bharti D, Sarkar P, Anis A, Kim D, Chałas R, et al. Selected applications of chitosan composites. Int J Mol Sci. 2021;22(20):10968.

22. Bao H, Pan Y, Ping Y, Sahoo NG, Wu T, Li L, et al. Chitosan-functionalized graphene oxide as a nanocarrier for drug and gene delivery. Small [Internet]. 2011;7(11):1569–78. Available from: www.small-journal.com

23. Liang S, Huang Q, Liu L, Yam KI. Microstructure and molecular interaction in glycerol plasticized chitosan/poly(vinyl alcohol) blending films. Macromol Chem Phys. 2009;210(10):832–9.

24. Kumar A, Han SS. PVA-based hydrogels for tissue engineering: A review. Int J Polym Mater Polym Biomater. 2017;66(4):159–82.

25. Qi YY, Tai ZX, Sun DF, Chen JT, Ma HB, Yan XB, et al. Fabrication and characterization of poly(vinyl alcohol)/graphene oxide nanofibrous biocomposite scaffolds. J Appl Polym Sci. 2013;127(3):1885–94.

26. Chowdhury UB and D. Functionalized Graphene Oxide Quantum Dots-PVA hydrogel : Colorimetric Sensor. Nanotechnology. 2016;27(145501).

27. Yang S, Lei P, Shan Y, Zhang D. Preparation and characterization of antibacterial electrospun chitosan/poly (vinyl alcohol)/graphene oxide composite nanofibrous membrane. Appl Surf Sci [Internet]. 2018 Mar 30 [cited 2022 Apr 25];435:832–40. Available from: https://doi.org/10.1016/j.apsusc.2017.11.191

28. Begum MHA, Hossain MM, Gafur MA, Kabir ANMH, Tanvir NI, Molla MR. Preparation and characterization of polyvinyl alcohol–starch composites reinforced with pulp. SN Appl Sci [Internet]. 2019 [cited 2023 Jan 5];1(9). Available from: https://doi.org/10.1007/s42452-019-1111-2

29. Aslam M, Kalyar MA, Raza ZA. Polyvinyl alcohol: A review of research status and use of polyvinyl alcohol based nanocomposites. Polym Eng Sci. 2018 Dec 1;58(12):2119–32.

30. Pandele AM, Ionita M, Crica L, Dinescu S, Costache M, Iovu H. Synthesis, characterization, and in vitro studies of graphene oxide/chitosan-polyvinyl alcohol films. Carbohydr Polym. 2014 Feb 15;102(1):813–20.

31. Kazemnejadi M, Eslahi H, Sardarian A. A New Approach to Cross-Linking of Polyvinyl Alcohol and Its Swelling studies. 2016;(April).

32. Belay M, Sonker AK, Nagarale RK, Verma V. Synergistic strengthening of composite films by

crosslinking graphene oxide reinforcement and poly(vinyl alcohol) with dicarboxylic acids [Internet]. Vol. 66, Polymer International. 2017. p. 1737–46. Available from: www.soci.org

33. Takeshita S, Yoda S. Chitosan Aerogels: Transparent, Flexible Thermal Insulators. Chem Mater [Internet]. 2015;27(22):7569–72. Available from: https://pubs.acs.org/sharingguidelines

34. Sonu SS, Rai N, Chauhan I. Multifunctional Aerogels: A comprehensive review on types, synthesis and applications of aerogels. J Sol-Gel Sci Technol. 2023;324–36.

35. Baetens R, Jelle BP, Gustavsen A. Aerogel insulation for building applications: A state-of-the-art review. Vol. 43, Energy and Buildings. NTNU; 2011. p. 761–9.

36. Salimian S, Zadhoush A, Naeimirad M, Kotek R, Ramakrishna S. A review on aerogel: 3D nanoporous structured fillers in polymer-based nanocomposites. Polym Compos. 2018;39(10):3383–408.

37. Hrubesh LW. Aerogel applications. J Non Cryst Solids. 1998;225(1–3):335–42.

38. Fricke J, Tillotson T. Aerogels: Production, characterization, and applications. Thin Solid Films. 1997 Apr 1;297(1–2):212–23.

39. Jiang J, Zhang Q, Zhan X, Chen F. A multifunctional gelatin-based aerogel with superior pollutants adsorption, oil/water separation and photocatalytic properties. Chem Eng J [Internet]. 2019;358(October 2018):1539–51. Available from: https://doi.org/10.1016/j.cej.2018.10.144

40. Hao-Yang Mi, Xin Jing, Alexander l. Politowicz, Edward Chen, Han-Xiong Huang L-ST. Highly compressible ultra-light anisotropic cellulose/graphene aerogel fabricated by bidirectional freeze drying for selective oil absorption. 2018. p. 199–209.

41. Yang X, Shang S, Li L. Layer-structured poly(vinyl alcohol)/graphene oxide nanocomposites with improved thermal and mechanical properties. J Appl Polym Sci. 2011 May 5;120(3):1355–60.

42. Henry Kuo Feng Cheng, Nanda Gopal Sahoo, Yan Pei Tan, Yongzheng Pan, Hongqian Bao, Lin Li, Siew Hwa Chan and JZ. Poly(vinyl alcohol) nanocomposites filled with poly(vinyl alcohol) grafted graphene oxide. ACS Appl Mater Interfaces. 2012;2387–94.

43. Wang C, Li Y, Ding G, Xie X, Jiang M. Preparation and characterization of graphene oxide/poly(vinyl alcohol) composite nanofibers via electrospinning. J Appl Polym Sci. 2013;127(4):3026–32.

44. Rodríguez-Rodríguez R, Espinosa-Andrews H, Velasquillo-Martínez C, García-Carvajal ZY. Composite hydrogels based on gelatin, chitosan and polyvinyl alcohol to biomedical applications: a review. Int J Polym Mater Polym Biomater. 2020;69(1):1–20.

45. Açik G, Kamaci M, Özata B, Özen Cansoy CE. Effect of polyvinyl alcohol/chitosan blend ratios on morphological, optical, and thermal properties of electrospun nanofibers. Turkish J Chem. 2019;43(1):137–49.

46. Moradi S, Hamedi H, Tonelli AE, King MW. Chitosan/graphene oxide composite films and their biomedical and drug delivery applications: A review. Appl Sci [Internet]. 2021;11(17). Available from: https://doi.org/10.3390/app11177776

47. Wahba MI. Enhancement of the mechanical properties of chitosan [Internet]. Vol. 31, Journal of Biomaterials Science, Polymer Edition. 2020. p. 350–75. Available from: https://www.tandfonline.com/action/journalInformation?journalCode=tbsp20

48. Shao L, Chang X, Zhang Y, Huang Y, Yao Y, Guo Z. Graphene oxide cross-linked chitosan nanocomposite membrane. Appl Surf Sci. 2013;280:989–92.

49. Li C, Shi G. Functional gels based on chemically modified graphenes. Vol. 26, Advanced Materials. 2014. p. 3992–4012.

50. Hu J, Zhu J, Ge S, Jiang C, Guo T, Peng T, et al. Biocompatible, hydrophobic and resilience graphene/chitosan composite aerogel for efficient oil−water separation. Surf Coatings Technol. 2020 Mar 15;385.

51. Zheng Z, Zhao Y, Hu J, Wang H. Flexible, Strong, Multifunctional Graphene Oxide/Silica-Based Composite Aerogels via a Double-Cross-Linked Network Approach. ACS Appl Mater Interfaces. 2020;12(42):47854–64.

52. Dang W, Wang B, Xu Z, Zhang X, Li F, Zhao K, et al. Pore structure, thermal insulation and compressive property of ZrO2 nanofiber aerogels with carbon junction fabricated by freeze drying. Vol. 600, Journal of Non-Crystalline Solids. 2023.

53. Babiarczuk B, Lewandowski D, Szczurek A, Kierzek K, Meffert M, Gerthsen D, et al. Novel approach of silica-PVA hybrid aerogel synthesis by simultaneous sol-gel process and phase separation. J Supercrit Fluids [Internet]. 2020;166:104997. Available from: https://doi.org/10.1016/j.supflu.2020.104997

54. Mi X, Huang G, Xie W, Wang W, Liu Y, Gao J. Preparation of graphene oxide aerogel and its adsorption for Cu 2+ ions. Carbon N Y. 2012 Nov;50(13):4856–64.

55. Rattana T, Chaiyakun S, Witit-Anun N, Nuntawong N, Chindaudom P, Oaew S, et al. Preparation and characterization of graphene oxide nanosheets. Procedia Eng. 2012;32:759–64.

56. Hontoria-Lucas C, López-Peinado AJ, López-González J de D, Rojas-Cervantes ML, Martín-Aranda RM. Study of oxygen-containing groups in a series of graphite oxides: Physical and chemical characterization. Carbon N Y. 1995 Jan 1;33(11):1585–92.

57. Yang X, Tu Y, Li L, Shang S, Tao XM. Well-dispersed chitosan/graphene oxide nanocomposites. ACS Appl Mater Interfaces [Internet]. 2010;2(6):1707–13. Available from: www.acsami.org

58. Díez N, liwak A, Gryglewicz S, Grzyb B, Gryglewicz G. Enhanced reduction of graphene oxide by high-pressure hydrothermal treatment. RSC Adv [Internet]. 2015 Sep 25 [cited 2022 Jun 1];5(100):81831–7. Available from: https://pubs.rsc.org/en/content/articlehtml/2015/ra/c5ra14461b

59. Choi KS, Park Y, Kim SY. Comparison of graphene oxide with reduced graphene oxide as hole extraction layer in organic photovoltaic cells. J Nanosci Nanotechnol. 2013 May;13(5):3282–7.

60. Chen D, Feng H, Li J. Graphene oxide: Preparation, functionalization, and electrochemical applications. Chem Rev. 2012 Nov 14;112(11):6027–53.

61. Zhang Y, Gao H, Niu J, Liu B. Facile synthesis and photoluminescence of graphene oxide quantum dots and their reduction products. New J Chem [Internet]. 2014 Sep 15 [cited 2022 Jun 1];38(10):4970–4. Available from: https://pubs.rsc.org/en/content/articlehtml/2014/nj/c4nj01187b

62. Mahendran GB, Ramalingam SJ, Rayappan JBB, Kesavan S, Periathambi T, Nesakumar N. Green preparation of reduced graphene oxide by Bougainvillea glabra flower extract and sensing application. J Mater Sci Mater Electron [Internet]. 2020 Sep 1 [cited 2023 Jan 27];31(17):14345–56. Available from: https://link.springer.com/article/10.1007/s10854-020-

03994-4

63. Jayathilaka LPI, Ariyadasa TU, Egodage SM. Development of biodegradable natural rubber latex composites by employing corn derivative bio-fillers. J Appl Polym Sci. 2020 Oct 20;137(40).

64. Sahoo P, Shubhadarshinee L, Jali BR, Mohapatra P, Barick AK. Synthesis and characterization of graphene oxide and graphene from coal. Mater Today Proc. 2022 Jan 1;56:2421–7.

65. Pandey N, Bohra BS, Tiwari H, Pal M, Negi PB, Dandapat A, et al. Development of biodegradable chitosan/ graphene oxide nanocomposite via spray drying method for drug loading and delivery application. J Drug Deliv Sci Technol. 2022 Aug;74:103555.

66. Arifin B, Sugita P, Masyudi DE. Chitosan and lauric acid addition to corn starch-film based effect: Physical properties and antimicrobial activity study. Int J Chem Sci. 2016;14(2):529–44.

67. Zuñiga Rodriguez TD, Peña Lara D, Diosa Astaiza JE. Comportamiento de fases de membranas nanoestruturadas basadas en PVA, CS, H3PO2 y Nb2O5. Rev EIA [Internet]. 2020 Nov 1 [cited 2023 Jan 26];17(34):1–7. Available from: https://revistas.eia.edu.co/index.php/reveia/article/view/1368

68. Khalid MN, Agnely F, Yagoubi N, Grossiord JL, Couarraze G. Water state characterization, swelling behavior, thermal and mechanical properties of chitosan based networks. Eur J Pharm Sci. 2002 Jun 1;15(5):425–32.

69. Mansur HS, Sadahira CM, Souza AN, Mansur AAP. FTIR spectroscopy characterization of poly (vinyl alcohol) hydrogel with different hydrolysis degree and chemically crosslinked with glutaraldehyde. Mater Sci Eng C. 2008 May 1;28(4):539–48.

70. Abureesh MA, Oladipo AA, Gazi M. Facile synthesis of glucose-sensitive chitosan–poly(vinyl alcohol) hydrogel: Drug release optimization and swelling properties. Int J Biol Macromol [Internet]. 2016 Sep 1 [cited 2023 Jan 6];90:75–80. Available from: https://www.researchgate.net/publication/283072317_Facile_synthesis_of_glucose-sensitive_chitosan-polyvinyl_alcohol_hydrogel_Drug_release_optimization_and_swelling_properties

71. Salman SA, Bakr NA. Physical Sciences DSC and TGA Properties of PVA Films Filled with...salt. 2018;(March):0–11.

72. Liu W, Speranza G. Tuning the Oxygen Content of Reduced Graphene Oxide and Effects on Its Properties. ACS Omega [Internet]. 2021 Mar 9 [cited 2023 Jan 27];6(9):6195–205. Available from: https://pubs.acs.org/doi/full/10.1021/acsomega.0c05578

73. Srinivasa PC, Ramesh MN, Kumar KR, Tharanathan RN. Properties and sorption studies of chitosan-polyvinyl alcohol blend films. Carbohydr Polym. 2003 Sep 1;53(4):431–8.

74. Borrás A, Gonçalves G, Marbán G, Sandoval S, Pinto S, Marques PAAP, et al. Preparation and Characterization of Graphene Oxide Aerogels: Exploring the Limits of Supercritical CO2 Fabrication Methods. Chem - A Eur J. 2018;24(59):15903–11.

75. Neto CGT, Giacometti JA, Job AE, Ferreira FC, Fonseca JLC, Pereira MR. Thermal analysis of chitosan based networks. Carbohydr Polym. 2005 Nov 10;62(2):97–103.